



Norwegian University
of Life Sciences

Master's Thesis 2018/2019 60 ECTS
Chemistry, Biotechnology and Food Science

Quantitative and qualitative analyses of cyanopeptides in crayfish using liquid chromatography – mass spectrometry

Edvarda Wevling Matre
Chemistry

Table of contents

Acknowledgements	IV
Abstract	V
Sammendrag	VI
Abberivations and defenitions	VIII
1. General introduction	1
<i>1.2 Aims of study</i>	<i>1</i>
2. Biological and toxicological theory	2
2.1 <i>Cyanobacteria</i>	2
2.1.1 Global rise of cyanobacterial blooms.....	3
2.1.2 Cyanotoxins.....	3
2.1.3 Other bioactive compounds.....	9
3. Instrumental and analytical theory	12
3.1 <i>Sample preparation</i>	12
3.2 <i>Analytical separation, chromatography</i>	12
3.2.1 High Preformance Liquid Chromatography.....	13
3.3 <i>Mass Spectrometry</i>	16
3.3.1 Electrospray ionization mass spectrometry, ESI-MS.....	17
3.3.2 Mass filters.....	19
3.3.3 Detectors used in mass spectrometry.....	21
3.3.4 Tandem mass spectrometry.....	21
3.4 <i>Thiol derivatisation for Mdha7/Dhb7 differentiation</i>	22
3.5 <i>Enzyme linked immunosorbent assay</i>	23
3.6 <i>Method validation</i>	24
3.6.1 Blank samples.....	25
3.6.2 Standards.....	25
3.6.3 LOD and LOQ.....	25
3.6.4 Spike recovery.....	26
4. Material and methods	26
4.1 <i>Chemicals and reference materials</i>	26
4.2 <i>Exposure of crayfish to NIVA CYA-98</i>	27
4.3 <i>Cyanobacterial sample and sample preparation</i>	28
4.4 <i>Crayfish samples and sample preparation</i>	28
4.5 <i>Liquid chromatography</i>	29

4.6 Ion-trap mass spectrometry analyses	30
4.7 High-resolution mass spectrometry (HRMS) analyses	30
4.7.1. HRMS/MS of microcystins using a mixed MC standard.....	31
4.7.2 HRMS/MS screening for microcystins	31
4.7.3 Parallel reaction monitoring	31
4.8. β -mercaptoethanol derivatisation for <i>Mdha</i> ⁷ / <i>Dhb</i> ⁷ differentiation.....	32
4.9 Correction of concentration of [<i>D-Asp</i> ³]MC-LR and [<i>Asp</i> ³]MC-RR standards.....	32
4.10 Microcystin and anabaenopeptin quantification using liquid chromatography – high resolution mass spectrometry.....	32
4.11 Evaluation of method performance	33
4.11.1. Spike recovery	33
4.11.2. Precision and limits of detection and quantification	33
4.11.3. Signal suppression and enhancement (SSE)	34
4.12 Calculations and statistical analysis.....	34
5. Results and discussions	34
5.1 LC – HRMS of microcystins	35
5.2 Screening of microcystins and other cyanopeptides in NIVA-CYA98 using LC – HRMS analyses	38
5.3 β -Mercaptoethanol derivatisation for <i>Mdha</i> ⁷ / <i>Dhb</i> ⁷ differentiation.....	43
5.4 MS fragmentation of microcystins and anabaenopeptins in NIVA CYA-98 using ion trap tandem mass spectrometry	47
5.5 MS fragmentation of microcystins and anabaenopeptins in NIVA CYA-98 using high-resolution tandem mass spectrometry.....	56
5.6 Correction of concentration	64
5.7 Microcystins and other cyanopeptides in NIVA-CYA98	65
5.8 Evaluation of method performance	66
5.8.1 LOQ and LOQ.....	66
5.8.2 Spike recovery	68
5.8.3 Precision	68
5.9 Quantification of microcystins and anabaenopeptins using liquid chromatography–high resolution mass spectrometry.....	68
5.9.1 Quantification of microcystins and anabaenopeptins in NIVA-CYA98 (crayfish feed).....	68
5.9.2 Quantification of microcystins and anabaenopeptins in crayfish tissue	70
5.10 Comparison with ELISA results	74
6. Suggestions for further work	75
7. Conclusion.....	76
8. References	77
Appendix A	i

Appendix B.....ii
Appendix Ciii
Appendix D..... X
Appendix E.....xiii
Appendix F.....xiii
Appendix Gxviii

Acknowledgements

The work presented in this thesis was carried out at the Norwegian University of Life Sciences, at the Faculty of Chemistry, Biotechnology and Food Science (NMBU), in collaboration with the Norwegian Veterinary Institute (NVI). The work was conducted during a period from August 2018 until May 2019 and represents 60 ECTS of a 120 ECTS master's degree in chemistry.

I would first and foremost like to thank my supervisor at NVI, Silvio Uligh, for giving me the opportunity to write this master thesis and advising me throughout the year. I couldn't possibly have asked for a better supervisor. I would also like to thank all of the employees at the section of chemistry and toxicology (NVI) for answering questions and supporting me during my work. A special thanks to Ingunn Samdal and Kjersti Løvberg who performed the ELISA analyses and helped me interpret and understand the results. Additionally, I want to thank Chris Miles for answering questions and expanding my horizon in the microcystin universe. I would also like to thank my supervisor at NMBU, Dag Ekeberg, for support during the writing process.

Lastly, I would like to thank my parents, friends and boyfriend, all of whom have been a source of support and positive energy throughout my studies, from start to finish. I am very grateful. A special thanks to my dear friend Kari, of whom I have shared an office with during the work at NVI and my sister Mina for always being there for me.

Edvarda Wevling Matre
Ås, may 2019

Abstract

Microcystins are hepatotoxic (liver toxic) heptapeptides produced by cyanobacteria. These compounds can occur in drinking water, recreational water and food originating from waterbodies. The compounds are highly toxic and are known to be a hazard for both humans and animals. The world health organization (WHO) has set a provisional guideline of 1 µg/L in drinking water or a tolerable daily intake (TDI) of 0.04 µg microcystin per kg body weight per day. There are more than 250 different microcystin congeners due to variations in the amino acid structure, mainly in position two and four.

In the presented work, microcystins and other cyanopeptides were quantified in hepatopancreas and muscle crayfish tissue samples originating from a feeding trial conducted at The Norwegian Veterinary Institute (NVI). The purpose of the feeding trial was to investigate uptake and distribution of microcystins in crayfish. The feeding trial consisted of three groups of European noble crayfish (*Astacus astacus*), one control group and two groups receiving toxic cyanobacteria as feed or added in the water. The cyanobacteria used in the trial was *Planktothrix rubescens* (strain NIVA-CYA98), which is one of the species dominating Lake Steinsfjorden – the source of most crayfish used for consumption in Norway. The samples were analysed by liquid chromatography – mass spectrometry (LC–MS) and liquid chromatography– high resolution mass spectrometry (LC–HRMS). For structure elucidation we additionally used tandem (MS²) mass spectrometry and β-mercaptoethanol derivatisation.

Four microcystins ([D-Asp³, Dhb⁷]MC-RR, [D-Asp³, Dhb⁷]MC-RR, [D-Asp³, Dhb⁷]MC-HtyR and oxygenated [D-Asp³, Dhb⁷]MC-RR) and three anabaenopeptins (Anabaenopeptin B, Anabaenopeptin A and Ocsillamide Y) were detected in NIVA-CYA98. All anabaenopeptins and two microcystins ([D-Asp³, Dhb⁷]MC-RR, [D-Asp³, Dhb⁷]MC-RR) were detectable in the crayfish samples.

The concentrations of microcystins in the crayfish muscle samples were low (<0.085 µg/g) and fell below the limit of quantification (LOQ) in most of the samples for the group of crayfish receiving NIVA-CYA98 as feed. In the group of crayfish with NIVA-CYA98 added to the water, most samples were not detected or below LOD. Since muscle tissue is considered as the edible part of the crayfish, the study shows that it is safe to eat crayfish.

Analysis of samples of hepatopancreas tissue showed that microcystins and anabaenopeptins are accumulating in this part of the crayfish. Crayfish receiving NIVA-CYA98 as feed yielded a mean result of 104 ng/g.

Samples were earlier analysed by enzyme linked immunosorbent assay (ELISA) which showed good correlation to LC-MS results.

Sammendrag

Mikrocystiner er hepatotoksiske (levertoksiske) heptapeptider produsert av cyanobakterier. Disse toksinene kan forekomme i drikkevann, rekreasjonsvann og mat fisket eller høstet fra vann. Forbindelsene er svært giftige og er kjent for å være en til fare for både mennesker og dyr. WHO har fastsatt en foreløpig grenseverdi på 1 µg / l i drikkevann eller et tolerabelt daglig inntak (TDI) på 0,04 µg mikrocystin per kg kroppsvekt per dag. Det finnes mer enn 250 forskjellige microcystiner, takket være variasjoner i aminosyrestrukturen, hovedsakelig i posisjon to og fire.

I det presenterte arbeidet ble mikrocystiner og andre cyanopeptider kvantifisert i hepatopankreas- og muskelkrepsvevsprøver som stammede fra en fôringsstudie utført ved Veterinærinstituttet (NVI). Hensikten med fôringsstudiet var å undersøke opptak og distribusjon av mikrocystiner i kreps. Eksperimentet besto av tre grupper Edelkreps (*Astacus astacus*), en kontrollgruppe og to grupper som mottok giftige cyanobakterier som fôr eller tilsatt i tankvannet. Cyanobakterien som ble brukt i forsøket var *Planktothrix rubes* (stamme NIVA-CYA98), som er en av artene som dominerende Steinsfjorden - kilden til de fleste kreps som brukes til mat i Norge. Prøvene ble analysert ved væskechromatografi - massespektrometri (LC-MS) og væskechromatografi- høyopløselig massespektrometri (LC-HRMS). For å bestemme microcystinenes struktur brukte vi i tillegg tandem (MS²) massespektrometri og β-merkaptanolderivatisering.

Fire mikrocystiner ([D-Asp3, Dhb7] MC-RR, [D-Asp3, Dhb7] MC-RR, [D-Asp3, Dhb7] MC-HtyR og oksygenert [D-Asp3, Dhb7] MC-RR) og tre anabaenopeptiner (anabaenopeptin B, anabaenopeptin A og oscillamid Y) ble påvist i NIVA-CYA98. Alle anabaenopeptinene og to mikrocystiner ([D-Asp3, Dhb7] MC-RR, [D-Asp3, Dhb7] MC-RR) var detekterbare i krepsprøvene.

Konsentrasjonene av mikrocystiner i krepsprøveprøver var lave ($<0,085 \mu\text{g} / \text{g}$) og falt under kvantifiseringsgrensen (LOQ) i de fleste av prøvene fra gruppen kreps som mottok NIVA-CYA98 som fôr. I gruppen kreps med NIVA-CYA98 tilsatt til vannet ble de fleste prøver ikke eller var under detekjsonsgrensen (LOD). Siden halemuskelen er betraktet som den spiselige delen av kreps, viser studien at det med stor sannsynlighet er trygt å spise kreps fra Steinsfjorden. Det er å anta at de naturlig forekommende konsentrasjonene av mikrocystiner vil ligge mellom verdiene på gruppen som fikk NIVA-CYA98 i fôr og tilsatt i vann.

Hepatopankreasvevsprøver viser at mikrocystiner og anabaenopeptiner akkumuleres i hepatopankreas. Krepsen som mottok NIVA-CYA98 som fôr ga et gjennomsnittlig resultat på $104 \text{ ng} / \text{g}$.

Studien viste også en god korrelasjon mellom ELISA og LC-MS.

Abberivations and defenitions

NVI	The Norwegian Veterenary Institute
NIVA	The Norwegian Institute for Water Research
MC	Microcystin
TDI	Tolerable Daily Intake
LC	Liquid Chromatography
GC	Gas Chromatography
HPLC	High Performance Liquid Chromatography
TMS	Trimethylsilyl
MS	Mass Spectrometry
EI	Electron Ionization
CI	Chemical Ionization
UV	Ultra Violet
ELISA	Enzyme-linked Immunosorbent Assay
RF	Radio Frequency
DC	Direct Current
AC	Alternating Current
LOD	Limit of Detection
LOQ	Limit of Quantification
RM	Reference Material
CRM	Certified Reference Material
Mdha	N-methyldehydroalanine
MAsp	D-erythro-methylaspartic acis
Addaa	(2S,3S,8S,9S)-3-amino-9methoxy-2,6,8-trimethyl-10-phenyldeca-4,6-dienoic acid
Dhb	Dehydrobutyrine
MDhb	Methyldehydrobutyrine
Arg	Arginine
Ala	Alanine
Leu	Leucine
Asp	Asparagine
Ile	Isoleucine
Tyr	Tyrosine

Phe	Phenylalanine
M	Methyl
Hty	Homotyrosine
Rpm	Rounds per minute
SSE	Signal suppression/enhancement
AGC	automatic gain control

1. General introduction

The last decades there has been an increasing focus on cyanobacteria and their toxins (Chorus et al., 2000). Cyanobacteria have been found in a broad variety of climates (Meriluoto et al., 2017) and the presence of cyanobacterial blooms are increasing on a global scale due to global warming, higher CO₂ levels and nutrient enrichment of aquatic ecosystems (Huisman et al., 2018). Many cyanobacteria are able to produce several different cyanotoxins. Out of these, microcystins is the best studied and most frequently detected group (Gault & Marler, 2009). Microcystins may be produced by more than ten different genera of cyanobacteria and pose a high risk to humans, animals and aquatic organisms due to their high toxicity.

Cyanobacterial blooms have also been an issue of concern in Norway. Lake Steinsfjorden in Buskerud is one of the places that has been subject for regular cyanobacterial blooms. This lake is used for recreational purposes and is also where the Norwegian population obtain most crayfish for food consumption. The blooms in Lake Steinsfjorden are dominated by the microcystin producing cyanobacteria *Planktothrix agardhii* and *Planktothrix rubescens*. Biomass from these species may be a potential source of food for the omnivorous European crayfish (*Astacus astacus*) that inhabits the lake. Microcystins have been reported in hepatopancreas and muscle tissue from omnivorous crayfish originating from Lake Steinsfjorden (Aune, 1997). Due to the high toxicity of microcystins and global increase of cyanobacterial blooms there is a need to gain more knowledge on microcystin uptake, cyanobacterial distribution, peptide synthesis and toxicity of different microcystins and their analogs. There is little information concerning microcystin uptake in crayfish, both in Norway and internationally.

1.2 Aims of study

The aims of this study was to:

- 1) To obtain a complete microcystin and cyanopeptide profile in a strain of toxic cyanobacteria (NIVA-CYA98) used in a feeding trial conducted at the Norwegian Veterinary Institute.
- 2) Quantify microcystins and other cyanopeptides in tissue (muscle and hepatopancreas) from European noble crayfish (*Astacus astacus*) originating from the feeding trial
- 3) Compare the LC-MS results with earlier obtained ELISA results of the same samples

2. Biological and toxicological theory

2.1 Cyanobacteria

Cyanobacteria are highly adaptable organisms that can survive extreme environmental conditions. They are known to inhabit both marine water, fresh water and brackish water. They can also occur on the top of rocks and soils or attached to plants in the shoreline. Cyanobacteria have even been observed in the desert (Meriluoto et al., 2017). These organisms have a global distribution and the phylum consists of a range of different species which all have in common that they are oxygenic phototrophs. By obtaining their energy through photosynthesis and producing oxygen, cyanobacteria were responsible for creating the earth's aerobic atmosphere 2200-2400 million years ago (Meriluoto et al., 2017). When the aquatic environment offers favourable conditions, for instance high concentrations of phosphorus, cyanobacteria can form blooms. These can be defined as a marked visible discoloration of the water by cyanobacteria and take place after exponential reproduction (Fig. 1). The blooms can have a negative impact on the water quality and can be formed by several genera of cyanobacteria. The most common bloom-forming cyanobacteria are *Aphanizomenon*, *Cylindrospermopsis*, *Dolichospermum*, *Microcystis*, *Nodularia*, *Planktothrix* and *Trichodesium*. These organisms can cause hypoxia and anoxia due to microbial degradation of blooms. Hypoxia is a phenomenon where the level of dissolved oxygen in the water decrease, and anoxia is when the concentration of dissolved oxygen become extremely low or reach zero. This can be lethal for aquatic flora and fauna. Cyanobacteria may also produce cyanotoxins. There are several different types of cyanotoxins, and they can cause liver, digestive and neurological disease if consumed by birds or mammals (Huisman et al., 2018).



Figure 1: a) photo of cyanobacterial blooming in southeast Florida, 2016. Adopted from (Florida Atlantic University, 2018). b) photo of cyanobacterial blooming taken Landsat 8 satellite, 2017. Adopted from (Finnish Environment Institute, 2017).

2.1.1 Global rise of cyanobacterial blooms

Although cyanobacteria have occupied aquatic environments throughout much of earth's history, there are now evidence indicating that the occurrence of harmful cyanobacterial blooms is increasing on a global scale. This has happened during the last decades and is believed to expand further in the coming ones. The explanation for this rise is understood to be caused by global warming, higher CO₂ levels and nutrient enrichment of aquatic ecosystems. The input of nutrients is caused by human activities such as agriculture and industry (Huisman et al., 2018).

2.1.2 Cyanotoxins

Cyanobacteria have been known to cause poisoning in animals for more than 120 years. In 1996, 76 people died after being exposed to a water source contaminated with cyanotoxins at a dialysis clinic in Brazil (Carmichael et al., 2001). The leading cause of death was believed to be intravenous exposure to microcystins. In 1999 approximately 30 000 flamingos were killed by a cyanobacterial bloom in Kenya (Krienitz et al., 2003), and in 2012 over 750 birds died because of a toxic cyanobacterial bloom in Maryland, USA (Foss et al., 2018).

Toxicological experiments have confirmed that cyanobacteria can produce a variety of different toxins. Without the exception of saxitoxin, which can also be produced by dinoflagellates, these types of toxins are only produced by cyanobacteria (Webb et al., 2006). Because cyanobacterial blooms mainly occur in freshwater and brackish water, these waters are also the major route of exposure. This includes food caught or harvested from

waterbodies. In some cases, the poisoning can also happen due to inhalation of aerosols contaminated with cyanotoxins or through skin contact with blooms (Meriluoto et al., 2017).

The different cyanotoxins can be separated into groups according to their chemical structure. The majority of cyanotoxins are of low weight and vary from 118 Da (β -N-methylamino-L-alanine [BMAA and 2,4-diaminobutyric acid [DAB]) to ~1000 Da (microcystins) (Meriluoto et al., 2017). Lipopolysaccharides (LPS) is the largest group of cyanotoxins and consists of molecules ranging from 10 to 20 kDa (Meriluoto et al., 2017). Table 1 provides a summary of different cyanotoxins, their chemical structure, the types of bacteria that may produce the toxin and the toxins modes of action.

Table 1: Displays the different cyanotoxins, what group of chemical structure they are divided into, cyanobacteria producers and the toxins mode of action.

Cyanotoxin	Chemical structure	Modes of action	Cyanobacteria producers
Microcystins	Cyclic heptapeptides	Hepatotoxic, tumor promoting, inhibition of eukaryotic protein phosphatase PP1, PP2A, and phosphatases PPP4, PPP5	<i>Microcystis</i> , <i>Anabaena</i> , <i>Nostoc</i> , <i>Planktothrix</i> , <i>Phormidium</i> , <i>Oscillatoria</i> , <i>Radiocystis</i> , <i>Gloeotrichia</i> , <i>Anabaenopsis</i> , <i>Rivularia</i> , <i>Tolypothrix</i> , <i>Hapalosiphon</i> , <i>Plectonema</i>
Nodularins	Cyclic pentapeptides	The modes of action as microcystins, in addition to weak carcinogenicity	<i>Nodularia spumigena</i> , <i>Nostoc</i> (symbiotic)
Cylindrospermopsins	Tricyclic guanidine alkaloids	Multiple organ toxicity, neurotoxic, genotoxic, protein synthesis inhibitor	<i>Cylindrospermopsis</i> , <i>Umezakia</i> , <i>Anabaena</i> , <i>Oscillatoria</i> , <i>Parhidiopsis</i> , <i>Aphanizomenon</i>

Anatoxin-a	Bicyclic alkaloids	Neurotoxic, binds competitively at acetylcholine receptors	<i>Anabaena, Phormidium, Aphanizomenon</i>
Anatoxin-a(S)	Phosphorylated cyclic N-hydroxyguanine	Neurotoxic, inhibits acetylcholine esterase	<i>Anabaena</i>
Saxitoxins	Alkaloids	Neurotoxic, blocks voltage-gated sodium channels	<i>Aphanizomenon, Anabaena, Lyngbya, Cyndrospermopsis, Planktothrix</i>
Lyngbyatoxins, Aplysiatoxins	Indole alkaloids	Tumor-promoting, binds eukaryotic protein kinase C	<i>Lyngbya, Oscillatoria, Schizothrix</i>
BMAA, DAB	Diamino acids	Neurotoxic, developmental toxin, erroneous insertion into proteins	Many genera
LPS	Lipopolysaccharides	Inflammatory, promotion of cytokine secretion	All genera

Table adopted from (Meriluoto et al., 2017).

Microcystins

Microcystins are the most frequently detected and best described group of cyanotoxins (Gault & Marler, 2009). This is also the most diverse group of cyanotoxins (Neilan et al., 2013) with more than 250 identified and reported structurally diverse analogues (Foss et al., 2018; Miles & Stirling, 2017), and new ones being discovered regularly (Meriluoto, J. et al., 2017).

Microcystins can be produced by several genera within the phylum of cyanobacteria (Table 1) and are released during cell rupture. Some strains in the genus, such as *Microcystis aeruginosa*, have a global distribution and are well adapted to different climates. This makes microcystins a significant hazard for human health (Pearson et al., 2010).

Microcystins are cyclic hepatotoxic (livertoxic) heptapeptides produced by non-ribosomal peptide synthesis. This synthesis is carried out by a large multi-enzyme complexes according to the thio-template mechanism (Welker & Von Döhren, 2006). The molecules have the general formula cyclo (D-Ala-L-X-D-erythro-β-methylAsp-L-Z-Adda-D-Glu-N-

methyldehydro-Ala), where X and Z represent the amino that vary the most. They act as specific inhibitors of protein phosphatase (PPs) type 1, 2A, 3 (for MC-LA), 4, 5 and in some extent 2B. The inhibition of PP1 and PP2A result in an increased phosphorylation of proteins in liver cells which affects several processes that may result in severe liver damages. They are shown to be tumour promoters, endocrine disruptors and immunotoxicants as well as inducing oxidative DNA damage and activation of proto-oncogenes (Gault & Marler, 2009).

Microcystins comprise of several rare amino acids that are more or less conserved in the chemical structure (Fig. 2). One amino acid that is characteristic for microcystins, is 3-amino-9-methoxy-2-6,8-trimethyl-10-phenyldeca-4,6-dienoic acid (Adda), which occur in position 5 of the microcystin skeleton. Microcystins also contain both L- and D- amino acids and N-methyldehydroalanine (Mdha) (Pearson et al., 2010). The most varying amino acids are the ones in position 2 and 4 (Appendix A, Fig 1A.). Another common variation is to observe MDha instead of Dhb in position 7 and methylation on D-Asp in position 3.

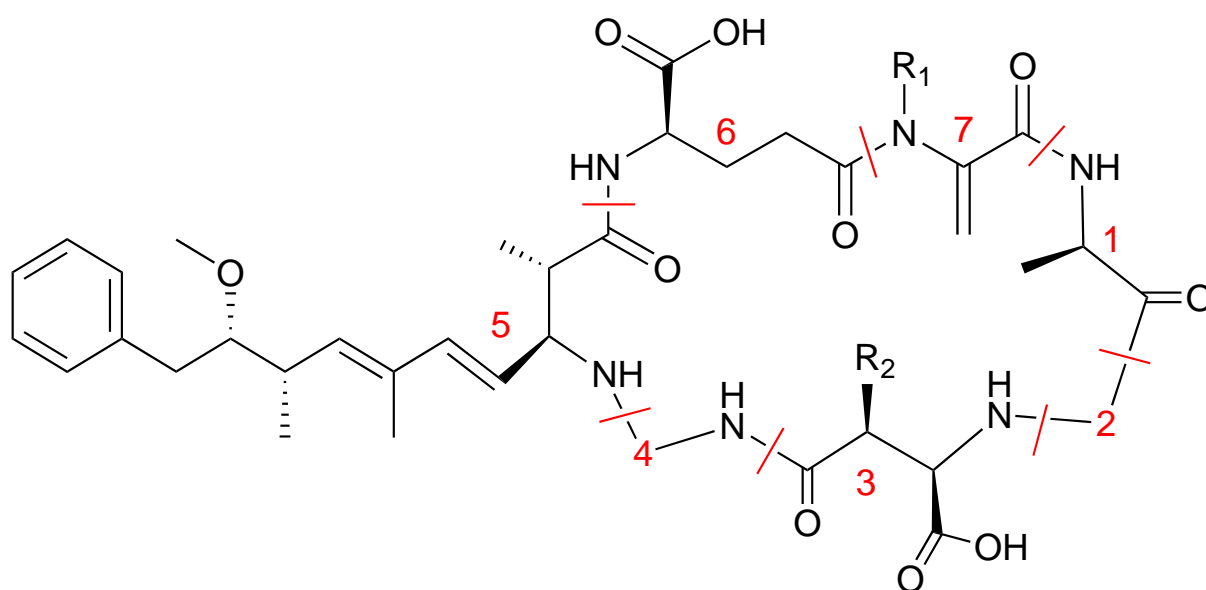
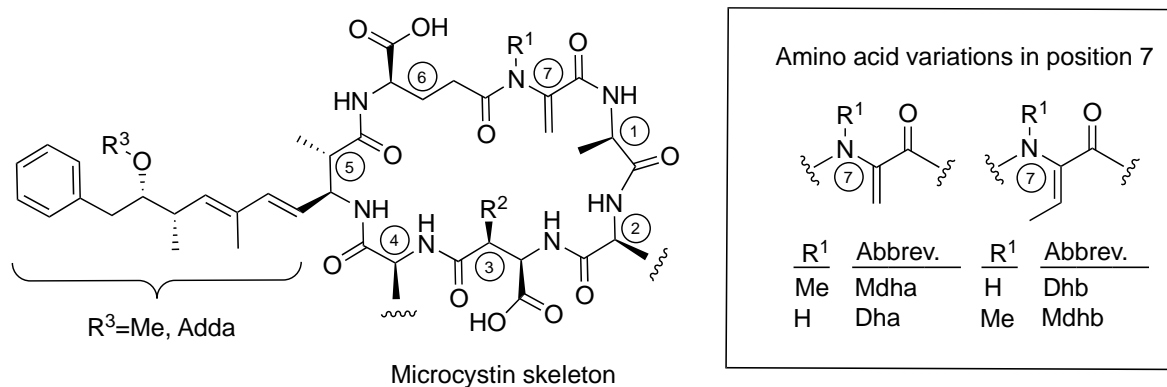


Figure 2: General structure of a microcystin. Red lines are separating the different amino acids, and the numbers are indicating the position of the amino acids. Position 2 and 4 are marked in red. R₁ and R₂ show common sites of methylation.

MC-LR is the most frequently occurring and most toxic microcystin. MC-LR is also the most studied microcystin, and is considered as the most “normal” one (World Health Organization, 2017). MC-LR has Adda in position 5, M-Asp in position 3, Mdha in position 7 and methyl in R₁ and R₂ (see Fig. 3). Variation in molecular structure that differ from MC-LR, except in

position 2 and 4, are denoted by putting them in square brackets. E.g. [D-Asp³, Dhb⁷]MC-LR, where there is no methylation of asparagine in position 3 and the microcystin has Dhb instead of Mdha in position 7.

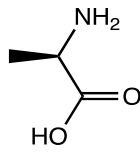
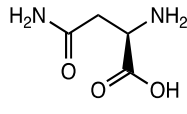
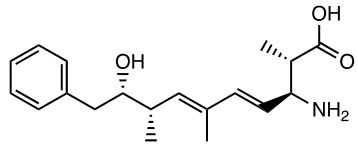
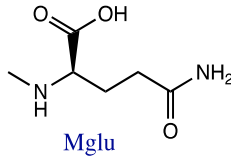
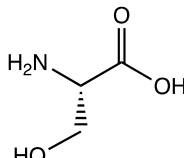
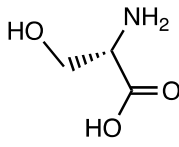
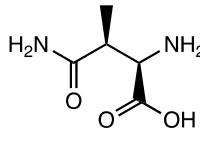
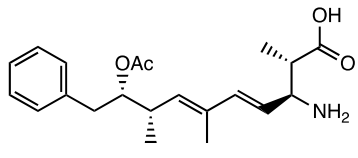
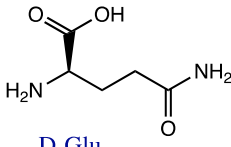
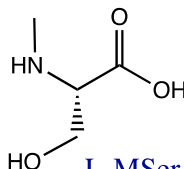
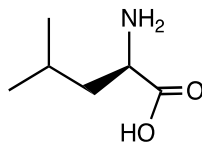
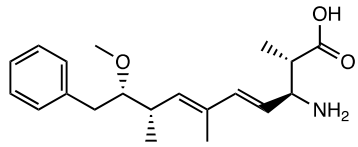
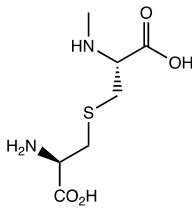
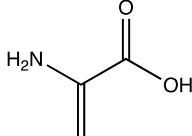
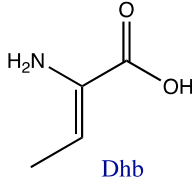
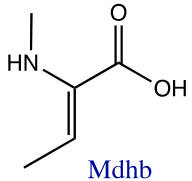
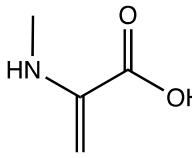


	2	4	7	R1	R2	[M+H] ⁺
MC-RR	Arg	Arg	Mdha	Me	Me	1038.5731
MC-LF	Leu	Phe	Mdha	Me	Me	986.5233
MC-LW	Leu	Trp	Mdha	Me	Me	1025.5342
MC-LY	Leu	Tyr	Mdha	Me	Me	1002.5183
MC-LA	Leu	Ala	Mdha	Me	Me	910.4920
MC-LR	Leu	Arg	Mdha	Me	Me	995.5560
[D-Asp ³]MC-LR	Leu	Arg	Mdha	Me	H	981.5404
[D-Asp ³ ,Dhb ⁷]MC-LR	Leu	Arg	Dhb	H	H	981.5404
[Dha ⁷]MC-LR	Leu	Arg	Dha	H	Me	981.5404
MC-YR	Arg	Tyr	Mdha	Me	Me	1045.5353
MC-RY	Tyr	Arg	Mdha	Me	Me	1045.5353
[D-Asp ³ , Dhb ⁷]MC-HtyR	Hty	Arg	Dhb	H	H	1045.5353
[D-Asp ³]MC-HtyR	Hty	Arg	Mdha	Me	H	1045.5353
[Dha ⁷]MC-HtyR	Hty	Arg	Dha	H	H	1045.5353
[D-Asp ³]MC-RR	Arg	Arg	Mdha	Me	H	1024.5574
[Dha ⁷]MC-RR	Arg	Arg	Dha	H	Me	1024.5574
[D-Asp ³ ,Dhb ⁷]MC-RR	Arg	Arg	Dhb	H	H	1024.5574

Figure 3: structure of microcystins discussed in the text, given with their name abbreviation, the amino acids they have in the most varying positions, R groups and [M+H]⁺.

Even though the amino acids in position 1, 3, 5, 6 and 7 are more conserved than the amino acids in position 2 and 4, there may still be some variations (Tab. 3).

Table 3: Amino acids that can occur in position 1, 3, 5, 6 and 7. These are the more conserved positions and do not have as many amino acid alternatives as position 4 and 2.

Position 1	Position 3	Position 5	Position 6	Position 7
 D-Ala	 D-Asp	 DMAdda	 Mglu	 L-Ser
 L-Ser	 D-MAsp	 ADMAdda	 D-Glu	 L-MSer
 D-Leu		 Adda		 MeLan
				 Dha
				 Dhb
				 Mdhb
				 Mdha

The Table is adopted from Chris Miles personal data, with permission.

Variations in position 2, 4, 7, R1 and R2 is the main reason for all the structural isoforms of microcystins.

Toxicity guidelines for microcystins

Microcystin-LR is the most studied microcystin and is the only microcystin which has enough toxicological data obtained about it to make a provisional guideline value. The World Health Organization (WHO) has derived a Tolerable Daily Intake (TDI) of 0,04 µg/kg body weight and a Provisional guideline value of 1 µg/L (considering a consumption of 2 liter/day). Both values include both cell-bound and free microcystin-LR. Due to the fact that only one microcystin has a guideline value and microcystins is a group of large variety, it is challenging to determine the risk of consuming water and/or foods contaminated with microcystins (WHO, 2017).

2.1.3 Other bioactive compounds

Cyanobacteria are able to produce several different bioactive compounds. Bioactive compounds produced by cyanobacteria is a heterogenous group of chemicals, that for instance includes biogenic amides, alkaloid structures and derivatives of lipids. The most widely studied group of bioactive cyanobacterial compounds is the peptides. Three common ways to classify peptides are according to their biosynthetic pathway, their chemical structure or their primary target organ. So far, more than 600 peptides or peptidic secondary metabolites have been identified (Welker & Von Döhren, 2006). These peptides are described from various taxa and many of them are assumed to be synthesized by non-ribosomal synthetase.

It is shown that other cyanopeptides may occur just as frequently as microcystins, and that these compounds have received way too little attention (Janssen, 2019). The toxic effects caused by cyanobacterial extracts can often not be explained by microcystins alone and must be caused by other bioactive compounds. Because of this, there is expressed a need for more studies and risk assessment, not only of microcystins, but also other peptides produced by cyanobacteria. The following sub-chapters give some examples of bioactive secondary metabolites produced by cyanobacteria (Janssen, 2019).

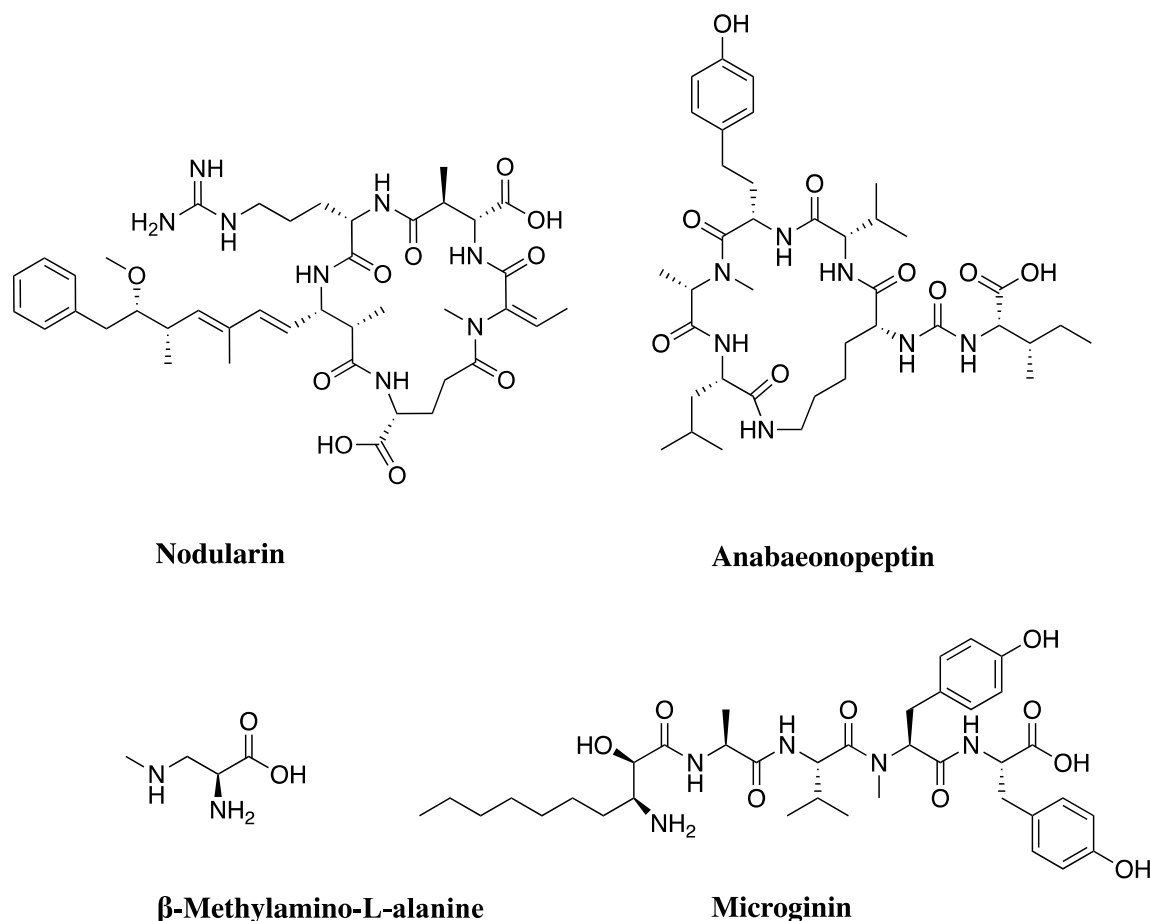


Figure 4: Four bioactive compounds produced by cyanobacteria. The name of the group/molecule is given with the molecular structure of a molecule in the group. The figure shows Nodularin R, Anabaenopeptin I, β-Methylamino-L-alanine (not a group) and Microginin 713.

Anabaenopeptins

Anabaenopeptins (Fig. 3) are a group of structurally diverse non-ribosomal, cyclic peptides. The group includes molecules with a mass ranging from 759 Da (Anabaenopeptin I) to 956 Da (Oscillamide C). Anabaenopeptins all consists of a cyclic pentapeptide with a single amino acid residue side chain (usually Arg, Ile, Tyr or Phe) attached through a uredio bridge with the α -amide of D-lysine. Anabaenopeptines have been identified in cyanobacteria from the genera *Dolichospermum/Anabaeno*, *Chrysochlorum/Aphanizomenon*, *Planktothrix*, *Microcystis*, *Nodularia*, *Nostoc*, *Lyngbya/Planktolingybia* and *Schizothrix*. The different anabaenopeptins have different biological activity depending on amino acid composition. Anabaenopeptin F, Oscillamide B and Oscillamide C inhibits the activity of protein phosphatase (PP) due to the positively charged Arg in position 1 and a hydrophobic residue of N-MEHty in position 5. These molecules may also be active towards proteolytic enzymes (Martens, 2017).

Microginins

Microginins (Fig. 3) is a group consisting of 25 different linear, nonribosomal peptides. They have mainly been isolated from *Microcystis aeruginosa*, but have also been found in various bloom forming cyanobacteria strains. This is a group of peptides that can be drug candidates to treat hypertension and associated diseases such as chronic heart failure and diabetic nephropathy (Gault & Marler, 2009).

β-Methylamino-L-alanine

β-Methylamino-L-alanine, or BMAA, (Fig. 3) is an amino acid originating from alanine, with a methylamino side chain. The amino acid can be produced by a variety of cyanobacteria, and functions as a neurotoxin in mammals. The toxin has been associated with the occurrence of neurodegenerative diseases such as ALS, parkinson and alzheimer (Caller et al., 2018),(Gault & Marler, 2009).

Nodularins

Nodularins, or NODs, are cyclic pentapeptides with the general structure cyclo(-D-erythro-β-methylAspo(iso-linkage)-L-Z-Adda-D-Glu(iso-linkage)-2-(methylamino)-2(Z)-dehydrobutyric acid). These peptides share several structural and functional properties with microcystins. NODs are also produced through nonribosomal peptide synthesis and functions as a hepatotoxin (liver toxin). Nodularins were first identified in the cyanobacteria *Nodularia spumigena*. Since the first discovery during the late 1800s, toxic blooms of *Nodularia spumigena* has been documented in brackish water and lakes all over the world (Gault & Marler, 2009).

Secondary metabolites in NIVA-CYA98

Genes associated with biosynthesis of microcystins, anabaenopeptins, aeruginosins, microginins, microviridins and cyanopeptolins have previously been identified in *P. rubescens* (Kurmayer et al., 2016). The possession of these genes does not however mean that the species is able to or do actually produce the toxins or peptides. There may also exist non-producing strains. In 2008 an article regarding a field program conducted in Lake Steinsfjorden also showed that *P. rubescens* can form subpopulations with dissimilar ecological traits. The study revealed that 11 different cyanopeptides were been found in,

NIVA-CYA98, which is the strain used in the feeding trial prior to this study (Rohrlack et al., 2008).

3. Instrumental and analytical theory

3.1 Sample preparation

In order to obtain a representative sample, the sample material has to be homogenous. Heterogenous samples, such as tissue, acquires sample preparation. This can be done by mixing, grinding, crushing and decomposition, depending on what you want to analyse. When using HPLC–MS, it is important that the sample is particle free to not destroy the capillary needle. A particle free sample can be obtained by filtration, sedimentation or centrifuging (Skoog et al., 2014).

3.2 Analytical separation, chromatography

Separation is an important area within the field of chemistry, and chemists are constantly trying to challenge old principals to obtain better separation techniques. Methods for separation can be both preparative and analytical. While preparative separation is often used for purification, analytical separation aims to measure the relative proportions of analytes in a mixture. This information can be used in qualitative and quantitative analysis. Today, there are numerous analytical methods for separations. Some common examples are distillation, electrophoresis, chemical or electrolytic precipitation and chromatography (Skoog et al., 2014).

According to James M. Miller (2005)., chromatography is the most important procedure for isolating and purifying chemicals common for all types of chromatography, is that they use a stationary and mobile phase to separate the components of a mixture. The mobile-phase components will interact differently with the stationary phase. The variation of equilibrium reactions with the stationary phase, will cause the components of the analytical mixture to migrate with different rates through the stationary phase (often a column). This is the basis of a chromatographic separation. The components are carried through the stationary phase together with a mobile phase. The mobile phase can be either a liquid, a supercritical liquid or a gas. This aspect is one way to separate different types of chromatographic systems. How long time a component uses to migrate through the stationary phase, is determined by the composition of the stationary phase, the composition of the mobile phase and the temperature.

In this study, high performance liquid chromatography has been used for all analysis.

3.2.1 High Performance Liquid Chromatography

Chromatographic methods where the carrier medium is a liquid solvent are called liquid chromatography (LC). High performance liquid chromatography (HPLC) is the most versatile and widely used type of liquid chromatography (Miller, 2005).

HPLC is carried out in columns packed with small particles. Due to the close packing in the column, the particles produce a high resistance to fluid flow. This creates a need for high pressure pumps to obtain sufficient flow of the mobile phase. HPLC systems requires a much higher pumping pressure than the initial, more simple forms of column chromatography. Because of this HPLC was previously referred to as high *pressure* liquid chromatography. A HPLC system (Fig.5) consists of a mobile phase reservoir, pumps, injector, a column for separation and a detector (Skoog et al., 2014).

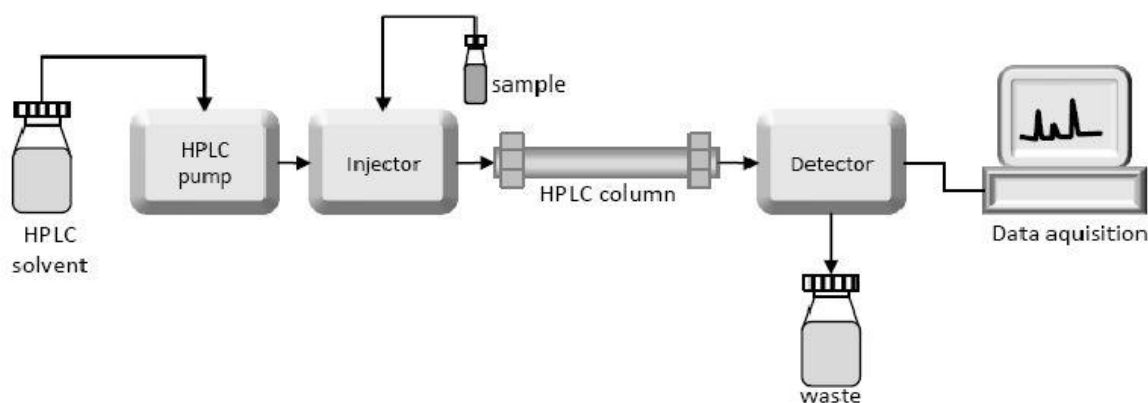


Figure 5: Schematic representation of a HPLC system. Adopted from (Laboratoryinfo, 2019)

The pumps pass the mobile phase through the column. Many HPLC systems contain mixing chambers to allow the use of gradient elution. Gradient elution is to change the proportions of two or more mobile phase solvents during the analysis. Gradient elution can make the separation of similar components easier and is also useful in developing new methods. One disadvantage with gradient elution is that the reproducibility of the method is not as good as an isocratic method, with an unchanging solvent mixture. The chromatographic column determines what kind of chromatography that will occur. This can be partition chromatography, adsorption chromatography, ion-exchange chromatography, size exclusion

chromatography, affinity chromatography or chiral chromatography. Today, it is possible to combine several interaction mechanisms to get a better separation (Skoog et al., 2014).

Phenomenex F5

The column used in this study, Kinetex F5 from Phenomenex, inhabits 5 different interaction mechanisms and core shell technology to separate components of a mixture. These types of columns are relatively universal and can be used on a variety of different mixtures. Figure 6 illustrates the particles used in Kinetex F5.

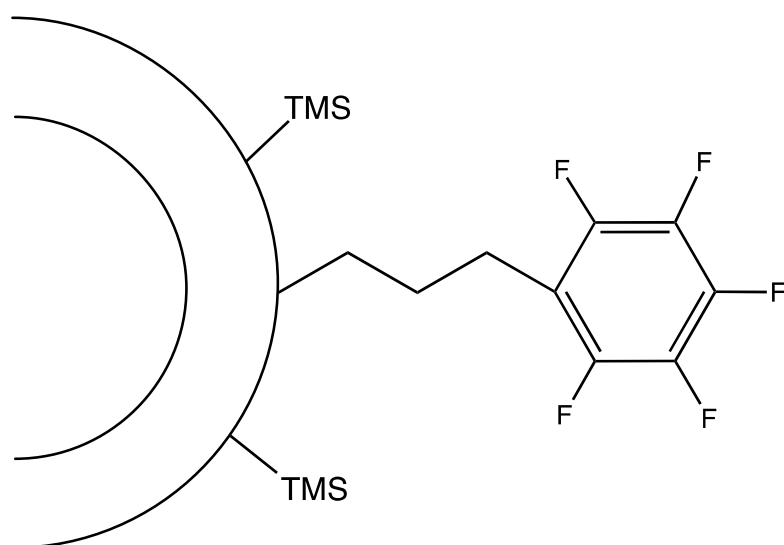


Figure 6: Illustration of a particle used in Kinetex F5. The particle has a solid core and is bound to 1-butyl-2,3,4,5,6-pentafluorobenzene and trimethylsilyl (TMS).

Trimethylsilyl (TMS) is used to derivatise accessible silanol groups on the particle. This is often referred to as endcapping and prevents tailing on the peaks of polar compound. The carbon skeleton of the linker and the ring (Fig. 6) promotes neutral/hydrophobic retention. In non-acetonitrile mobile phases, the π - π -electrons in the ring can interact with the π - π -electrons in the analyte. The electronegativity of the fluorine groups creates dipole moments, promoting polar compound retention. Induced dipole moments can also aid neutral compound retention. Shape selectivity allows the column to do isomeric separations that are otherwise impossible on traditional alkyl phases. When polar functional groups in the analyte interacts with the fluorine, hydrogen bonding will cause effective retention mechanisms (Phenomenex, 2019).

Today HPLC is compatible with different detectors, such as UV, RI, fluorescence and MS. HPLC is carried out using packed columns, usually with a length of 5 to 30 cm and an inside diameter of 1-5 mm. Porous silica particles are the most usual packing material in HPLC columns. These particles can get a variety of coatings and modifications to get different features (Skoog et al., 2014).

Core shell particles

Core shell particles were first reported in the 1960s (Halasz & Horvath, 1964) but did not have a real impact on HPLC separations until after 2006, when the 2,7 μm Halo core-shell particle of Advanced Material Technologies was introduced (Gritti et al., 2007), (Guiochon & Gritti, 2011). Core shell particles comprise of a solid core with a thin and porous external layer (in the range of 0,2-0,7 μm). Today most core-shell particles used in chromatography consist of a porous layer and a core, both made of silica. The core may however be made out of a different material. The particle size, core and shell are adapted to suit different chromatographic methods, and today there is a number of shell particles commercially available. Microscope pictures of different core-shell particles is provided in Figure 7.

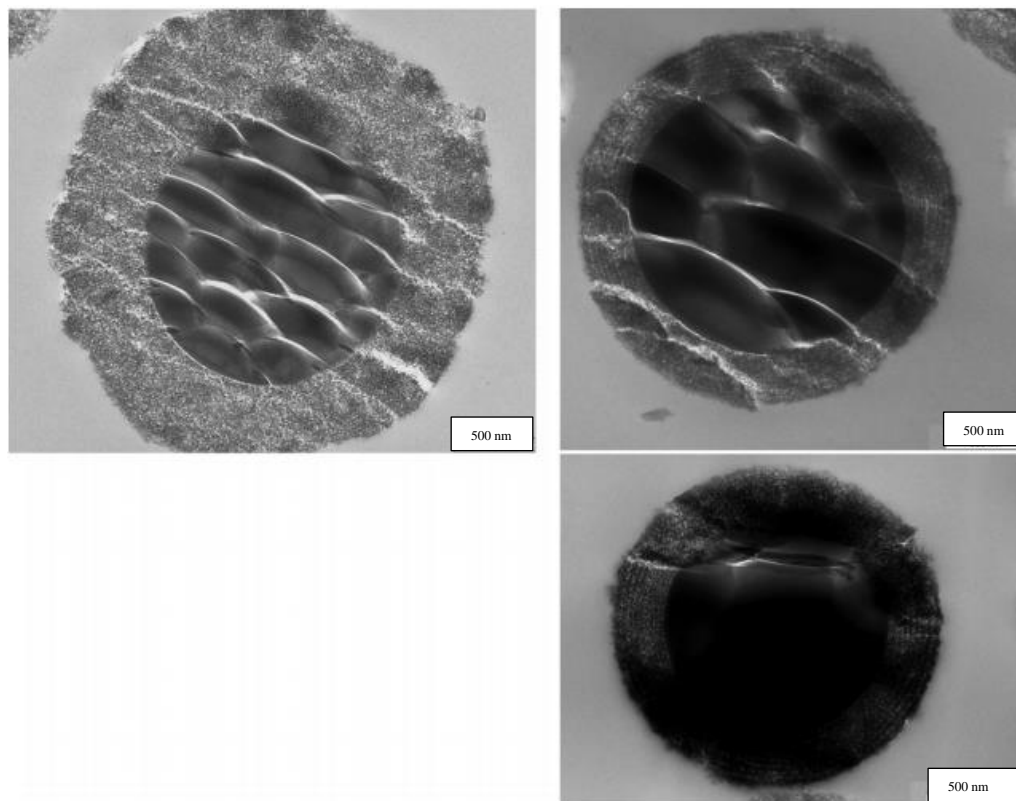


Figure 7: Pictures of core-shell particles taken with a scanning electron microscope (SEM). The top left picture shows a 2,7 μm Halo core-shell particle, the top right picture shows a 2,6 μm Kinetex core-shell particle, and the

bottom right picture shows a 1,7 μm Kinetex core shell particles. Both the Kinetex particles show a layer stratification of the porous shell, revealing that they were made by a layer-by-layer (LbL) approach. Many core-shell particles for chromatography applications are prepared this way. Adopted from (Guiochon & Griitti, 2011).

Core-shell particles are used to increase the efficiency of chromatographic columns. The efficiency of a column is affected by Eddy diffusion, longitudinal diffusion and resistance to mass transfer, which are terms in the van Deemters equation, shown in equation 1.

$$h = A + \frac{B}{v} + Cv \quad (1)$$

h is the plate height, A is Eddy diffusion, v is the mobile phase linear velocity, B is longitudinal diffusion and C is mass transfer.

h in van Deemters equation is used as a measure of efficiency, and the smaller h is, the better is separation. Particles with a solid core have a rougher surface than fully porous particles and are tolerant to shear stress. This gives a better and more homogenous packing, which decrease the value of A . The B term will decrease because the core design reduces the amount of mobile phase in the column. This will reduce the amount of dead volume in the column which gives less longitudinal diffusion. The resistance to mass transfer is reduced by the solid core as the diffusional path of the analytes is limited by the depth of the shell. However, this effect varies with the size of the analytes and is more significant for larger molecules like proteins and oligonucleotides. Compared to fully porous particles, methods using core-shell particles can result in equal separation using lower back-pressure (Hayes et al., 2014).

3.3 Mass Spectrometry

Mass spectrometry is both an individual analytical tool and a chromatographic detector. In mass spectrometry, analyte molecules are ionized and separated according to their mass-to-charge ratio (m/z). A detector converts the number of ions into an electrical signal. By plotting signal strength against m/z , one obtains a mass spectrum. There are several different types of mass spectrometers which vary widely in size, resolution, flexibility and cost. They are however built up of the same components. A mass spectrometer (Fig.8) contains a sample inlet, an ion source, a mass filter and a detector. The inlet introduces the sample to the ion source, where it is transferred to ions by bombardment of high energy electrons, photons, ions or molecules. After ionization, positive or negative gaseous ions will be accelerated into the

mass filter, using a repeller. The mass filter separates the ions based on their m/z value. The results are then collected and converted into electrical signals by the ion transducer. The signal processor, today a data handling system, process the results to make a mass spectrum (Skoog et al., 2014).

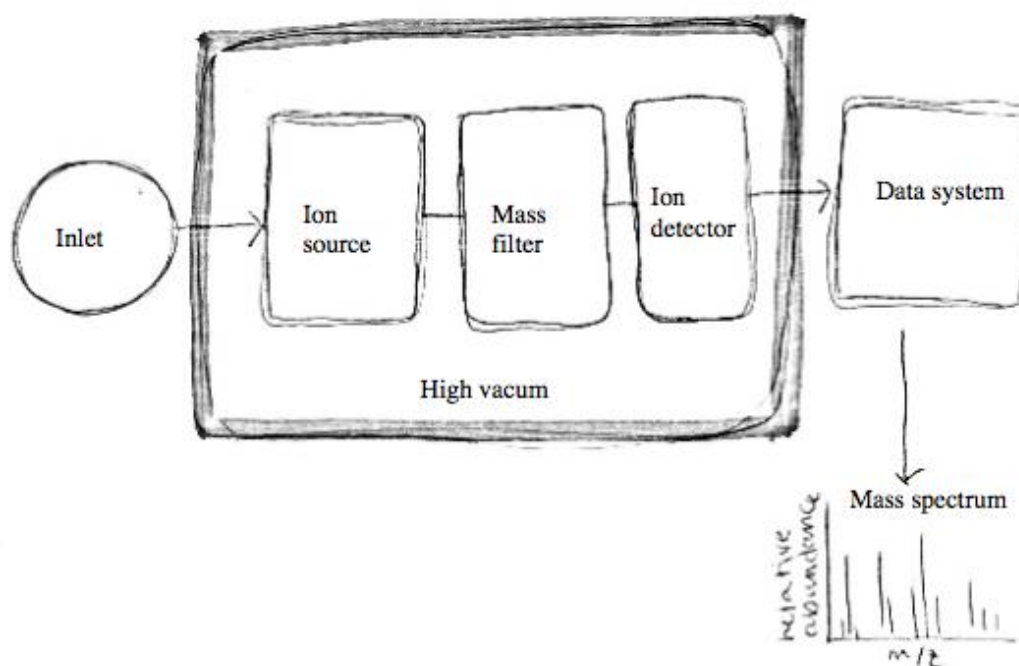


Figure 8: Schematic presentation of a mass spectrometer. The illustration shows the ion source, mass filter and ion detector under high vacuum, as well as the sample inlet and data system. The arrow indicates that the data system will generate a mass spectrum.

3.3.1 Electrospray ionization mass spectrometry, ESI-MS

After the chromatographic separation, the mobile-phase-components are transported to the mass spectrometer for detection. Electrospray ionization (ESI) is a technique that take advantage of electric chemistry to transfer ionic species from the liquid phase to the gaseous phase. The work of John Fenn, Koichi Tanaka and colleagues built the fundament of ESI as we know it today. This also gave them the Nobel prize in chemistry in 2002 (organisation, 2002). Electrospray ionization (Fig. 9) is a relatively universal ionisation technique that can be used on both small inorganic and large organic compounds, like peptides and nucleic acid polymers (Kearle & Tang, 1993). Because of this, ESI have been an important tool in the development of biological analytical chemistry. This technique is the most widely used atmospheric pressure ionization (API) method and is preferred when doing LC-MS.

There are three steps in the formation of charged molecules; the creation of an electrically charged spray, reduction of droplet size by solvent evaporation and release of fully dissolved ions.

A voltage of typically 2-3 kV is applied to a small capillary needle where the elute from the LC is pumped through. There is produced a potential difference between the capillary and the mass spectrometer inlet. Microdroplets are formed from the capillary needle, and the high voltage is producing an aerosol of charged droplets. As the solvent evaporates from the droplets, the charge concentrates at the surface of the droplets due to the decreasing size. When the droplet gets small enough, it will explode when the Columbian repulsion overcomes the droplets surface tension. This creates several smaller, lower charged droplets (Gross & Roepstorff, 2011; Ho et al., 2003),.

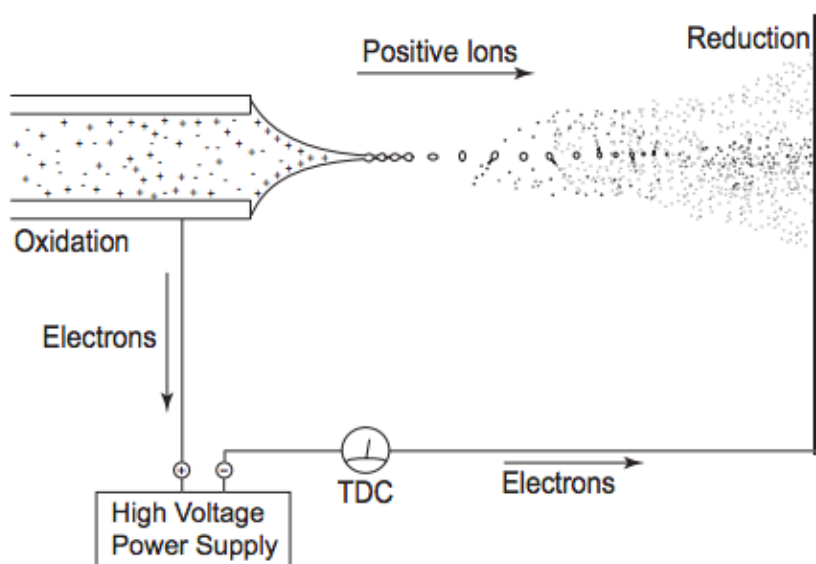


Figure 9: Illustrates the ions in the mobile phase and how they migrate through the capillary needle to form a Taylor cone. Repulsive forces break the cone into small highly charged droplets that eventually will become ions in the gaseous phase. This figure shows the scenario in positive ionization mode. Adopted from (Kearle & Tang, 1993).

3.3.2 Mass filters

A mass filter is the part of a mass spectrometers (Fig. 8) that separates the ions according to their m/z . There are several different mass filters, the ones described in the following sub-chapters are used during this study.

Quadrupole mass filters

The quadrupole mass analyser (Fig.10) is considered a standard instrument in many laboratories, due to their light weight, high transmission, low price, low acceleration voltage and the fact that they allow high scan speed, since scanning is realized by solely sweeping electric potentials ^[13]. In linear quadrupoles, the ions are led into an oscillating electric field situated between four hyperbolic or cylindric rods. The electric field is generated by applying a direct current and an alternating current to the opposite rods. This is combined with a radio frequency (rf) voltage. The rf voltage give the rods the opportunity to oscillate between positive and negative polarities, and this is the basis of the separation in a quadrupole. Only the selected ions, with a specific m/z , will get a stable oscillatory trajectory along the quadrupole. These ions will reach the detector. Ions with different m/z values will acquire unstable oscillation patterns and collide into the rods and be discharged. The desired m/z can be changed by varying the dc and rf voltages (Gross & Roepstorff, 2011), (Rønning, 2017).

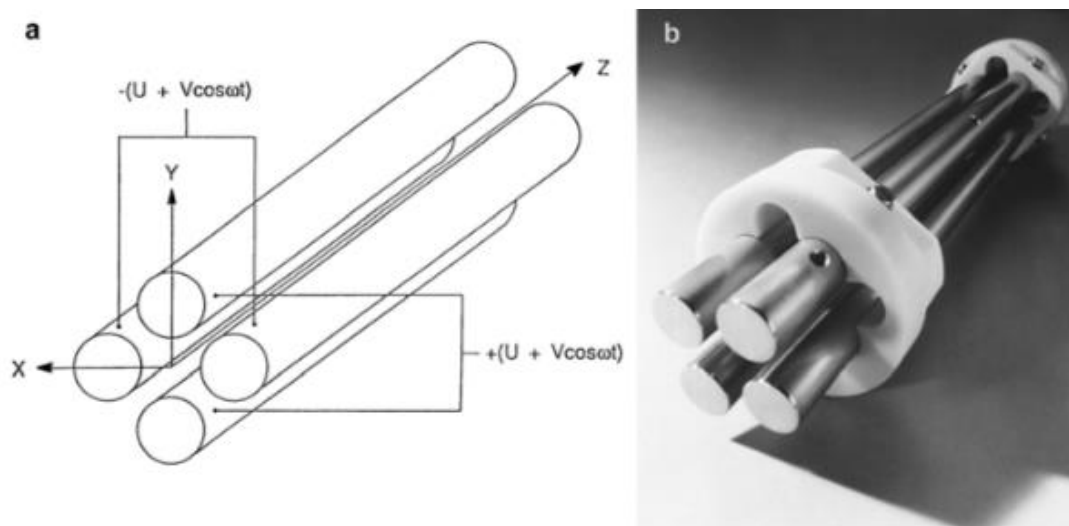


Figure 10: a) schematic drawing of the cylindric rods by courtesy of JEOL, Tokyo, b) a picture of a linear quadrupole by Waters Corp., MS Technologies, Manchester, UK. Adopted from (Gross & Roepstorff, 2011).

Ion trap mass filters

Ion traps (Fig. 11) separate different m/z values based on the behaviour of ions in an electric field (similar to quadrupoles). Ion traps also take advantage of a direct current and an alternating current in a radio frequency field. The ions will gain either stable or unstable oscillations based on their m/z . Unlike the quadrupoles, the ion trap detects the ions with unstable oscillations.

The ions are led into the ion trap and are ionized using electric or chemical ionization. When setting up the oscillating electric field, the ions will get stable or unstable oscillations based on their m/z . Ions with unstable oscillations, will be kicked out of the ion trap through source slits. The ions are then received by a detector.

There are two different ion traps. 3D- ion traps and linear quadrupole ion traps (Rønning, 2017).

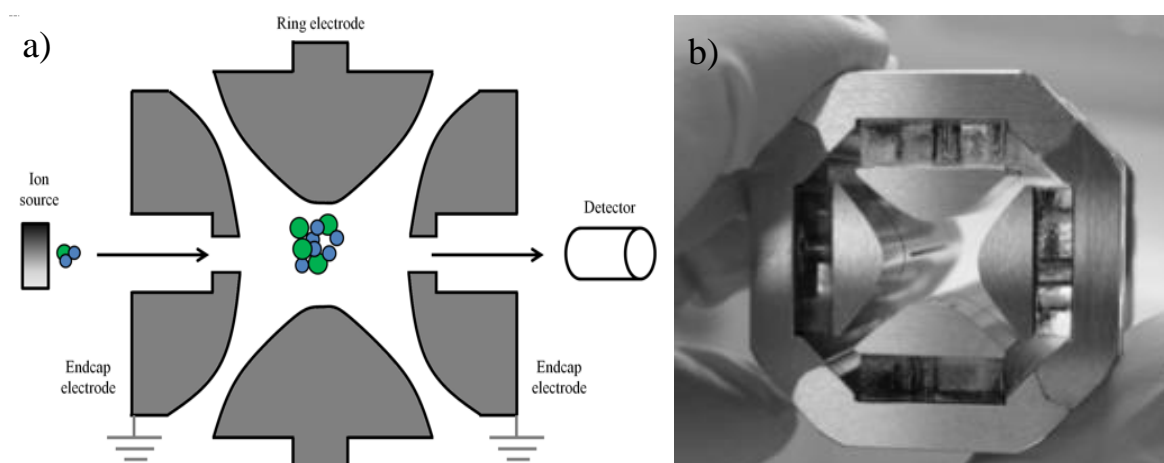


Figure 11: a) cross section of an ion trap. The illustration shows that the ions enter the entrance endcap electrode and get caught in the ring electrode. Ions with unstable oscillations will be let out through the exit endcap electrode. Adopted from (National Programme on Technology Enhanced Learning) b) picture of an LTQ ion trap. Adopted from (Mass Spectrometry Geekery, 2012)

Orbitrap mass filters

Orbitrap mass filters (Fig. 12) are relatively new constructions. These are electronic ion traps made of a spindle-shaped inner central electrode and a split outer electrode, separated with a dielectric ring. After the ions are injected into the orbitrap, they are collected in a C-trap. The ions will then be transferred to the orbitrap in packages with a high speed. In the orbitrap, the ions will acquire a stable circular movement back and forth along an inner central electrode. The oscillatory motion of the ions induces a transient current

in the split outer electrode. Because the periodicity of the axial oscillation is proportional to the m/z , Fourier transformation of the measured current gives the individual oscillation frequencies, and the ions m/z . Due to this trait, there is no need for an external detector when using an orbitrap mass analyser (John Gravas, 2013). Orbitraps are high-resolution mass filters, meaning that they produce more narrow peaks due to better peak separation than for instance an ion trap mass filter.

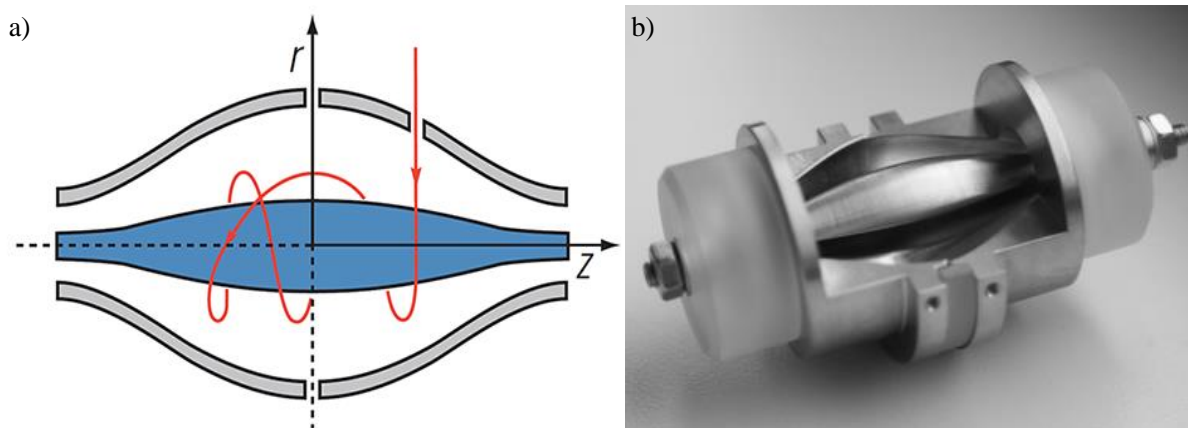


Figure 12: a) cross section of an orbitrap mass analyser. The figure shows the inner central electrode surrounded by a line with arrows, illustrating the orbitrap path of the ions. Adopted from (*Orbitrap mass analyzer*). b) picture of an orbitrap. Adopted from (*Orbitrap mass analyzer*, 2012).

3.3.3 Detectors used in mass spectrometry

Detectors are used in mass spectrometry analysis to convert an electric current to a readable signal in the form of a mass spectrum. The orbitrap is an example of an instrument where mass analysis and detection are performed at the same time. Mass spectrometers containing this type of mass analysers do not need an ion detector. The most used detector constructions are electron multipliers and photomultipliers.

3.3.4 Tandem mass spectrometry

Tandem mass spectrometry, also known as MS/MS or MS², is the name of a technique where more than one step of mass analysis is used for the detection of specific ions. Tandem MS is divided into two categories; tandem MS in time and tandem MS in space. In-time instruments perform MS/MS by using the same mass filter more than one time. Instruments designed to do tandem MS in space perform several steps of mass analysis using more than one mass filter. Ion traps are examples of tandem-in-time instruments, while an orbitrap-quadrupoles are examples of tandem-in-space instrument (Gross & Roepstorff, 2011).

Tandem MS in space is typically conducted by isolating a precursor ion which fragments further, either spontaneously or by activation from an inert gas. The fragmentation is usually carried out between the mass filters. This can be done in field free regions (where fragmentation happens spontaneously) or in collision cells with inert gas. Fragmentation of the precursor ion gives product ions and neutral fragments. Tandem mass spectrometry can be applied for experimental purposes and during structure elucidation. During studies of microcystins it is common to use different acquisition modes for confirmation of masses and in the search for new structural isoforms. All ion fragmentation is an acquisition mode that often is used for targeting characteristic parts of the molecule. In this acquisition, all precursor ions are fragmented without a pre-selection. Adda⁵ or DMAdda⁵ give characteristic fragments at m/z 135.0804 or m/z 121.0647 in positive mode. When a precursor includes one of these fragments, it's highly possible that it is a microcystin. One can gain this information by opening an extracted ion chromatogram in the range 135.0804 or 121.0647. The structure of Adda and DMAdda is shown in Table 3 (Gross & Roepstorff, 2011). Another scanning mode that is widely used, is selected ion monitoring (SIM). In this acquisition mode, the instrument only acquires information about selected ions. This leaves more detector time to ions with a m/z of interest and thus increase the sensitivity. Data-dependent acquisition (DDA) is an acquisition mode where a selected number of precursor ions are fragmented and analysed in a second mass filter. Data independent acquisition is a scanning mode that practice sequential isolation and fragmentation in an optional precursor window. Several precursor windows may be added until the desired mass range is covered (John et al., 2004).

3.4 Thiol derivatisation for Mdha7/Dhb7 differentiation

Mdha and Dhb (Table 3) are two amino acids that can be found in position 7 in the microcystin structure (Fig. mc). These amino acids both have a m/z of 1001.1050, and have thus been challenging to separate on LC-MS.

Miles and co-workers have developed a method to distinguish between microcystins containing Mdha or Dhb in position 7 of the microcystin heptapeptide (Miles et al., 2012; Miles et al., 2013). The method is based on derivatisation of the microcystins with a suitable thiol, making the differentiation of the two groups easier. Figure 13 shows an example of a thiol derivatisation (using mercaptoethanol) with Mdha versus Dhb.

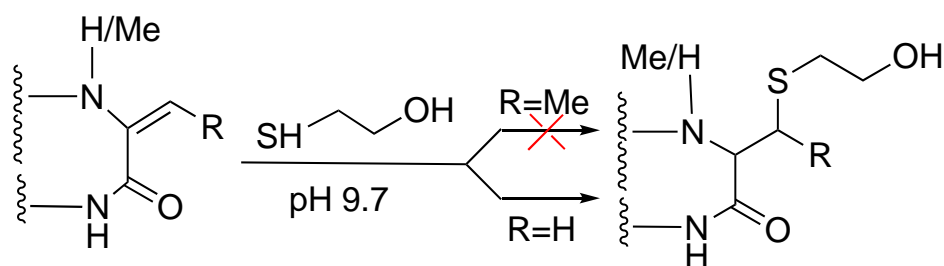


Figure 13: Derivatisation of Mdha/Dhb in position 7 with mercaptoethanol under basic conditions. The arrow with a red cross show that the reaction will not happen instantly when having a methylated R-group in position 7 of the microcystin structure. This methylation is associated with the amino acid Dhb. Adopted from (Miles et al., 2013)

Reactions as the example shown in Figure 13, happens because the α - β unsaturated alkene in amides are reactive towards thiol. Miles and co-workers showed that [Mdha⁷]-congeners reacted several hundred-folds faster with mercaptoethanol than the [Dhb⁷] containing microcystines, due to the extra methyl group in Dhb.

When using mercaptoethanol as the selected thiol, like in figure 13, the microcystins will gain a mass of 78,0134 amu (Miles et al., 2012; Miles et al., 2013). Only microcystins containing Mdha in position 7 will be observed with this addition of mass. In extracted ion chromatograms, it is therefore possible to observe a decrease in peak area corresponding to the microcystin and an increase in peak area of the conjugated microcystin, when the reaction occurs.

3.5 Enzyme linked immunosorbent assay

The enzyme linked immunosorbent assay (ELISA) is an analytical biochemistry assay that can detect analytes based on an enzymatic response through recognition and binding of antibodies.

Antibodies, or Immunoglobulins (Igs), are proteins made by the immune system to protect against foreign substances, antigens, like viruses, fungi, bacteria, food allergens or cancer cells. Antigens can be defined as the elements causing an immune response (Hosseini, 2018). The technology of ELISA takes advantage of this recognition system for both research and applied purposes. With the use of relevant enzyme substrates, it is possible to cause a colour change that is proportional to the concentration of the analyte of interest. This colour change (Fig. 14) can be quantified using specially designed spectrometers. ELISA is a highly

sensitive method that makes it possible to do a rapid analysis of a large numbers of samples (Crowther, 1995).

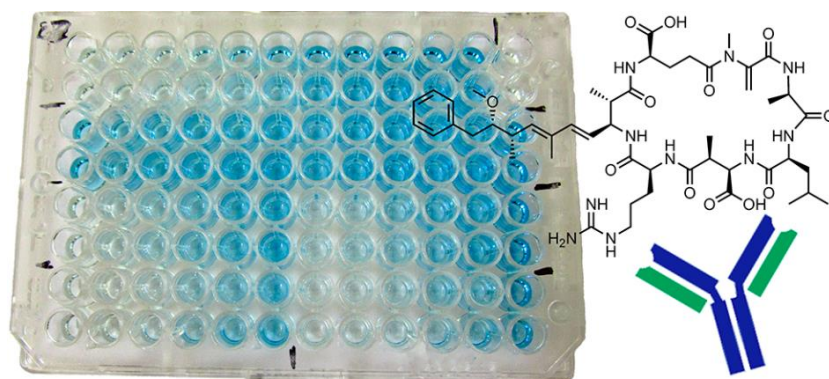


Figure 14: ELISA plate after after addition of the colourless chemical producing the blue colour, a microcystin structure and an antibody. Adopted from (Samdal et al., 2014)

Because LC–MS require expensive instrumentation and trained operators, it is essential to have an alternative detection method for microcystins. Especially for use in developing countries where bloom forming cyanobacteria often occur more frequently.

A new competitive ELISA was developed by Samdal et al. (2014), with an aim to include as many microcystins as possible in a single analysis. The antibody used in this method was developed to recognize the general cyclic peptide structure of the microcystins and nodularins. This ELISA hence has a high cross-reactivity, which means that it can recognize many different analogs with equal response. This results in broad specificity and good sensitivity, and is therefore a valuable tool for measuring the total content of microcystins and nodularins in a sample (Samdal et al., 2014).

3.6 Method validation

Method validation determines the suitability of the analysis used for obtaining a specific result. Validation can be done by the analyst, but can also be performed by supervisory personnel. Requirements in standards, such as ISO/IEC 17025, ISO 15189 and ISO 15195 have helped to clarify the need to demonstrate that methods are fit for purpose. There are a number of different ways to validate an analytical method. The most common are; analysis of standard reference materials, analysis performed using a different analytical method, estimation of the loss of analyte (spike recovery) and analysis of synthetic samples resembling the composition of the test sample (Örnemark, 2014),.

3.6.1 Blank samples

Blank samples are used to estimate how much of the measured signal is caused by the analyte and how much of the signal is caused by noise or contamination. If the signal caused by contamination of the blank sample is significant and over LOQ, it can be subtracted from the analytical result. Various types of blanks can be used for this purpose. Reagent blanks are treated similar to the analytical samples during sample preparation and are being analysed to decide if the reagents are contributing to the signal of measurement. Sample blanks consist of sample matrices with no analyte present. These blanks are analysed to estimate the presence of interferences in the matrix. In the context of HPLC–MS, the reagent blanks also decrease the carry-over from the previous sample (Skoog et al., 2014; Örnemark, 2014).

3.6.2 Standards

Standards are substances with a specific known concentration. Standards may be used to calibrate an analytical instrument, like a LC–MS, or to make calibration curves for quantitative analysis. This is not necessarily the same standard. Standards are often referred to as reference materials (RMs). Reference materials can be any material used as a basis for reference. Certified reference materials (CRMs) is something significantly different, both in the way they are used and how they are characterised. Certified reference materials require metrological traceability, uncertainty and documentation. When using a CRM with the same matrix and concentration in the same region as the samples, it is possible to estimate the bias (Örnemark, 2014).

3.6.3 LOD and LOQ

The limit of detection (LOD) refers to the lowest quantity of analyte that can be detected in a sample, with a given level of confidence. The quantification limit (LOQ) is the smallest amount of analyte which can be quantified, with a given level of confidence. These limits have to be decided experimentally. Some common methods for detecting the LOD and LOQ are visual definition, calculation from signal-to-noise ratio, calculation from the standard deviation (SD) of the blank and calculation from the calibration line at low concentrations (Vial & Jardy, 1999). When the method does not involve background noise, a way to obtain the LOD and LOQ is through linear regression. When using this method, LOD and LOQ will be expressed as follows:

$$\text{LOD}=3S_a/b \quad (2)$$

$$\text{LOQ}=10 S_a/b \quad (3)$$

In equation 2 and 3, S_a is the SD of the response and b is the slope of the calibration curve. S_a may be estimated by the standard deviation of the y-residuals or y-intercepts of regression lines.

3.6.4 Spike recovery

When the analyte of interest is part of a complex matrix, the matrix material can interfere with the analyte and cause a decrease or increase in response. The sample preparation may also include steps that can lead to loss of analyte, such as extraction or filtration. For instance, the analyte can remain in the matrix after extraction or it can adsorb to the surface of equipment used during sample preparation. These factors can cause significant inconsistencies between laboratories due to different practices and lack of general guidelines (Thompson et al., 1999), (Örnemark, 2014).

Methods for estimating the loss of analyte includes reference materials, isotope dilution, internal standard and spiking (spike recovery). Spiking is one of the most widely used methods to gain information about recovery. This approach is cost efficient compared to the other methods and particularly easy to use if there is a matrix blank available (a matrix sample that does not contain any analyte). When the spiked sample is prepared and analysed in the same way as the other samples, the recovery of the analyte could be estimated (Thompson et al., 1999).

4. Material and methods

4.1 Chemicals and reference materials

Microcystin ([Asp³]MC-RR, MC-LF, MC-LY, MC-LA, [D-Asp³]MC-LR, MC-YR, MC-RR) and Nodularin-R (NOD-R) were purchased from Enzo Life Sciences, Inc., Farmingdale, NY, USA. NMR-quantitated standards (certified reference materials) of [Asp³]MC-LR and [Asp³, Dhb⁷]MC-RR were obtained from The National Research Council of Canada (NRC, Halifax, NS, Canada). Anabaenopeptins (anabaenopeptin A, anabaenopeptin B and oscillamide Y)

were purchased from Enzo Life Science. Mercaptoethanol was purchased from Sigma-Aldrich, (St. Louis, MO, USA. Methanol, acetonitrile and water of Optima LC–MS grade was used for mobile phases during the study, all purchased from Thermo Fisher Scientific (Waltham, MA, USA). Methanol for sample extraction was of HPLC quality (Romil, Cambridge, UK). Formic acid was of p.a. quality and purchased from Merck (Darmstadt, Germany). A microcystin-producing *Planktothrix rubescence* culture (NIVA-CYA98) was provided by The Norwegian Institute for Water Research (NIVA). The culture was grown in a Z8 medium⁶ with a light/dark cycle of 16 h/8 h at ca. 20 °C. A large scale culture of NIVA-CYA98 was freeze-dried at NIVA and provided for experiments at The Norwegian Veterinary Institute (NVI)

4.2 Exposure of crayfish to NIVA CYA-98

Adult noble crayfish were divided into three treatment groups and held separated from each other during the feeding trial. Group one received food pellets made from a mixture of ground shrimp, peas and agar, spiked with freeze-dried biomaterial from NIVA-CYA98. This group was held in boxes containing normal tap water. Group two received food pellets made from a mixture of ground shrimp, peas and agar without added NIVA-CYA98. However, the water in the boxes containing these crayfish was spiked with NIVA-CYA98.

Group three served as control group and received the same food as group 2, consisting of pellets made from a mixture of ground shrimp, peas and agar. This group were held in boxes containing normal tap water.

A total of 108 crayfish were used in the feeding trial, randomly distributed into one of the three groups. Hence each treatment group consisted of 36 individuals. Per group, all individuals were kept in boxes of four, totalling nine boxes per treatment group.

The experiment was carried out throughout a period of 6 weeks. Each week, 6 crayfish were removed from each treatment group. The selection of these crayfish was made through randomisation before the experiment was conducted. An illustration and a picture from the feeding trial are shown in Figure 15.

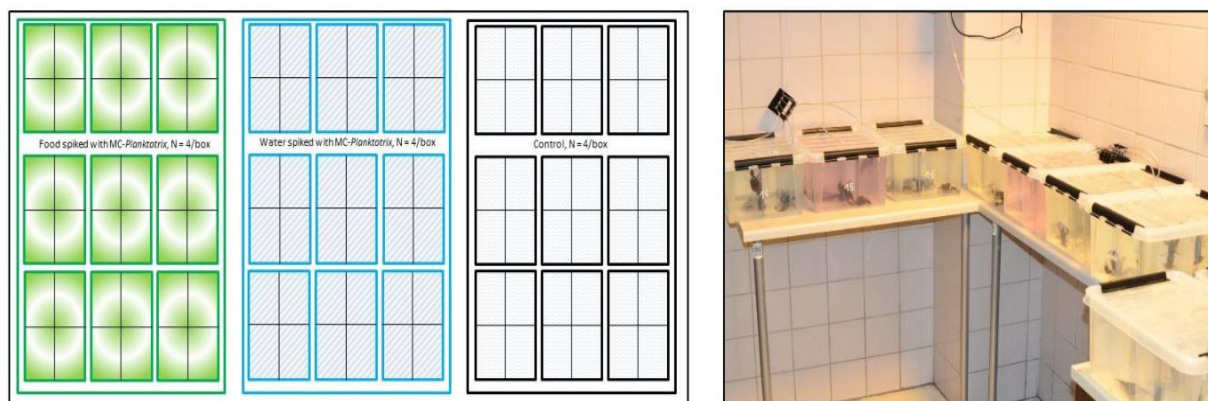


Figure 15: Experimental set-up to the left, with green boxes representing crayfish receiving food spiked with *P. Rubescens* biomaterial, blue boxes representing crayfish living in water spiked with *P. Rubescens* biomaterial, and white boxes representing the control group. The picture to the right shows the experimental facility.

4.3 Cyanobacterial sample and sample preparation

Freeze-dried NIVA-CYA98 (0.0976 g) was weight into an 8 mL glass vial and 8.0 mL of MeOH/H₂O (1:1 v/v). The sample was sonicated for 5 minutes and placed on a sample tray for 40 minutes. The sample was stored in the freezer overnight. An aliquot of the supernatant (ca 1 mL) and filtered (Spin X Micro-centrifuge, 0,22 µm, Costar Inc., Corning, NY, USA). Dilutions of 1:10, 1:100 and 1:100 were prepared by adding the appropriate amount of methanol/water (1:1). All extracts were stored in -20 °C.

4.4 Crayfish samples and sample preparation

Crayfish that were removed from the experiment were put in a freezer of -80 °C for euthanisation. After thawing the crayfish, tissue from gills, hepatopancreas, stomach, muscle and intestine were transferred to centrifuge tubes before further preparation. Only tissue from muscle and hepatopancreas was analysed during this study. For ELISA analysis, methanol was added to the crayfish sample (9 times the wet weight of the crayfish tissue in mL), followed by homogenization with an Ultra-Turrax T25, (Janke and Kunkel, Staufen im Breisgau, Germany). Crayfish samples and extracts were stored at -20 °C until processing and/or analysis. After homogenization, the mixture was allowed to sediment and approximately 1 mL of the supernatant was filtered (Spin-X centrifuge tubes, 0,22 µm, 5 min, 5000 rpm). The filtered sample was transferred to a chromatography vial and stored at -20 °C until analysis by LC-MS. Figure 16 shows pictures of crayfish before and during dissection.



Figure 16: European noble crayfish (*A. Astacus*) before and during dissection.

4.5 Liquid chromatography

Liquid chromatography was performed on a $150 \times 2,1$ mm i.d Kinetex F5 column (2,5 μ m particle size, Phenomenex, Torrance, CA, USA), either using a Waters Acquity UPLC pump and autosampler (Milford, MA, USA) or a Dionex Ultimate RS3000 UHPLC pump and autosampler (Thermo Fisher Scientific) in connection with ion-trap mass spectrometry, or a Vanquish Horizon UHPLC pump and autosampler (Thermo Fisher Scientific) in connection with high-resolution mass spectrometry.

Two methods, with different mobile phase gradients (Appendix B, Fig. B1-B2) were used during the study.

Gradient 1: (t in min): t_0 , B=30%; t_{15} , B=50%; $t_{15,5}$, B=100%; $t_{17,5}$, B=100%; t_{18} , B=30%, total run time; 20,5 min.

Gradient 2: t_0 , B=15%; t_{15} , B=40%; $t_{15,5}$, B=100%; $t_{17,5}$, B=100%; t_{18} , B=15%, total run time; 20,5 min.

Mobile phase A consisted of 0,01% (V/V) formic acid in H₂O and mobile phase B consisted of 0,01% (V/V) formic acid in Acetonitrile.

4.6 Ion-trap mass spectrometry analyses

All ion-trap mass spectrometry analyses were conducted using *gradient 1*. The ion-trap mass spectrometer used was a Thermo Fisher Scientific LTQ. The mass spectrometer was equipped with an electrospray ionization interface, operated in positive ion mode. The mass analyser was scanned in the mass range m/z 400-1500 during full-scan analyses. MS² spectra of microcystins were acquired by selecting the [M+H]⁺ ions of target microcystins and using two scan segments of two MS² scan events each. LC-MS¹ and LC-MS² were done separately to give more scans/peak. During MS², the isolation width was 2.0 m/z and the normalized collision energy (NCE) was 35%. The Activation Q was 0.250 and the activation time was 30 ms. Important interface parameters included a source voltage of +3.50 kV (-4.5 kV for negative ionization mode), a capillary temperature of 275 °C, a sheat gas flow of 45 units and an auxiliary gas flow of 27 units.

Ion-trap mass spectrometry analyses of anabaenopeptins other than microcystins was performed using an LCQ Fleet ion trap mass spectrometer (Thermo Fisher Scientific), equipped with an electrospray ionization interface. Important interface parameters included a source voltage of +3.50 kV (-4.5 kV for negative ionization mode), a capillary temperature of 270 °C, a sheat gas flow of 45 units and an auxiliary gas flow of 27 units. The mass spectrometer was operated in both positive and negative ionization mode in the mass range m/z 200-1200. For LC-MS², the [M+H]⁺ ions of anabaenopeptin A, anabaenopeptin B and oscillamide Y were selected in segmented analyses using an isolation width of 2.0 m/z and a normalized collision energy (NCE) of 35%. The Activation Q was 0.250 and the activation time was 30 ms.

4.7 High-resolution mass spectrometry (HRMS) analyses

The instrument used was a Q-Exactive high-resolution mass spectrometer (Thermo Fisher Scientific), equipped with a heated electrospray interface. Full-MS and HRMS/MS data were acquired for microcystins and other cyanopeptides in the NIVA-CYA98 extract, both in positive and negative ion mode mode. *Gradient 1* was used for LC-HRMS and HRMS/MS of the cyanobacterial extract. For FullMS analyses of the cyanobacterial extract, the mass spectrometer was scanned in the mass range m/z 500.0000-1200.0000 (positive mode) and m/z 800.0000-1200.0000 (negative mode). Other important instrumental settings included mass

resolution 70,000, AGC target 3×10^6 , maximum ion inject time 250 ms, sheat and auxillary gas flow at 35 and 10 units N_2 , a spray voltage of 3.20 kV, transfer capillary temperature 280 °C, S-lens RF level 55 and auxillary gas heater temperature of 300 °C.

Crayfish samples were analysed with *Gradient 2*.

4.7.1. HRMS/MS of microcystins using a mixed MC standard

High resolution tandem mass spectrometry was performed on the same column as described in section 4.5 and the same LC–MS system and with *Gradient 1*. The 1:100 and 1:1000 dilutions of NIVA CYA-98 were analysed with calibration standards containing the microcystins [Asp³]MC-RR, MC-LF, MC-LY, MC-LA, [D-Asp³]MC-LR, MC-YR, NOD-R and MC-RR. The calibration standards had the following concentrations: 0.01 ng/mL, 0.04 ng/mL, 0.06 ng/mL, 0.08 ng/mL 0.1 ng/mL, 1.0 ng/mL, 50 ng/mL, 100 ng/mL, 150 ng/mL and 200 ng/mL and were dissolved in MeOH-H₂O (1:1).

4.7.2 HRMS/MS screening for microcystins

The extract of NIVA-CYA98 was analysed using Full MS–AIF (all-ion-fragmentation). FullMS was performed as described in sub-chapter 4.7. AIF was scanned in the mass range m/z 500.0000-1200.0000 with a mass resolution of 35,000, ACG target 3×10^6 , maximum ion injection time 200 ms, a normalized collision energy of 35%. The m/z 135.0804 was used to extract microcystins from HRMS/MS chromatograms. Data independent analysis (DIA) was performed using a resolution of 17,500, ACG target 2×10^5 , maximum ion injection time was set to auto, an isolation window of 62.0 m/z , a fixed first mass of 120.0 m/z and a stepped collision energy of 30, 60 and 80 kV. Data dependent MS² (ddMS²) was done using a resolution of 17,500, ACG target 1×10^5 , maximum ion injection time 50 ms, a loop count and TopN of 5, an isolation window of 2.0 m/z and a normalized collision energy of 75 kV. dd settings included a minimum AGC t. of 8.00×10^3 , intensisty thresh 1.6×10^5 , Apex trigger 1 to 2 s and dynamic exclus on 30.0 s.

4.7.3 Parallel reaction monitoring

HRMS/MS spectra of putative microcystins as well as anabaenopeptins A and B and Oscillamide Y were acquired using parallel reaction monitoring (PRM). The inclusion list contained the $[M + H]^+$ and $[M + H]^-$ ions for microcystins and other cyanopeptides.

Instrumental settings for PRM included a mass resolution of 17500, ACG target of 2×10^5 , a maximum injection time of 200 ms and an isolation window of 2,0 m/z. The analysis was done one time using a normalized collision energy (NCE) of 35% and one time using a stepped collision energy of 30, 60 and 80 eV. This analysis was performed on a 100 ng/mL mixed standard solution of anabaenopeptin A, anabaenopeptin B, oscillamide Y, [D-Asp³, Dhb⁷]MC-RR and [D-Asp³]MC-LR and an undiluted sample the NIVA-CYA98 extract.

4.8. β -mercaptoethanol derivatisation for Mdha⁷/Dhb⁷ differentiation

Sodium carbonate buffer (0.2 M, pH 9,41) was added (50 μ L) to the microcystin standard mixture (100 μ L, 100 ng/mL) and to the NIVA-CYA98 extract (100 μ L, 1:100 dilution). The samples were tempered to 25 °C in the autosampler before mercaptoethanol (1.0 μ L) was added to two aliquots of the buffered solutions. The mixture was vortexed before analysis by LC-MS. The underivatised (i.e., no thiol addition) aliquots were used as controls. The reaction was performed on the standard solution containing [D-Asp³]MC-RR, MC-LF, MC-LY, MC-LA, [D-Asp³]MC-LR, MC-YR, NOD-R and MC-RR, as well as NIVA-CYA98. The sample of NIVA-CYA98 was stored in a fume cabinet for one month to observe the reaction over time.

4.9 Correction of concentration of [D-Asp³]MC-LR and [Asp³]MC-RR standards

The concentrations of the standards were adjusted using NMR-quantitated standards of [Asp³]MC-LR and [Asp³, Dhb⁷]MC-RR from NRC, Halifax, NS, Canada. New calibration curves were prepared with NRC standards. The previously used standards of [Asp³]MC-LR and [Asp³]MC-RR from Enzo Life Sciences were treated as samples and analysed with the new calibration curves. The concentration of [Asp³, Dhb⁷]MC-LR and [Asp³, Dhb⁷]MC-RR was then corrected according to the NRC standards.

4.10 Microcystin and anabaenopeptin quantification using liquid chromatography – high resolution mass spectrometry

Mixed standards containing anabaenopeptin B, anabaenopeptin A, oscillamide Y, [D-Asp³]MC-RR and [D-Asp³]MC-LR were prepared with the following concentrations 0.1 ng/mL, 0.5 ng/mL, 1 ng/mL, 5 ng/mL, 15 ng/mL, 25 ng/mL, 50 ng/mL and 100 ng/mL.

Matrix-matched crayfish samples of muscle and hepatopancreas tissue were prepared by adding 200 μL of the mixed standard solution to chromatography vials, evaporating them to dryness (with N_2) and adding 200 μL of crayfish extract from the control group.

High resolution mass spectrometry was performed on the column described in sub-chapter 4.5 with *Gradient 2*. The instrument operated in full MS positive ion mode with the settings described in section 3.7.

4.11 Evaluation of method performance

The following sub-chapters describes the tools used to validate the method performance of the analyses in the study.

4.11.1. Spike recovery

Frozen crayfish were taken from $-80\text{ }^\circ\text{C}$ and thawed in room temperature. Muscle and hepatopancreas tissue were weighted into centrifuge tubes and 25 μL of 1 $\mu\text{g}/\text{mL}$ mixed standard solution of microcystins and anabaenopeptins were added to the spike samples. Control samples were not spiked. All centrifuge tubes were stored in the fridge overnight. The next day a volume (mL) of H_2O -MeOH (1:1), nine times the wet weight of the tissue, were added to all centrifuge tubes. The samples were subsequently homogenized using an Ultra-Turrax T25, (Janke and Kunkel, Staufen im Breisgau, Germany), filtrated (Spin X Micro-centrifuge, 0,22 μm , Costar Inc., Corning, NY, USA) and transferred to chromatography vials. The homogenizer was rinsed with methanol and methanol/water (1:1) in between individual extractions. Sample extracts were stored in the freezer at $-20\text{ }^\circ\text{C}$ until analyses by LC-MS.

3.11.2. Precision and limits of detection and quantification

Standard calibration curves were acquired from blank standards, prepared in methanol/water (1:1), and matrix-matched standards (muscle and hepatopancreas). Linearity was obtained using linear regression analysis. The precision (repeatability and reproducibility) was assessed by repeated analysis of the same sample on six different days (inter-day precision) (Ivanova et al., 2017).

The limit of detection (LOD) and limit of quantification (LOQ) were calculated for each peptide. The calculations were based on the SD of 8 (muscle) and 7 (hepatopancreas) experiments) of the y-intercept of the respective regression line and its corresponding slope(s). The following equations were used; $LOD=3SD/s$ and $LOQ=10SD/s$ (Ivanova et al., 2017).

4.11.3. Signal suppression and enhancement (SSE)

Signal suppression and enhancement (SSE) due to coeluting matrix components was evaluated for each analyte and defined as the slope of the matrix-matched standard calibration curve divided by the slope of the corresponding standard calibration curve in solvent. The SSEs were calculated in percentages. Numbers 100% indicated matrix enhancement.

4.12 Calculations and statistical analysis

Xcalibur 2.2 software was used for instrument control and data evaluation (Thermo Fisher Scientific), while version 4.2 was used for data processing (integration and quantification). Qualbrowser, a module within Xcalibur, was used to calculate the molecular formulae and the mass error of the target compounds, while Quanbrowser was used for quantification.

Microsoft Excel (Redmond, WA, USA) was used for basic statistics.

5. Results and discussions

The following sub-chapters presents results and discussion of

- 1) characterization of microcystins and other cyanopeptides in NIVA-CYA98 (used in crayfish feed)
- 2) quantification of microcystins and other cyanopeptides in hepatopancreas and muscle samples from crayfish

The gradient profile in the LC–MS method was changed during the study to obtain better separation between anabaenopeptin B (1.7 min) and oxygenated [D-Asp³, Dhb⁷¹]MC-RR (1.8 min). Though the latter turned out to not be detectable in crayfish tissue, the results show NIVA-CYA98 analysed with *Gradient 1* and crayfish samples analysed with *Gradient 2*. The other cyanopeptides are all in the group anabaenopeptins. They are thus referred to as both cyanopeptides and anabaenopeptins.

5.1 LC – HRMS of microcystins

Microcystins (MCs) are major hepatotoxic peptides that are produced by *Planktothrix rubescens* and other cyanobacteria. Previous studies on *P. rubescens* have shown that NIVA-CYA98 is a MC-producing strain (Rohrlack et al., 2008). A working standard mixture of nine MCs and nodularin (NOD-R) was prepared in methanol/water (1:1) and used for initial training.

Extracted ion chromatograms using the $[M+H]^+$ or $[M+2H]^{2+}$ ions for individual MCs or NOD-R resulted in linear calibration curves with $R^2 > 99$ (Appendix F, Fig. F1) The chromatograms (Fig. 17-18) showed good separation and peaks of acceptable shape.

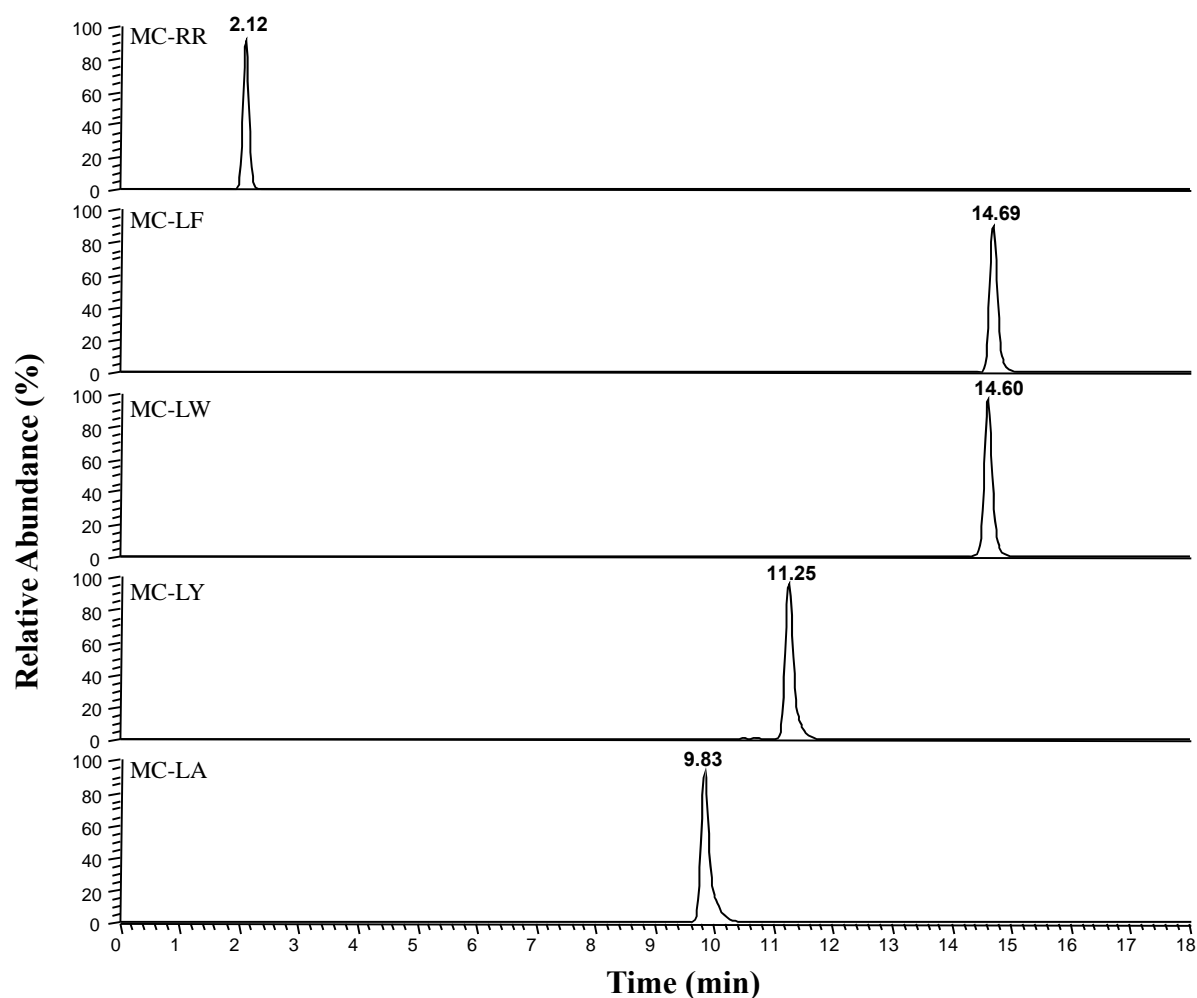


Figure 17: chromatograms of MC-RR, MC-LF, MC-LW, MC-LY and MC-LA in the mixed standard solution, 200 ng/mL. Relative abundance (%) on y-axis and time on x-axis. Retentiontime (in minutes) shown above the peaks.

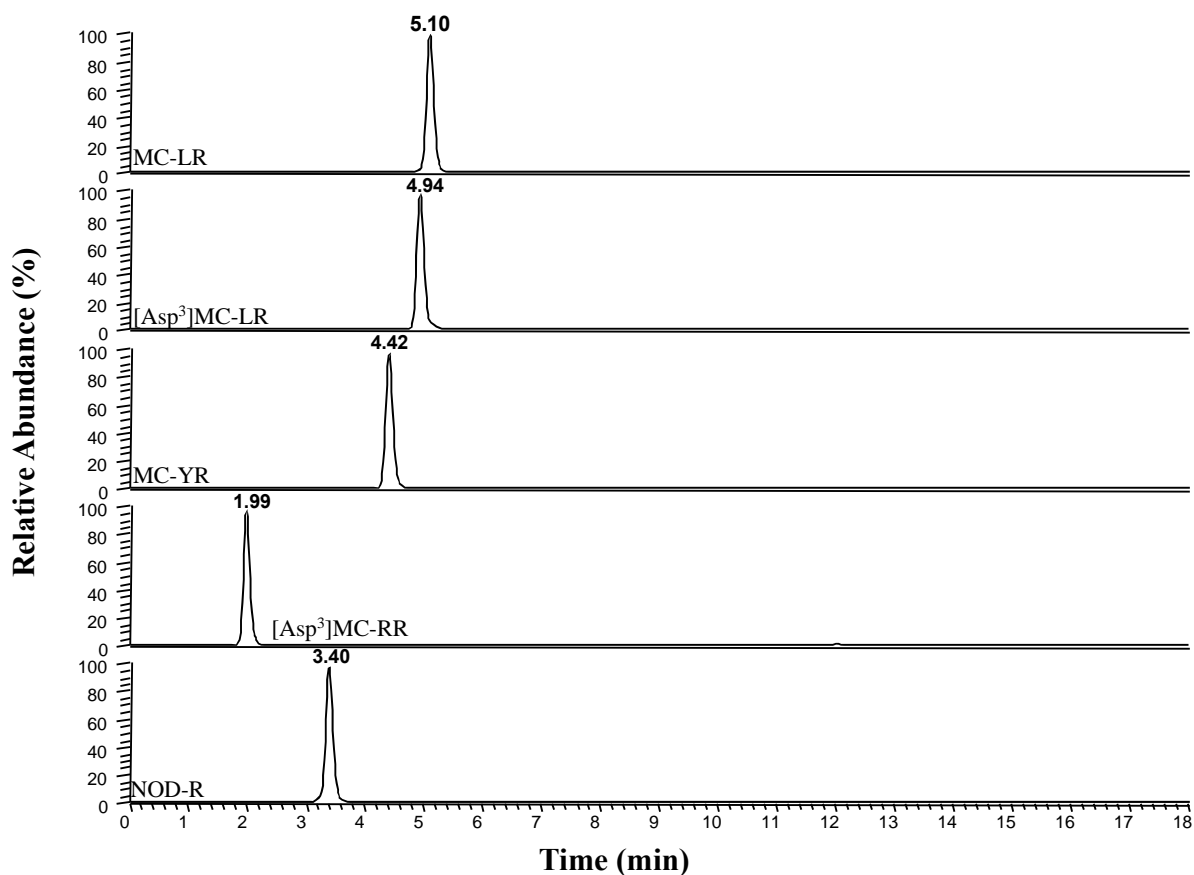


Figure 18: chromatograms of MC-LR, [Asp³]MC-LR (later identified as [Asp³,Dhb⁷]MC-LR), MC-YR, [Asp³]MC-RR and NOD-R in the mixed standard solution, 200 ng/mL. Relative abundance (%) on y-axis and time on x-axis. Retentiontime (in minutes) shown above the peaks.

Full mass spectra (Appendix C, Fig. C1-C2) of the standards gave the molecular ions m/z , which gave rise to the molecular formula and accuracy (Tab. 4).

Tab. 4: Microcystins and nodularin in the 200 ng/mL mixed standard solution, presented with their molecular formula, exact *mass* in positive mode, *m/z* in positive mode and the associated accuracy (ppm).

Compound	Molecular formula	Exact mass	<i>m/z</i>	Accuracy(ppm)
MC-RR	C ₄₉ H ₇₆ O ₁₂ N ₁₃ /	1038.5731/	1038.5725/	0.579/
	C ₄₉ H ₇₇ O ₁₂ N ₁₃	519.7902	519.7913	2.090
MC-LF	C ₅₂ H ₇₂ N ₇ O ₁₂ ⁺	986.5233	986.5239	0.571
MC-LW	C ₅₄ H ₇₃ O ₁₂ N ₈ ⁺	1025.5342	1025.5342	-0,064
MC-LY	C ₅₂ H ₇₂ O ₁₃ N ₇ ⁺	1002.5183	1002.5191	0.816
MC-LA	C ₄₆ H ₆₈ O ₁₂ N ₇ ⁺	910.4920	910.4931	1.135
MC-LR	C ₄₉ H ₇₅ O ₁₂ N ₇ ⁺	995.5560	995.5568	0.789
[Asp ³]MC-LR	C ₄₈ H ₇₃ O ₁₂ N ₁₀ ⁺	981.5404	981.5410	0.577
MC-YR	C ₅₂ H ₇₃ O ₁₃ N ₁₀ ⁺	1045.5353	1045.5356	0.260
[Asp ³]MC-RR	C ₄₈ H ₇₄ O ₁₂ N ₁₃ ⁺ /	1024.5574/	1034.5572/5	-0.196/
	C ₄₈ H ₇₅ O ₁₂ N ₁₃ ⁺	512.7824	12.7834	2.069
NOD-R	C ₄₀ H ₆₁ O ₁₀ N ₈ ⁺	825.4505	825.4212	0.828

The same analysis was performed on NIVA-CYA98, and three microcystins were detected (Fig. 19).

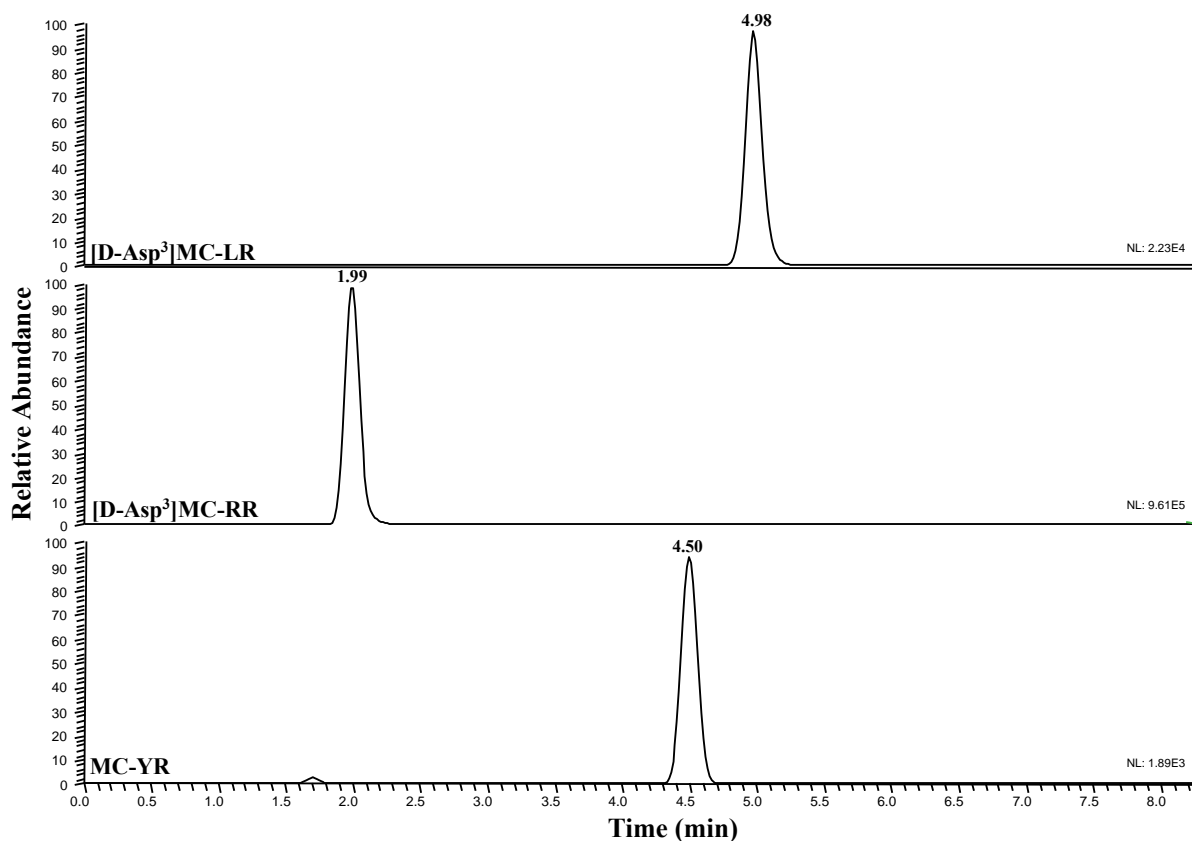


Figure 19: Full ms chromatograms of the microcystins found in a 1:100 dilution of NIVA CYA-98. MC-YR was later identified as [D-Asp³]MC-HtyR. [D-Asp³]MC-RR and [D-Asp³]MC-LR were later identified as [D-Asp³, Dhb⁷]MC-RR and [D-Asp³, Dhb⁷]MC-LR.

The analysis of a 1:100 dilution of NIVA-CYA98 provided chromatograms (Fig. 19) of acceptable peak shape and good separation. The corresponding mass spectra (Appendix C, Fig C3) revealed that the NIVA-CYA98 contains microcystins with the following m/z ; 981.5404 ([D-Asp³]MC-LR), 1024.5574 ([D-Asp³]MC-RR) and 1045.5353 (MC-YR), later identified as [D-Asp³, Dhb⁷]MC-RR and [D-Asp³, Dhb⁷]MC-LR.

Because NIVA-CYA98 was analysed with the mixed standard solution, the detection (and quantification) will be based on these analytes. There are however many structural isomers of microcystins resulting in similar mass spectra. Eight microcystins with m/z 981.5404, five with m/z 1045.5353 and five with m/z 1024.5574 are reported (Miles & Stirling, 2017). Given the difference in retention time between the microcystins in the mixed standard solution and NIVA-CYA98, this needed to be investigated further.

5.2 Screening of microcystins and other cyanopeptides in NIVA-CYA98 using LC – HRMS analyses

An extract (methanol/water, 1:1) from freeze-dried culture material of *P. rubescens* NIVA-CYA98 was used in order to screen for MC analogues using various LC–HRMS approaches. Determining the microcystin profile in NIVA-CYA98 was essential in order to know which MCs to quantify in the crayfish tissue. The vast majority of MCs contains an intact Adda⁵ moiety (Fig. 20), which gives a prominent m/z 135.0804 product ion in the LC–HRMS/MS mass spectra.

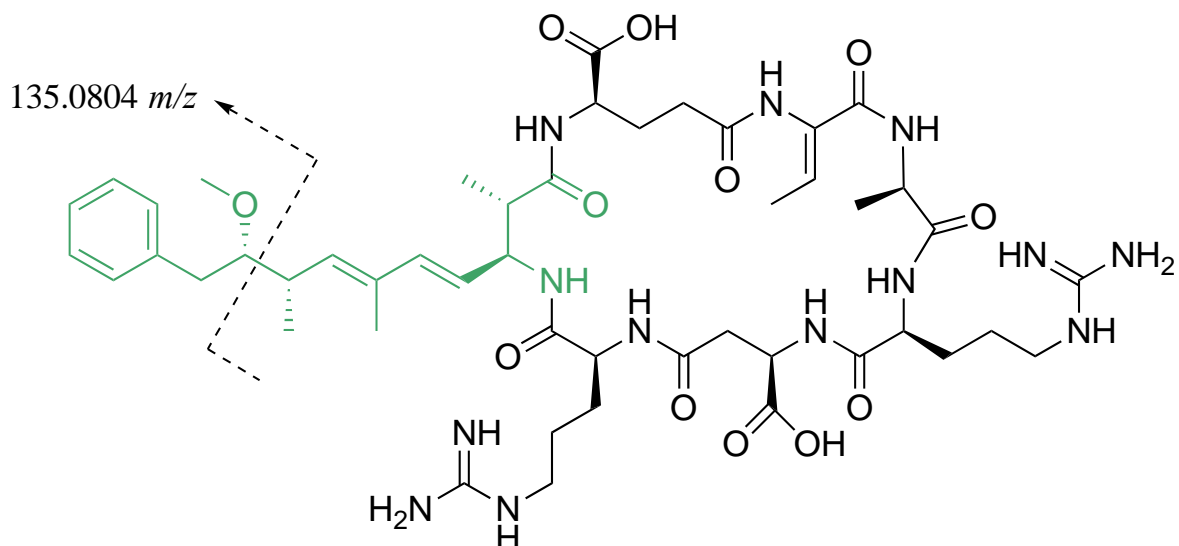


Figure 20: [D-Asp³, Dhb⁷]-RR, with the amino acid Adda marked in green. The Adda fragment is shown with a dashed line.

If a molecule in the extract included the amino acid Adda, it was reasonable to anticipate that it was most likely a MC or NOD.

Screening for the Adda fragment (Fig. 20) by all ion fragmenting (AIF) revealed that NIVA-CYA98 contains four species holding the Adda fragment (Fig 21).

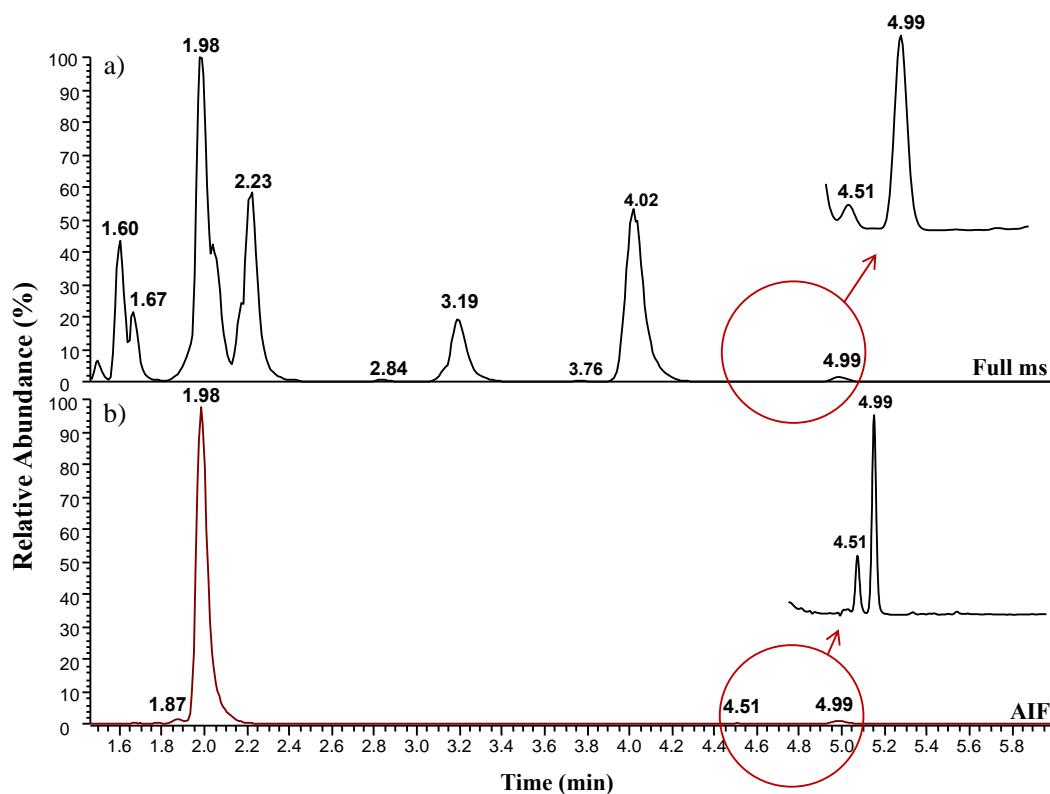


Figure 21: A methanol/water extract from NIVA-CYA98 (1:10 dilution) analysed by LC–HRMS(/MS) using the Full-MS/All-Ion-Fragmentation (AIF) mode; a) Full-MS, positive ion mode b) extracted ion chromatogram (m/z 135.0804, \pm 5.0000 ppm) from AIF. Enlarged traces represent the peaks at 5.51 and 4.99 min.

We thus used the presence of a m/z 135.0804 product ion (Fig. 21, b)) in the LC–HRMS/MS data to trace possible MCs in the NIVA-CYA98 extract. We used three different instrumental approaches to screen for the characteristic Adda fragment, i.e. AIF (all-ion-fragmentation, ddMS² (data-dependent scanning) and DIA (data-independent analysis). All three approaches revealed one major MC, as well as three minor MCs. The major MC eluted relatively early (1.98 min), and afforded mainly double-charged, protonated ions of m/z 512.7824 (Appendix C, Fig. C4). In addition, mono-charged protonated ions were observed at m/z 1024.5574 (Appendix C, Fig. C4). These data were in agreement with a molecular formula $C_{48}H_{74}N_{13}O_{12}^+$ Earlier reports have shown that NIVA-CYA98 produces mainly desmethyl-MC-RR, and the molecular formula of the MC eluting at 1.98 min was indicative of [D-Asp³]MC-RR. Comparing the LC–HRMS characteristics of the putative desmethyl-MC-RR in the extract with that of [Asp³]MC-RR in the mixed standard (Fig. 18) showed that the compounds eluted at 1.98 and 1.99 min and were hence either identical or a closely-related. Possibilities of common structural isomers include [Dha⁷]MC-RR or [D-Asp³, Dhb⁷]MC-RR (Fig. 3 for structural isomers). The specie eluting at 4.99 min mainly provided single charged

protonated ions of m/z 981.5404 (Appendix C, Fig C5). The data were in agreement with a molecular formula $C_{48}H_{73}N_{10}O_{12}^+$. Comparing the LC–HRMS characteristics of the putative [D-Asp³]MC-LR (Fig. 18) from the mixed standard, one can see that the species has a retention time at 4.94 (vs. 4.99), which suggest that they were either identical or strongly related. Other possible structural isomers are [D-Asp³, Dhb⁷]MC-LR or [Dha⁷]MC-LR (Fig. 3), which has the same molecular formula. [D-Asp³, Dhb⁷] probably has a closely related retention time. The specie eluting at 4.51 min afforded a single-charged, protonated ion of m/z 1045.5353. The data were in agreement with a molecular formula $C_{52}H_{73}N_{10}O_{13}^+$. Chromatograms of the putative MC-YR (Fig. 18) showed a retention time of 4.50 min. The mixed standard showed that MC-YR has a retention time of 4.42. This difference in retention time indicates that the specie might be another MC. Ather possible structural isomers are MC-RY, [D-Asp³]MC-HtyR, [D-Asp³, Dhb⁷]MC-HtyR and [Dha⁷]MC-HtyR (Fig. 3).

It has been reported that oxygenation of microcystins can occur in several different positions (Kim et al., 2017). It has also been disclosed that oxygenated analogs have been observed in nature (Miles, 2018). It was hence given advise to search for oxygenated analogs of the MCs already found in the dry material sample. An exact mass of 15.9949 (corresponding to oxygen) was added to the mass of the already identified microcystins. Extracted ion chromatograms were plotted, employing the exact masses of the $[M+H]^+$ ions of putative oxygenated MCs, i.e. m/z 1040.5523, m/z 997.5353 and m/z 1061.5302. Only m/z 1040.5523 gave a significant peak in the chromatograms (mass spectrum shown in Appendix C, Fig. C7). A m/z 135.0804 product ion was also observed in the AIF chromatograms at the same retention time as the m/z 1040.5523 compound. Thus, since desmethyl-MC-RR was the dominating MC analogue in the sample (Fig. 21, b)) it supported that the m/z 1040.5523 compound was equivalent to an oxygenated desmethyl-MC-RR.

The mentioned species elute at 1.87 min, 1.98 min, 4.51 min and 4.99 min. The species eluting earlier than 1.87 (Fig. 21, b)) have been inspected and were found not to be related to Microcystins or Nodularins.

According to Rohrlack et al. (2008), NIVA-CYA98 can contain the cyanopeptides oscillagin B, aeruginosin, oscillagin A, aeruginosin A, anabaenopeptin B, anabaenopeptin A, anabaenopeptin F, oscillamide Y, desmethyl-microcystin LR, desmethyl-microcystin RR, and oscillapeptin G . A dilution (1:10) of the *P. rubescens* extract (Appendix G, Fig. G1-G2) was investigated to see if NIVA-CYA98 contains any other cyanopeptides than MCs.

Extracted ion chromatograms were plotted using the exact mass of the $[M+H]^+$ ions of these peptides. The search showed three peaks from ions that could arise from $[M+H]^+$ of anabaenopeptins A and B, as well as oscillamide Y including four microcystins.

Table 5: The cyanopeptides and microcystins that provided molecular formula within the uncertainty limit (5.00 ppm), presented with exact *mass* in positive and negative mode, *m/z* in positive mode, *m/z* in negative mode, the associated uncertainty and the neutral molecular formula.

Compound and neutral molecular formula	Exact mass positive mode	Exact mass, negative mode	<i>m/z</i> , positive mode	<i>m/z</i> , negative mode	Accuracy (ppm) pos. mode	Accuracy (ppm) neg. mode
Anabaenopeptin A (C ₄₄ H ₅₇ N ₇ O ₁₀)	844.4240	842.4094	844.4225	842.4105	-1.517	1.242
Anabaenopeptin B (C ₄₁ H ₆₀ N ₁₀ O ₉)	837.4618	835.4472	837.4605	835.4479	-1.260	0.890
Oscillamide Y (C ₄₅ H ₅₉ N ₇ O ₁₀)	858.4396	856.4251	858.4381	856.4257	-1.537	0.696
[D-Asp ³]MC-LR (C ₄₈ H ₇₂ N ₁₀ O ₁₂)	981.5404	979.5258	981.5404	979.5280	-0.014	2.225
[D-Asp ³ ,Dhb ⁷]MC-RR (C ₄₈ H ₇₃ N ₁₃ O ₁₂)	1024.5574	1022.5429	1024.5543	1022.5439	-3.084	1.039
Oxygenated [D-Asp ³ ,Dhb ⁷]MC-RR (C ₄₈ H ₇₃ N ₁₃ O ₁₃)	1040.5524	1038.5378	1040.5506	1038.5398	-1.726	1.914
[D-Asp ³ ,Dhb ⁷]MC-HtyR (C ₅₂ H ₇₂ N ₁₀ O ₁₃)	1045.5353	1043.5208	1045.5351	1043.5231	-0.219	2.218

The results (Tab. 5) show that NIVA-CYA98 holds the molecules with a molecular formula that corresponds to anabaenopeptin A (*m/z* 844.4240), anabaenopeptin B (*m/z* 837.4618), oscillamide Y (*m/z* 858.4396), Desmethyl MC-RR (*m/z* 981.5404), Desmethyl MC-LR *m/z* (1024.5574), Oxygenated desmethyl MC-RR (*m/z* 1040.5525), and Desmethyl MC-HtyR (1045.5353), within an accuracy (ppm) of 5.00 ppm. All the results (Tab. 5) are far below the accuracy limit in both negative and positive mode which makes it highly probable that NIVA-CYA98 contain the mentioned compounds. Structural isomers were nevertheless still an issue, as they would have provided the same accuracy.

5.3 β -Mercaptoethanol derivatisation for Mdha7/Dhb7 differentiation

β -mercaptoethanol derivatisation was performed to determine if the microcystins in NIVA-CYA98 contained the amino acid Mdha or Dhb in position 7 of the amino acid structure (Miles et al., 2012). Microcystins with Mdha in positions 7 will be derivatised almost immediately, while a derivatisation of microcystins with Dhb in position 7 will take about hundred-fold longer time. It is hence possible to follow the reaction by observing the peak area of the MCs and the thiol-addition product over time. Determining the amino acid in position 7 would exclude many structural isoforms (see Fig. 3) in the search for a microcystin profile in NIVA-CYA98. The derivatisation was first performed on the microcystins in the mixed standard solution ([Asp3]MC-RR, MC-LF, MC-LY, MC-LA, [D-Asp3]MC-LR, MC-YR, MC-RR and NOD-R). To follow the reaction, LC–HRMS analyses were performed on the same sample over a time period of 195 minutes. A graphic representation of peak area of the MCs and NOD-R as a function of time is demonstrated in Figure 22.

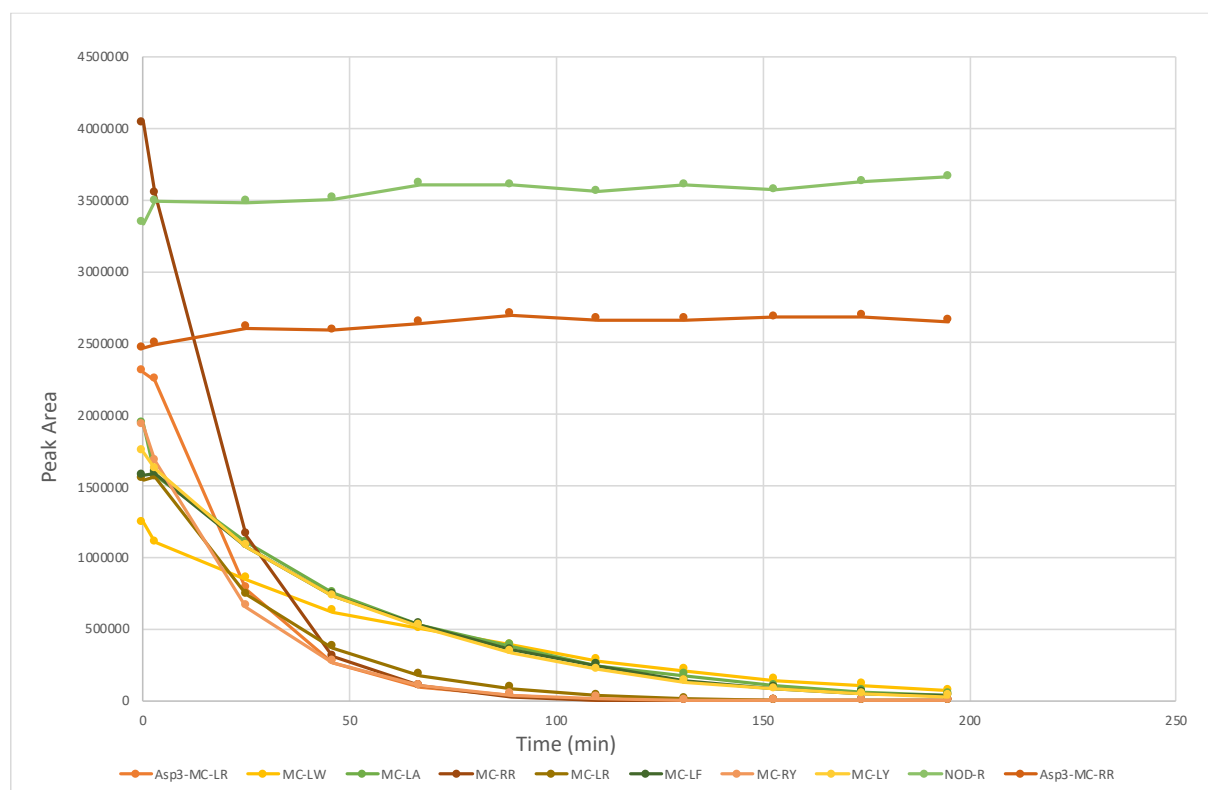


Figure 22: graphic representation of the $[M+H]^+$ peak area for all microcystins/nodularin as a function of time in the mixed standard solution after addition of mercaptoethanol at pH 9.41, $n=1$.

A decrease in peak area indicated that the original m/z was no longer detectable due to β -mercaptoethanol derivatisation. Another way of showing this is to extract an ion chromatogram associated to the MC-thiol conjugate, which is expected to increase exponentially in peak area. The derivatisation experiment showed that eight MCs reacted with half-lives of approximately 30 min, while NOD-R and [Asp³]MC-RR did not react within the same time period (Fig. 22). While it was expected that NOD-R reacts only slowly (it contains Mdhb⁵, which is known to react very slowly), [Asp³]MC-RR was expected to react as fast as the other MCs in the mixture. Thus, the [Asp³]MC-RR standard from Enzo Life Science must in fact be [Asp³, Dhb⁷]MC-RR, which is a structural isomer of [Asp³]MC-RR and hard to distinguish from the Dhb⁷ analogue by mass spectrometry alone.

β -Mercaptoethanol derivatisation was also attempted using the NIVA-CYA98 extract. The reaction was followed by LC–HRMS over a time frame of 176 minutes. A graphic representation of the peak areas of MCs in NIVA-CYA98 as a function of time is shown in figure 23.

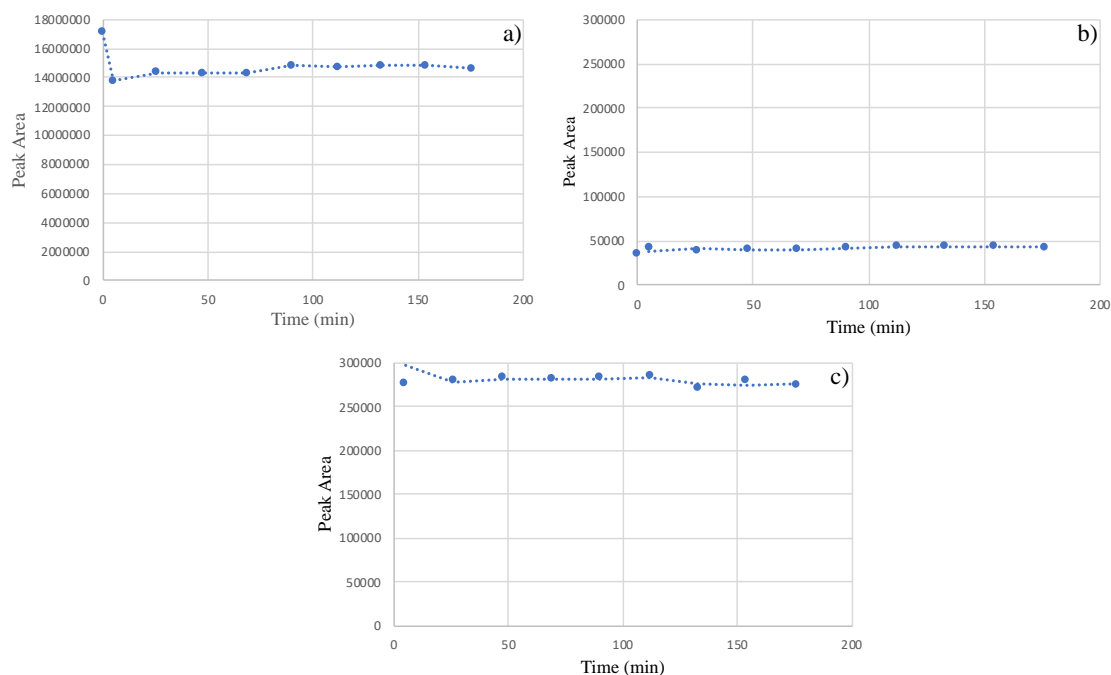


Figure 23: graphic representation of peak area as a function of time for the microcystins in NIVA-CYA98. a) [D-Asp³, Dhb⁷]MC-RR, b) [D-Asp³, Dhb⁷]MC-HtyR (earlier believed to be MC-YR), c) [D-Asp³, Dhb⁷]MC-LR.

The results indicated that there was no significant decrease in peak area for any of the microcystins in NIVA-CYA98 (Fig. 22). This indicates that all the detected microcystins in NIVA-CYA98 contain [Dhb] in position 7.

As mentioned, the nucleophilic addition of mercaptoethanol to Dhb happens with time, but it takes about hundred times longer than for Mdha (or Dha). The reaction was followed over the course of two weeks, showing that the thiol indeed was added to the α,β -unsaturated double bond (Fig. 24).

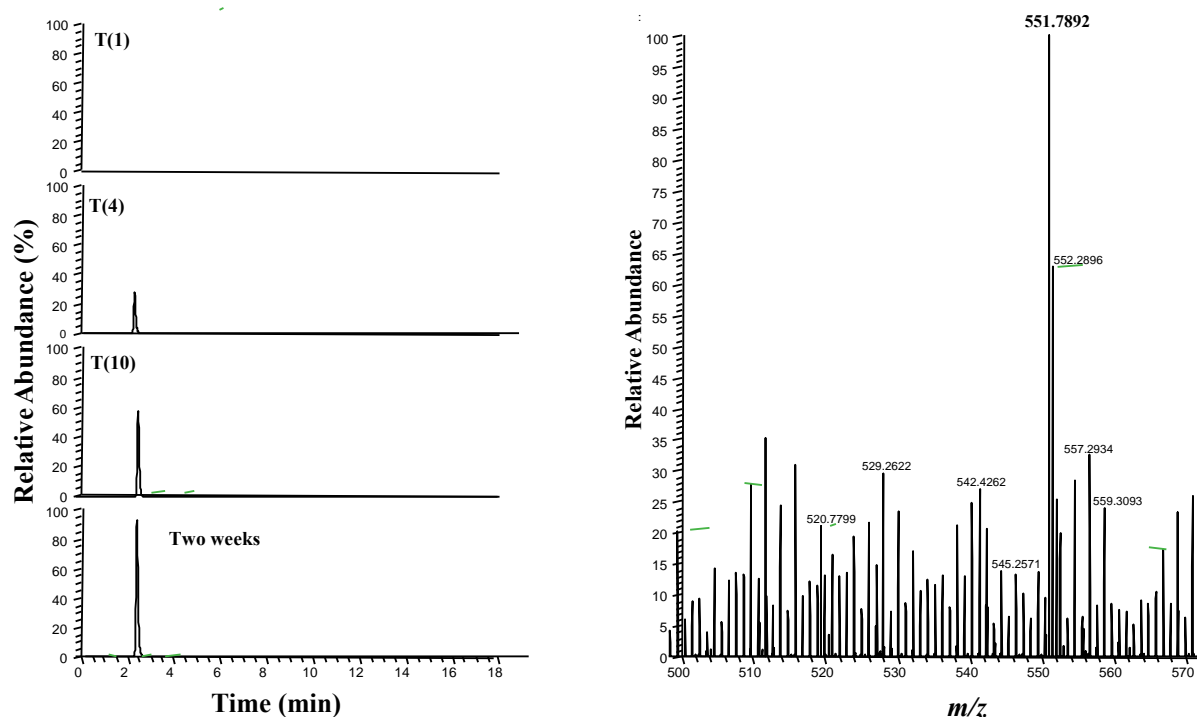


Figure 24: Chromatograms representing the relative abundances of the thiol-derivatised [D-Asp³, Dhb⁷]MC-RR at t(1), t(4), t(10) and t(two weeks) to the left. T represents the different injections. T(1) is injected immediately after addition of mercaptoethanol, T(10) is the tenth injection, which corresponds to approximately 80 min and 200 min for the second and third chromatogram. The representation is given with fixed scale at 10⁶ NL. The mass spectrum to the right shows the [M+2H]²⁺ of [D-Asp³, Dhb⁷]MC-RR conjugated with mercaptoethanol.

The Chromatograms (Fig. 24) showed that the peak area of [D-Asp³, Dhb⁷]MC-RR conjugated to mercaptoethanol increased over a time period of two weeks. T represents the different injections. This demonstrated that also microcystins with Dhb in position 7 of the microcystin structure will react with the mercaptoethanol over time. The reaction will give a [D-Asp³, Dhb⁷]MC-RR-thiol conjugate (Fig. 25).

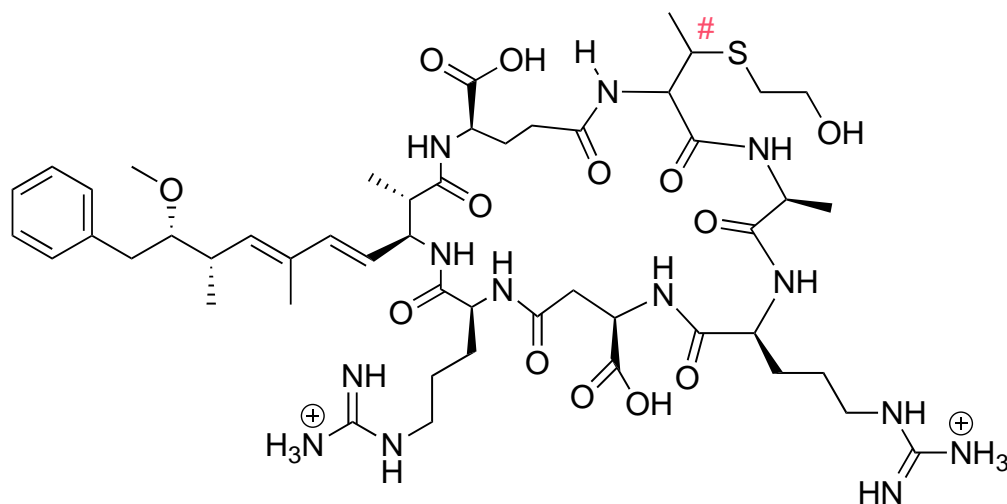


Figure 25: the mercaptoethanol conjugate of [D-Asp³, Dhb⁷]MC-RR.

The molecular structure shown in Figure 25 is representative for all MC-thiol conjugates where the microcystin has Dhb in position 7. Microcystins containing Mdha in position 7 will lack a methyl group in the site of the reaction, marked with #.

When mercaptoethanol (or any other thiol or nucleophile) reacts with a Dhb⁷-containing microcystins, it will create a stereogenic center, and the reaction may lead to four different stereoisomers. As this cannot happen with a Dha- or Mdha-containing MC, the presence of several isomeric reaction products is an additional confirmation of a Dhb⁷MC.

Pentafluorophenyl (PFP)-functionalized particles, are especially well suited for separating structural isomers. The column used in this study, Phenomenex F5, contains propyl-PFP functionalized particles, and separated two major thiol-addition products for [D-Asp³, Dhb⁷]MC-LR, while two minor products were partially separated (Fig. 26).

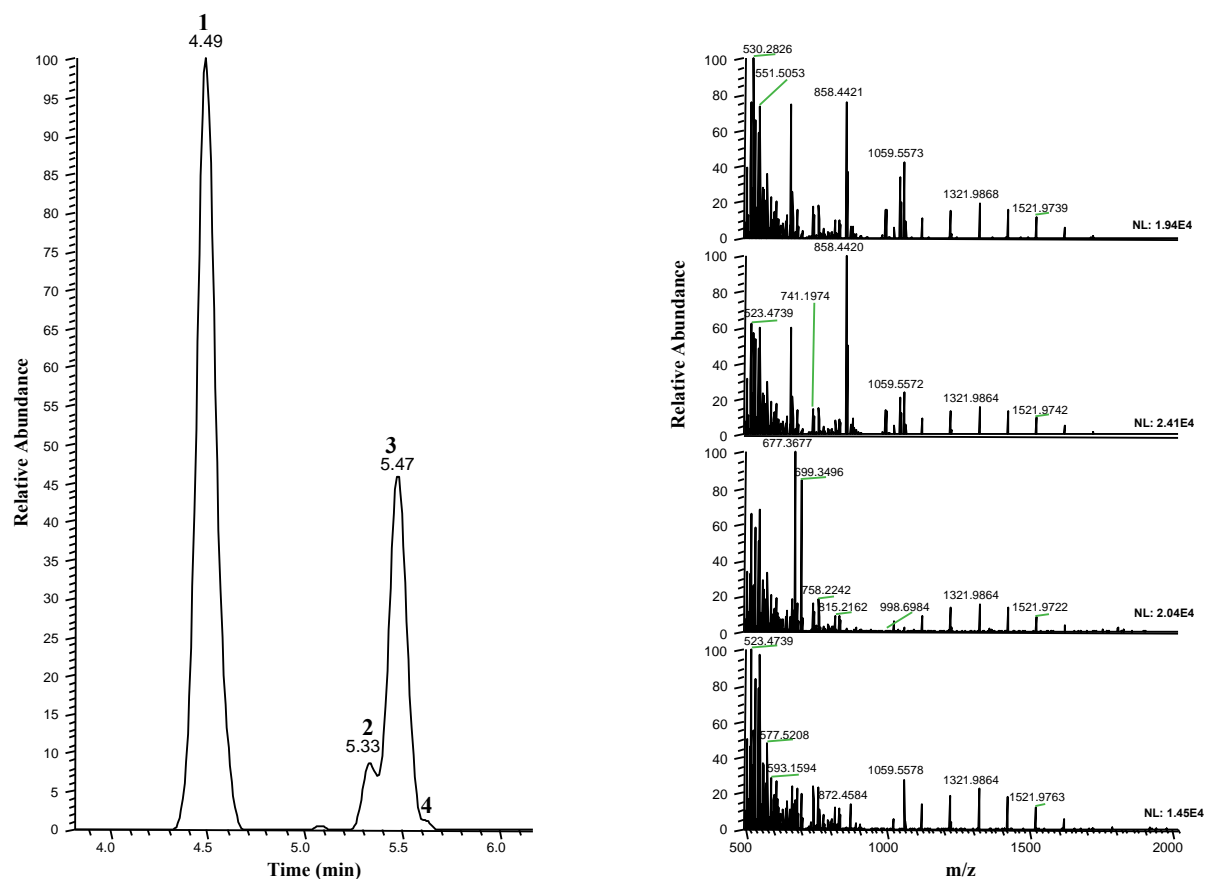


Figure 26: Extracted ion chromatogram ($[M+H]^+$) of the thiol-derivative of $[D\text{-Asp}^3, Dhb^7]MC\text{-LR}$ (m/z 1059.5543, ± 5.0000 ppm) giving rise to four peaks

5.4 MS fragmentation of microcystins and anabaenopeptins in NIVA CYA-98 using ion trap tandem mass spectrometry

Liquid chromatography–ion trap tandem mass spectrometry was used to confirm the identity of MCs and the three other cyanopeptides in NIVA-CYA98. Table 6 summarizes the observed m/z values of the product ions from collision-induced dissociation (CID) of the $[M+H]^+$ ions of $[D\text{-Asp}^3, Dhb^7]MC\text{-HtyR}$, $[D\text{-Asp}^3, Dhb^7]MC\text{-LR}$ and $[D\text{-Asp}^3, Dhb^7]MC\text{-RR}$ and oxygenated $[D\text{-Asp}^3, Dhb^7]MC\text{-RR}$.

Table 6: Assignments of the observed product ions and their m/z from collision-induced dissociation of $[M+H]^+$ of [D-Asp³,Dhb⁷]MC-HtyR, [D-Asp³,Dhb⁷]MC-LR, [D-Asp³,Dhb⁷]MC-RR and oxygenated [D-Asp³,Dhb⁷]MC-RR.

Fragment Ion Assignment	[Asp ³ , Dhb ⁷] MC- HtyR (a)	[Asp ³ , Dhb ⁷] MC-LR (b)	[D-Asp ³ , Dhb ⁷] MC-RR (c)	[D-Asp ³ , Dhb ⁷]MC- RR (oxygenated) (d)
$[M - NH_3 + H]^+$	1028.5	964.5	1007.6	1023.6
$[M - H_2O + H]^+$	1027.6	963.6	1006.6	1022.6
$[M - CO + H]^+$	1017.6	953.6	996.7	1012.8
$[M - CO - NH_2 + H]^+$	n.d.	n.d.	964.6	980.5
$[Arg^4-Adda^5-Glu^6-Dhb^7-Ala^1-2-NH_2 + 2H]^+$	947.5	883.6	925.6	942.8
$[Arg^4-Adda^5-Glu^6-Dhb^7-Ala^1-2 + H]^+$	930.6	866.6	909.6	925.5
$[Dhb^7-Ala^1-2-Asp^3-Arg^4-Adda^5 + H]^+$	916.6	852.5	895.5	n.d.
$[M-ADDAfrag. + H]^+$	n.d.	846.9	889.0	n.d.
$[M-ADDAfrag. - NH_3 + H]^+$	n.d.	829.9	872.5	n.d.
$[Arg^4-Adda^5-Glu^6-Dhb^7-Ala^1-2-CO + 2H]^+$	n.d.	894.7	937.6	n.d.
$[Arg^4-Adda^5-Glu^6-Dhb^7-Ala^1 + H]^+$	753.6	753.6	753.6	769.5
$[Asp^3-Arg^4-Adda^5-Glu^6 + H]^+$	714.4	714.5	714.5	714.5
$[Asp^3-Arg^4-Adda^5-Glu^6 - H_2O + H]^+$	696.4	696.4	696.7	696.4
$[Arg^4-Adda^5-Glu^6-Dhb^7 + H]^+$	682.6	682.4	682.6	682.5
$[Glu^6-Dhb^7-Ala^1-2-Asp^3-Arg^4 + H]^+$	n.d.	668.6	711.5	n.d.
$[Arg^4-Adda^5-Glu^6 + H]^+$	599.4	599.5	599.5	599.4
$[Arg^4-Adda^5-Glu^6 - NH_3 + H]^+$	n.d.	582.4	n.d.	n.d.
$[Arg^4-Adda^5-Glu^6 - CO + H]^+$	571.4	571.4	n.d.	n.d.

[Dhb ⁷ -Ala ¹ -2-D-Asp ³ -Arg ⁴ -NH ₂ + 2H] ⁺	620.4	556.5	n.d.	n.d.
[Dhb ⁷ -Ala ¹ -2-D-Asp ³ -Arg ⁴ + H] ⁺	603.5	539.4	n.d.	n.d.
[Ala ¹ -2-D-Asp ³ -Arg ⁴ + H] ⁺	520.4	456.4	n.d.	n.d.
[Ala ¹ -2-D-Asp ³ -Arg ⁴ - NH ₃ + H] ⁺	503.3	n.d.	n.d.	n.d.
[Adda ⁵ -Glu ⁶ -Dhb ⁷ - ADDAfrag. - NH ₃ + H] ⁺	n.d.	n.d.	n.d.	n.d.
[D-Asp ³ -Arg ⁴ -NH ₂ + H] ⁺	n.d.	n.d.	n.d.	n.d.
[D-Asp ³ -Arg ⁴ + H] ⁺	n.d.	n.d.	n.d.	n.d.

2 (amino acid in position 2) = Hty (a), Leu (b), Arg (c, d)

*Ala¹ is attached is oxygenated in specie d

All the MCs provided peaks of high intensity with m/z 599.5 (Tab. 6 and Fig. 29-30), associated to [Arg⁴-Adda⁵-Glu⁶ + H]⁺. Additionally they all provided peaks with m/z 682.5 associated to [Arg⁴-Adda⁵-Glu⁶-Dhb⁷ + H]⁺, m/z 696.4 associated to [D-Asp³-Arg⁴-Adda⁵-Glu⁶ - H₂O + H]⁺, and m/z 714.5 associated to [D-Asp³-Arg⁴-Adda⁵-Glu⁶ + H]⁺. This suggested that the only varying positions in the MC structure was position 1 (only concerning the oxygenated specie) and 2. [Asp³, Dhb⁷]MC-LR (b) and [Asp³, Dhb⁷]MC-LR (c) was compared with standards (200 ng/mL) which showed corresponding fragmentations. All product ions related to [Asp³, Dhb⁷]MC-HtyR (a) who included the varying amino acid in position 2 were shifted 64.0 m/z relative to the same product ions in [Asp³, Dhb⁷]MC-LR. This is equivalent to the m/z difference between Leu and Hty. All product ions which includes the amino acid in position 2 hence may confirm the presence of Hty (Tab. 6, marked in bold).

The analyses also showed that the oxygenated [D-Asp³,Dhb⁷]MC-RR analogue was oxygenated in the amino acid alanine (Ala¹). The m/z of the product ion [Arg⁴-Adda⁵-Glu⁶-Dhb⁷-Ala¹ + H]⁺ (Table 5, marked in red) was shifted by 15.9 m/z . relative to the same ion in [D-Asp³,Dhb⁷]MC-RR. The product ion [D-Asp³-Arg⁴-Adda⁵-Glu⁶ + H]⁺ (Table 6, marked in blue) was of identical m/z between the two analogues. The product ion [Arg⁴-Adda⁵-Glu⁶-Dhb⁷ + H]⁺ (Table 6, marked in green) also gave product ions with identical m/z , which further supports that the oxygen must be placed in Ala¹.

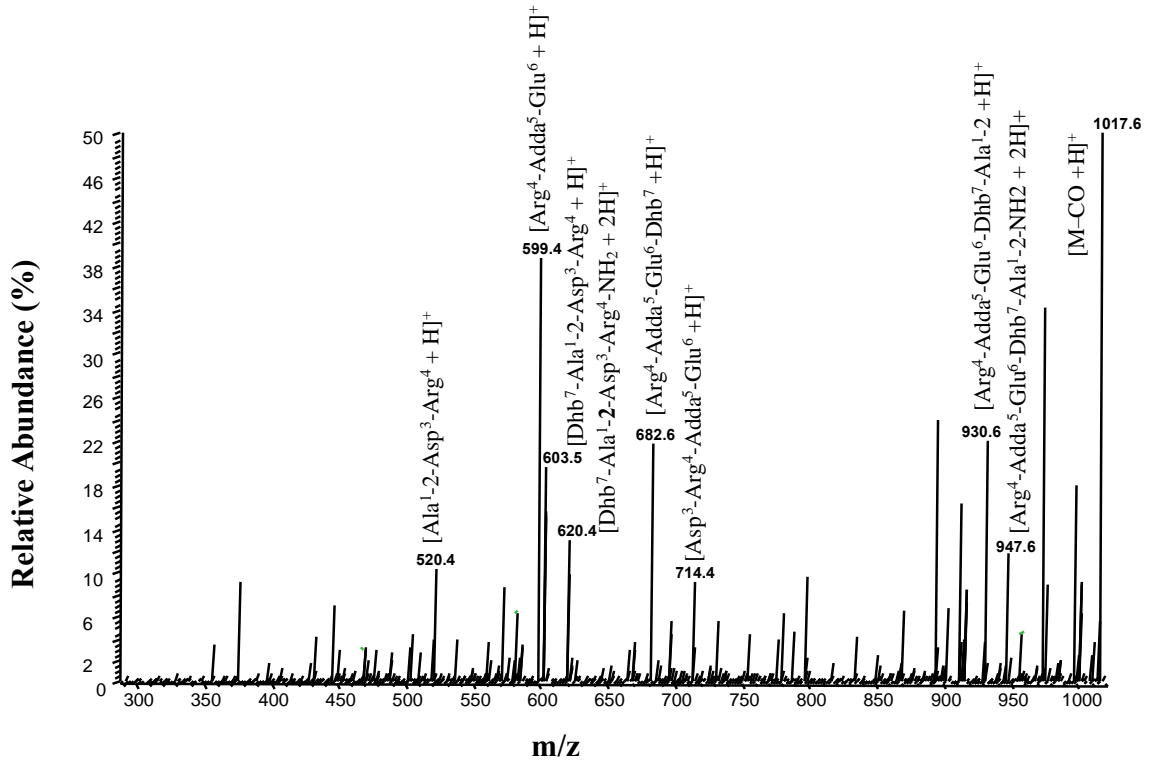


Figure 27: Tandem (MS²) mass spectrum from collision-induced dissociation of [M+H]⁺ of [Asp³, Dhb⁷]MC-HtyR (*m/z* of 1045.5). Product ions are shown with their assigned amino acid sequence in brackets. The product ion 1028.5 *m/z* (loss of NH₃) is off scale for better visualization of other and more diagnostic product ions.

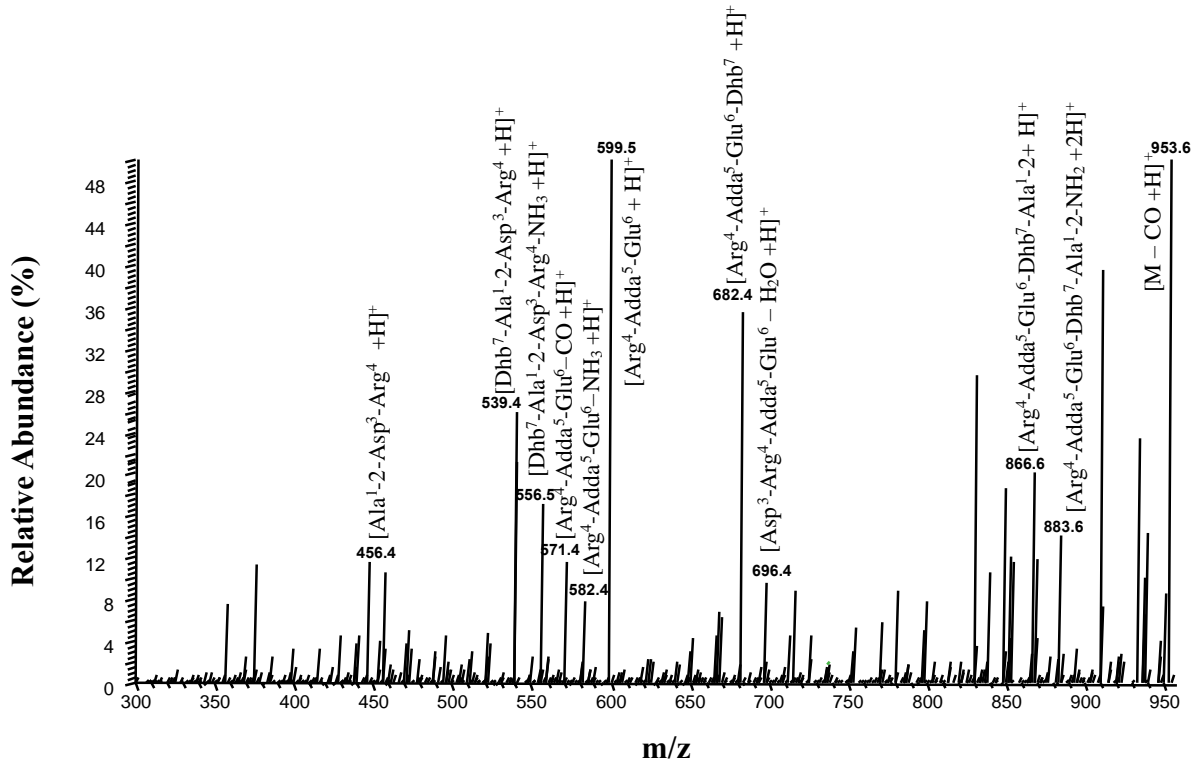


Figure 28: displays the tandem (MS^2) mass spectrum from collision-induced dissociation of $[M+H]^+$ of $[Asp^3, Dhb^7]MC-LR$ (m/z of 981.5). Product ions are shown with their assigned amino acid sequence in brackets. The product ion m/z 964.5 (loss of NH_3) and m/z 963.6 (loss of H_2O) are off scale for better visualization of other and more diagnostic product ions.

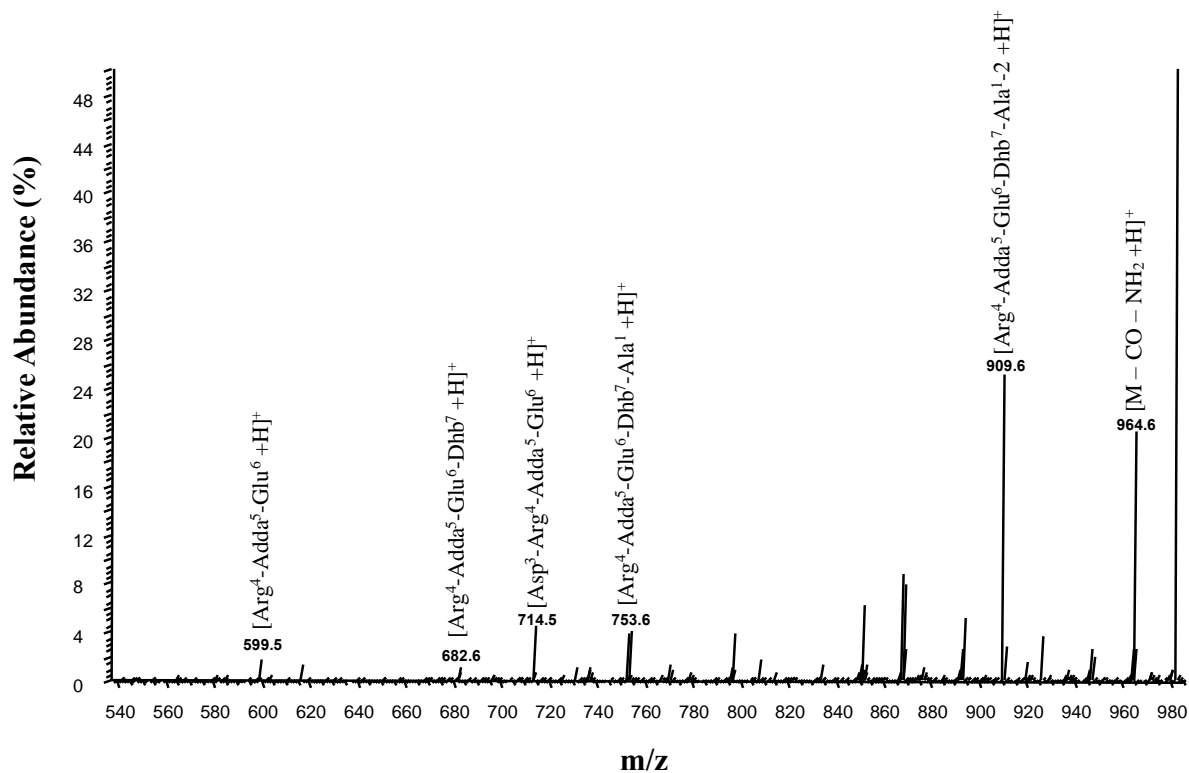


Figure 29: tandem (MS^2) mass spectrum from collision-induced dissociation of $[M+H]^+$ of $[Asp^3, Dhb^7]MC-RR$ (m/z of 1024.5574). Product ions are shown with their assigned amino acid sequence in brackets. The product ion m/z 1007.6 (loss of NH_3), m/z 1006.6 (loss of H_2O) and m/z 996.7 (loss of CO) are off scale for better visualization of other and more diagnostic product ions.

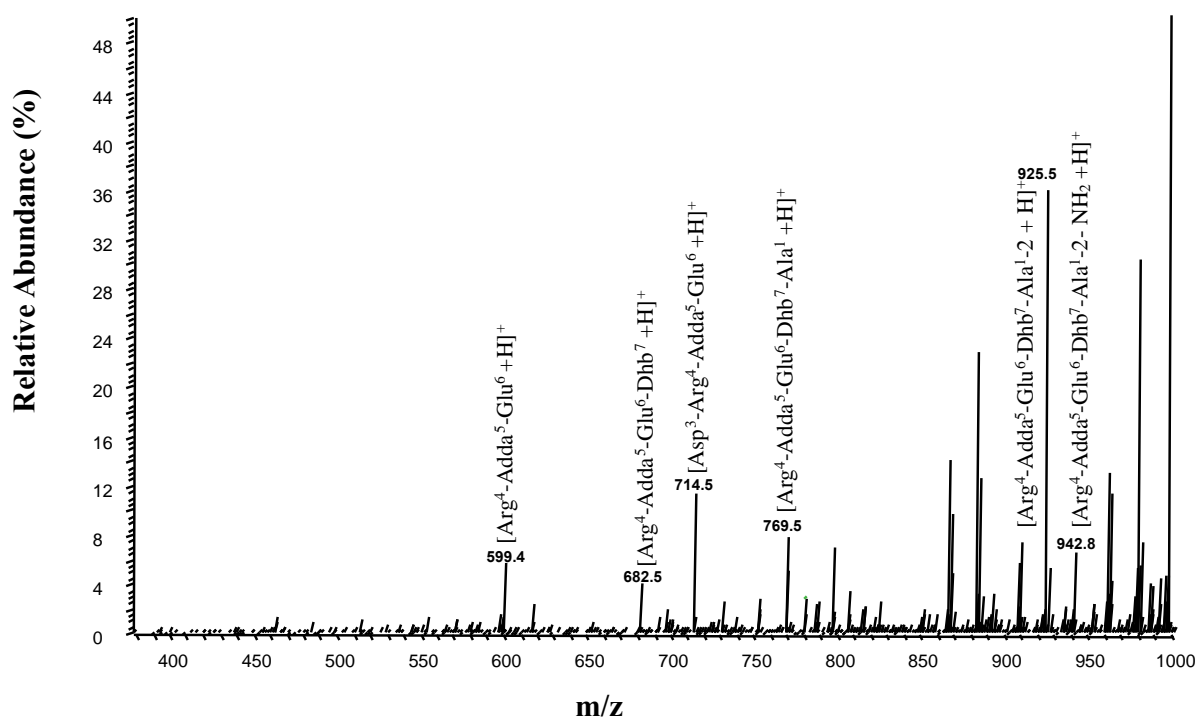


Figure 30: tandem (MS^2) mass spectrum from collision-induced dissociation of the oxygenated $[M+H]^+$ of $[Asp^3, Dhb^7]MC-RR$ (m/z of 1040.5). Product ions are shown with their assigned amino acid sequence in brackets. The product ion m/z 1023.6 (loss of NH_3), m/z 1022.6 (loss of H_2O) and m/z 1012.8 (loss of CO) are off scale for better visualization of other and more diagnostic product ions.

Table 7 summarizes the observed m/z values of the product ions from collision-induced dissociation (CID) of the $[M+H]^+$ ions of anabaenopeptin B, anabaenopeptin A and oscillamide Y.

Table 7: Assignments of the observed product ions and their m/z from collision-induced dissociation of $[M+H]^+$ of anabaenopeptin B, anabaenopeptin A and oscillamide Y.

Fragment Ion Assignment	Anabaenopeptin B	Anabaenopeptin A	Oscillamide Y
	(parent ion: m/z 837.5)	(parent ion: m/z 844.3)	(parent ion: m/z 858.6)
$[M - H_2O + H]^+$	819.4	826.3	840.3
$[M - MAIa^2 + H]^+$	752.6*	759.2	773.2
$[Ile/Val^4-Lys^5-Co-Tyr/Arg^3-Phe^1-MAIa^2+CH_2+H]^+$	n.d.	n.d.	695.4
$[Phe^1-MAIa^2-Hty^3-Ile/Val^4-Lys^5+H]^+$	637.3*	637.3*	651.4
$[Ile^4-Lys^5-CO-Tyr^6-Phe^1-Mala^2-2H]^+$	n.d.	n.d.	681.3*
$[Lys^5-CO-Tyr^6-Phe^1-Mala^2+2H]^+$	n.d.	568.1	568.0
$[Phe^1-Ala^2-Hty^3-Val^4-Lys^5+CO+NH_2+H]^+$	n.d.	n.d.	680.3
$[Val^4-Lys^5-Co-Tyr^6-Phe^1-MAIa^2+2H]^+$	n.d.	667.1	n.d.
$[Hty^3-Ile/Val^4+H]^+$	277.0	277.2	291.9
$[MAIa^2-Hty^3+H]^+$	n.d.	263.0*	263.0*

*Product ions marked with an asterisk are reported earlier (Bogialli et al., 2017).

The results (Tab. 7 and Fig. 31-33) showed that tandem (MS^2) spectra of the anabaenopeptins in NIVA-CYA98 compared well with the reference materials (200 ng/mL standards; anabaenopeptin A, anabaenopeptin b and oscillamide Y). Loss of water was a significant peak in the tandem (MS^2) spectra of anabaenopeptin A and oscillamide Y (Fig. 32-33). This peak could also be seen for anabaenopeptin B (Fig. 31). The base peak of anabaenopeptin b and anabaenopeptin originates from loss of the differing amino acid in the tail of the molecules (Fig. 34 for structures). This gave rise to identical base peaks of m/z 637.3. Loss of the corresponding amino acid in oscillamide Y provided a significant peak of m/z 651.4 (Fig.33).

This peak confirms the presence of isoleucine (vs. valine in anabaenopeptin A and B) in position four of the molecule structure (Fig. 34). The peak was assigned the amino acid sequence $[\text{Phe}^1\text{-MAIa}^2\text{-Hty}^3\text{-Ile}^4\text{-Lys}^5\text{+H}]^+$. The difference in 14 Da, originating from one CH_2 -group more in oscillamide Y, can also be observed for the peaks with the assigned amino acid sequence $[\text{Hty}^3\text{-Ile/Val}^4\text{+H}]^+$ (277.0 vs. 291.9). A peak of m/z 568.1 was found in both oscillamide Y and anabaenopeptin A (Fig. 32-33) were assigned to $[\text{Lys}^5\text{-CO-Tyr}^6\text{-Phe}^1\text{-Mala}^2\text{+2H}]^+$. These peaks confirm the common amino acids in oscillamide Y and anabaenopeptin A (Fig. 34).

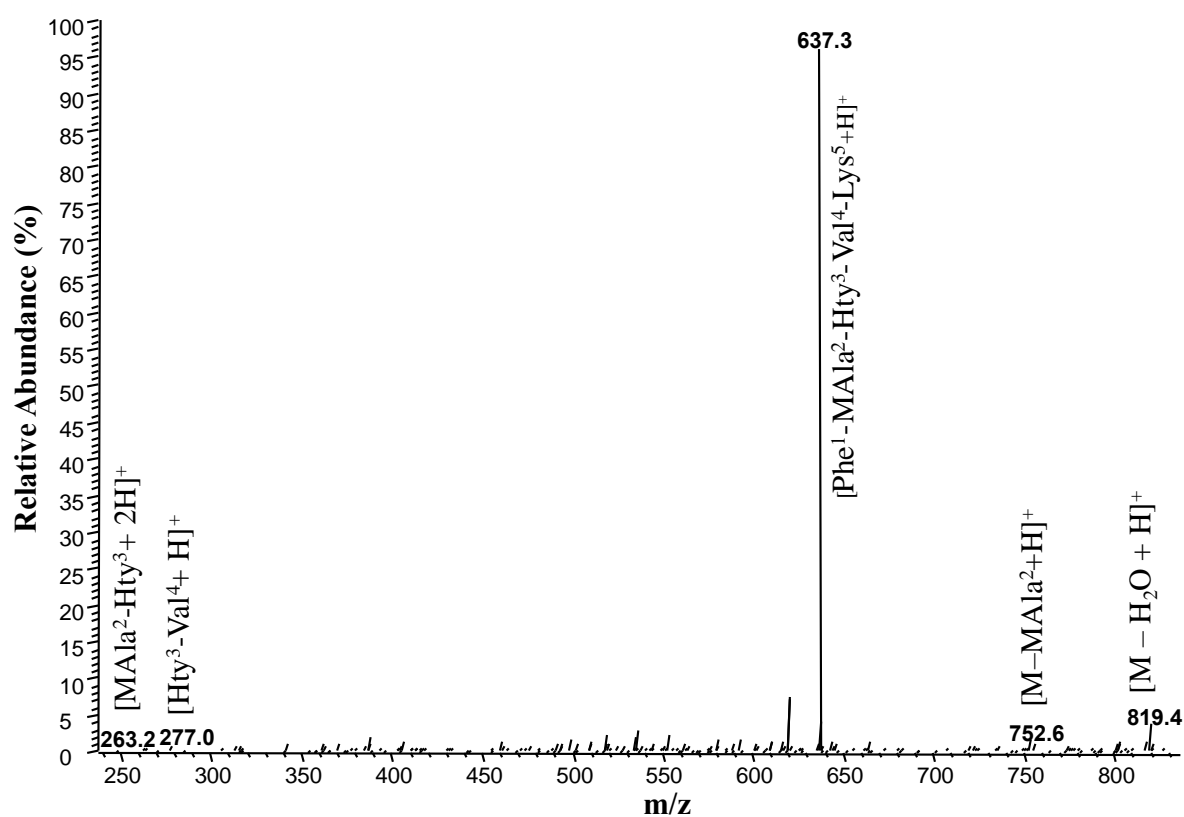


Figure 31: tandem (MS^2) mass spectrum from collision-induced dissociation of $[\text{M+H}]^+$ of anabaenopeptin B (m/z of 837.5). Product ions are shown with their assigned amino acid sequence in brackets.

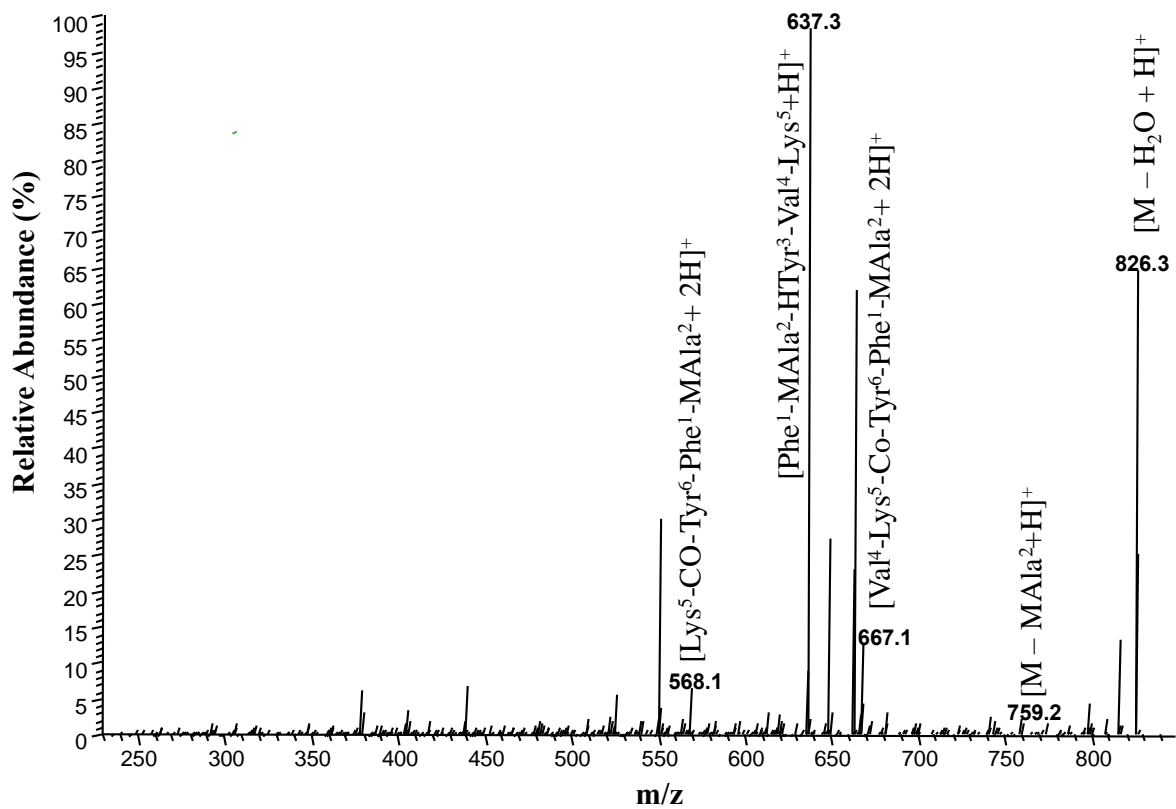


Figure 32: tandem (MS²) mass spectrum from collision-induced dissociation of [M+H]⁺ of anabaenopeptin A (*m/z* of 844.3). Product ions are shown with their assigned amino acid sequence in brackets.

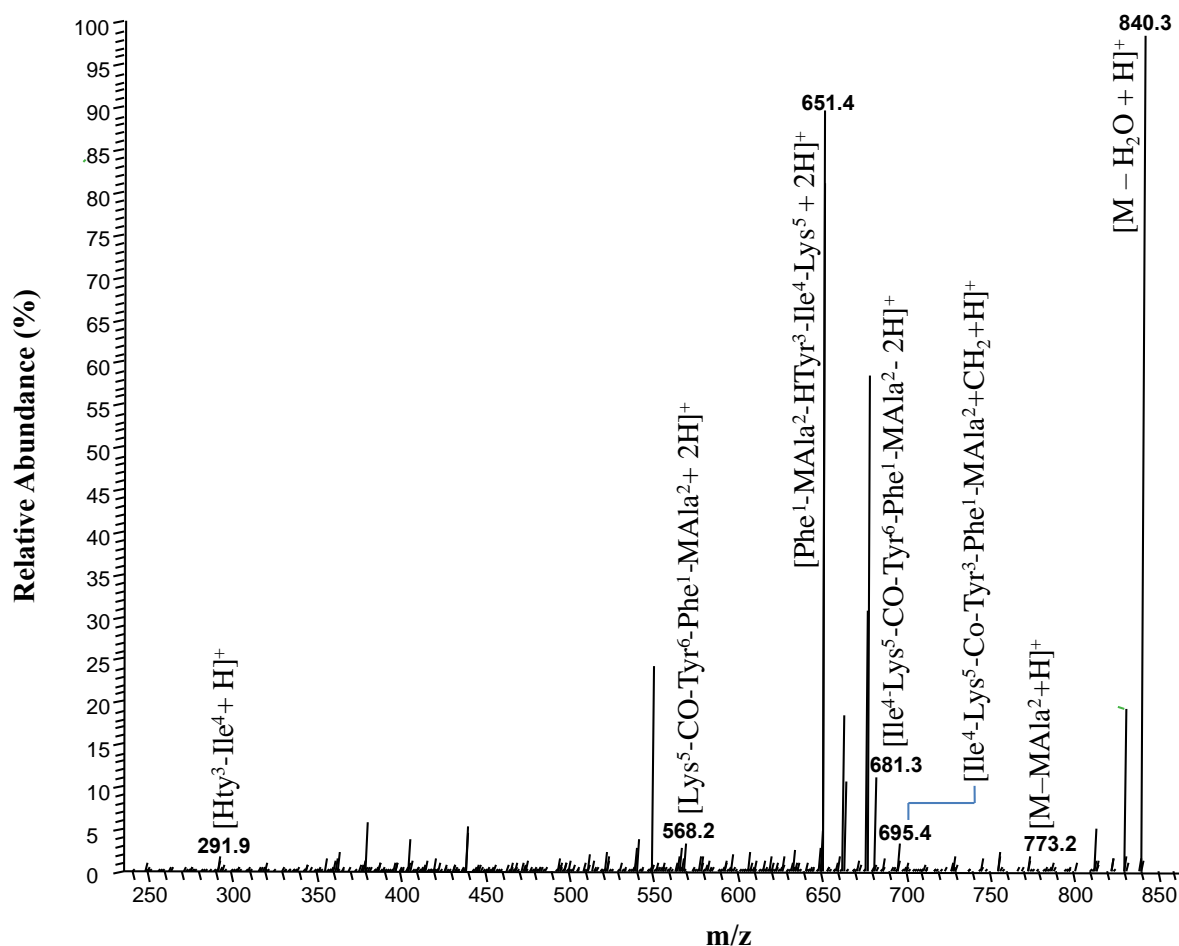


Figure 33: tandem (MS²) mass spectrum from collision-induced dissociation of [M+H]⁺ of Oscillamide Y (*m/z* of 858.6). Product ions are shown with their assigned amino acid sequence in brackets.

5.5 MS fragmentation of microcystins and anabaenopeptins in NIVA CYA-98 using high-resolution tandem mass spectrometry

Higher-energy collision dissociation (HCD) was performed using a quadrupole-Orbitrap hybrid high-resolution mass spectrometer. Product ion spectra from HCD are in many cases complementary to CID mass spectra and often give more product ions in the low-mass range. However, many product ions may be observed with both techniques, though at different relative intensities. The data from HRMS/MS (Tab. 8-12 and Fig. 35-39) was used to verify product ion assignments obtained from (low-resolution) CID-MS/MS.

Target-high-resolution tandem mass spectrometry analysis was only performed on the microcystins and other cyanopeptides that were detectable in the crayfish tissue (Fig. 34).

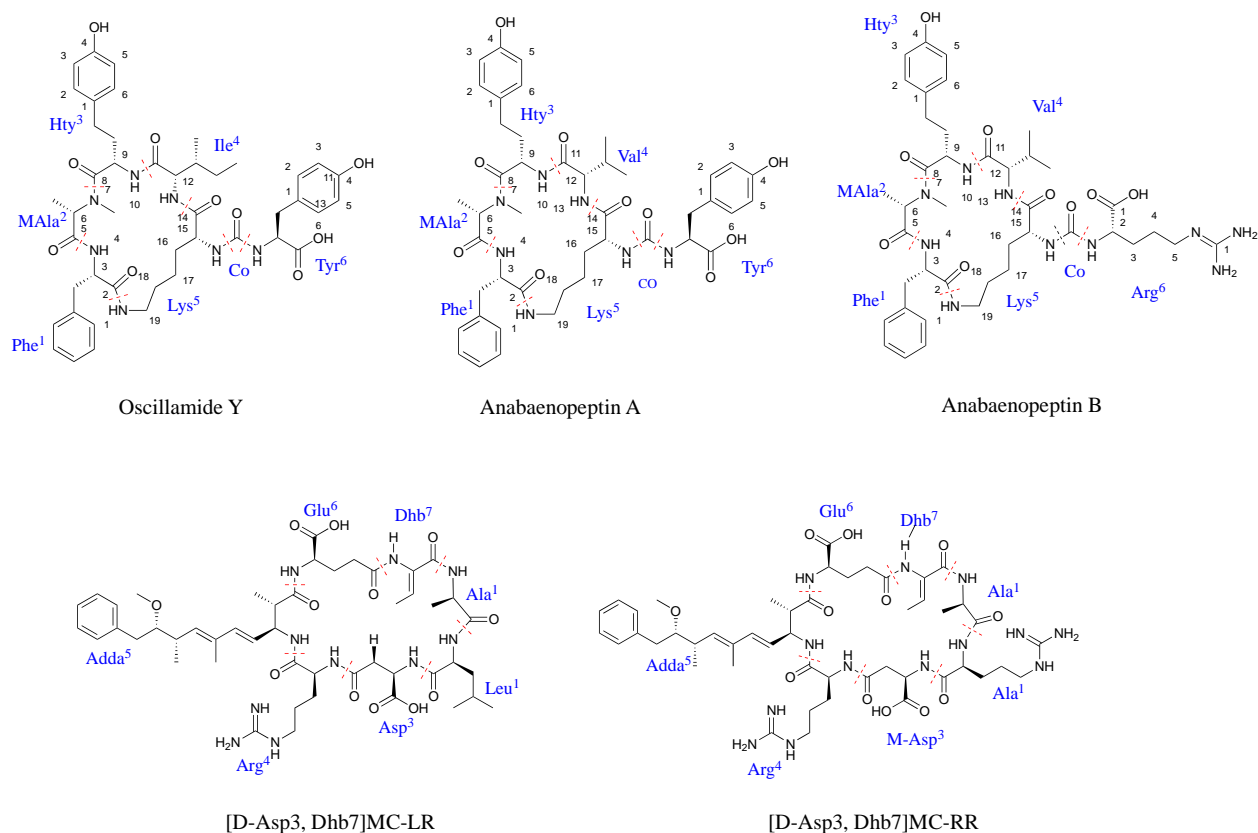


Figure 34: Microcystins and the anabaenopeptins detectable in crayfish tissue. Dashed, red, lines are separating the amino acids. The abbreviations of the amino acids/functional groups (CO) are marked in blue.

HRMS/MS spectra of the microcystins and anabaenopeptins (Fig. 35-39) gave several product ions confirming the molecular structure of the microcystins and anabaenopeptins detectable in crayfish tissue. The product ion spectra compared well to those obtained from HRMS/MS of the reference materials (standards; 200 ng/mL, anabaenopeptin A, anabaenopeptin B, Oscillamide Y, [D-Asp³, Dhb⁷]MC-RR and [D-Asp³, Dhb⁷]MC-LR) using PRM and an absolute, stepped CE of 30, 60, 80 eV (Tab. 8-12) or a NCE of 35%. Molecular formula of product ions obtained with an accuracy limit of 5.0000 ppm.

Table 8: Assignments of the observed product ions and their m/z from high energy collision induced dissociation with anabaenopeptin B as $[M+H]^+$. The exact mass of the product ions, the fragment formula and the accuracy is also shown.

Fragment ion assignment	Exact mass	m/z	Accuracy (ppm)	Molecular formula of product ion
[M+H] ⁺	837.4618	837.4603	-0.015	C ₄₁ H ₆₁ N ₁₀ O ₉ ⁺
[Phe ¹ -MAla ² -Hty ³ -Val ⁴ -Lys ⁵ +H] ⁺	637.3708*	637.3708	-0.015	C ₃₄ H ₄₉ N ₆ O ₆ ⁺
[MAla ² -Hty ³ -Val ⁴ +H] ⁺	362.2074	362.2067	-2.106	C ₁₉ H ₂₈ N ₃ O ₄ ⁺
[Hty ³ -Val ⁴ +H] ⁺	277.1547*	277.1534	-4.687	C ₁₅ H ₂₁ O ₃ N ₂ ⁺
[MAla ² -Hty ³ +H] ⁺	263.1390	263.1391	-0.232	C ₁₄ H ₁₉ N ₂ O ₃ ⁺
[MAla ⁴ +Co] ⁺	114.0550	114.0547	-2.324	C ₅ H ₈ O ₂ N ⁺
[MAla ² -Phe ¹ +H] ⁺	233.1285	233.1280	-1.992	C ₁₃ H ₁₇ O ₂ N ₂ ⁺
[Hty ³ -Val ⁴ +H] ⁺	249.1598	249.1596	-0.740	C ₁₄ H ₂₁ O ₂ N ₂ ⁺
[Co-Arg+H] ⁺	201.0982	201.0977	-2.769	C ₇ H ₁₃ O ₃ N ₄ ⁺
[Arg-NH ₂] ⁺	158.0924	158.0921	-2.044	C ₆ H ₁₂ O ₂ N ₃ ⁺
[Arg+H] ⁺	175.1190	175.11886	-0.840	C ₆ H ₁₅ O ₂ N ₄ ⁺
[MAla ² +H] ⁺	86.0600	86.0599	-2.097	C ₄ H ₈ O ₂ N ⁺

*Product ions also observed in tandem (MS²) ion trap mass spectra are marked with an asterisk.

Table 9: Assignments of the observed product ions and their m/z from higher-energy collision induced dissociation of anabaenopeptin A as [M+H]⁺. The exact mass of the product ions, the product ion formulae and the accuracy is also shown.

Fragment ion assignment	Exact mass	m/z	Accuracy (ppm)	Molecular formula of product ion
[M+H] ⁺	844.4240	844.4240	-0.015	C ₄₄ H ₅₈ N ₇ O ₁₀ ⁺
[M-MAla ² +H] ⁺	759.3712*	759.3724	1.562	C ₄₀ H ₅₁ O ₉ N ₆ ²⁺
[Val ⁴ -Lys ⁵ -Co-Tyr ³ -Phe ¹ -MAla ² +CH ₂ +H] ⁺	681.3606*	681.3601	-0.850	C ₃₅ H ₄₉ O ₈ N ₆ ²⁺
[Val ⁴ -Lys ⁵ -CO-Tyr ⁶ -Phe ¹ -MAla ² +H] ⁺	667.3450*	667.3450	-2.740	C ₃₄ H ₄₇ N ₆ O ₈ ⁺
[Phe ¹ -MAla ² -Hty ³ -Val ⁴ -Lys ⁵ +H] ⁺	637.3708*	637.3699	-1.396	C ₃₄ H ₄₉ N ₆ O ₆ ⁺
[Lys ⁵ -Co-Tyr ³ -Phe ¹ -Mala ² +H] ⁺	568.2766*	568.2759	-1.240	C ₂₉ H ₃₈ O ₇ N ₅ ⁺
[Val ⁴ -Lys ⁵ -Co-Tyr ⁶ -Phe ¹ +H] ⁺	582.2922	582.2932	1.726	C ₃₀ H ₄₀ O ₇ N ₅ ⁺
[Phe ¹ -Mala ² -Hty ³ -Val ⁴ +H] ⁺	509.2758	509.2753	-0.995	C ₂₈ H ₃₇ O ₅ N ₄ ⁺
[Mala ² -Hty ³ -Val ⁴ +2H] ⁺	362.2074	362.2061	-3.652	C ₁₉ H ₂₈ O ₄ N ₃ ⁺
[Hty ³ -Val ⁴ +H] ⁺	277.1547*	277.1541	-1.981	C ₁₅ H ₂₁ O ₃ N ₂ ⁺

[Mala ² -Hty ³ + H] ⁺	263.1390*	263.1385	-2.124	C ₁₄ H ₁₉ O ₃ N ₂ ⁺
[Mala ² -Phe ¹ + H] ⁺	233.1285	233.1282	-1.262	C ₁₃ H ₁₇ O ₂ N ₂ ⁺
[Hty ³ -Val ⁴ +H] ⁺	249.1598	249.1598	-0.062	C ₁₄ H ₂₁ O ₂ N ₂ ⁺
[M-Ala ² + H] ⁺	86.0600	86.05995	-1.051	C ₄ H ₈ ON ⁺
[Lys ⁵ -Co-NH ₂] ⁺				

*Product ions also observed in tandem (MS²) ion trap mass spectra are marked with an asterisk.

Table 10: Assignments of the observed product ions and their m/z from high energy collision induced dissociation with Oscillamide Y as [M+H]⁺. The exact mass of the product ions, the fragment formula and the accuracy is also shown.

Fragment ion assignment	Exact mass	m/z	Accuracy (ppm)	Molecular formula of product ion
[M+H] ⁺	858.4396	858.4383	-0.015	C ₄₅ H ₆₀ N ₇ O ₁₀ ⁺
[Ile ⁴ -Lys ⁵ -Co-Tyr ³ -Phe ¹ -MAla ² +CH ₂ +H] ⁺	695.3763*	695.3761	-0.200	C ₃₆ H ₅₁ O ₈ N ₆ ⁺
[Phe ¹ -MAla ² -Hty ³ -Ile ⁴ -Lys ⁵ + H] ⁺	651.3865*	651.3848	-2.517	C ₃₅ H ₅₁ N ₆ O ₆ ⁺
[Lys ⁵ -Co-Tyr ³ -Phe ¹ -MAla ² +H] ⁺	568.2766*	568.2740	-4.602	C ₂₉ H ₃₈ O ₇ N ₅ ⁺
[Ile ⁴ -Lys ⁵ -Co-Tyr ⁶ -Phe ¹ +H] ⁺	596.3079	596.3086	1.853	C ₃₁ H ₄₂ O ₇ N ₅ ⁺
[Phe ¹ -MAla ² -Hty ³ -Ile ⁴ + 2H] ⁺	523.2920	529.2907	-1.504	C ₂₉ H ₃₉ O ₅ N ₄ ⁺
[Mala ² -Hty ³ -Ile ⁴ + 2H] ⁺	376.2231	376.2225	-1.470	C ₂₀ H ₃₀ N ₃ O ₄ ⁺
[Hty ³ -Ile ⁴ + H] ⁺	291.1703*	291.1697	-2.058	C ₁₆ H ₂₃ O ₃ N ₂ ⁺
[MAla ² -Hty ³ + H] ⁺	263.1390*	263.1389	-0.300	C ₁₄ H ₁₉ N ₂ O ₃ ⁺
[MAla ² -Phe ¹ + H] ⁺	233.1285	233.1276	-3.536	C ₁₃ H ₁₇ O ₂ N ₂ ⁺
[Hty ³ -Val ⁴ +H] ⁺	291.1703	291.1697	-2.058	C ₁₄ H ₂₃ O ₃ N ₂ ⁺
[MAla ² + 2H] ⁺	86.0600	86.0598	-2.329	C ₄ H ₈ ON ⁺

*Product ions also observed in tandem (MS²) ion trap mass spectra are marked with an asterisk.

Table 11: Assignments of the observed product ions and their m/z from high energy collision induced dissociation with [D-Asp³, Dhb⁷]MC-RR as [M+H]⁺. The exact mass of the product ions, the fragment formula and the accuracy is also shown.

Fragment ion assignment	Exact mass	m/z	Accuracy (ppm)	Molecular formula of product ion
[M+H] ⁺	1024.5574	1024.5549	-2.431	C ₄₈ H ₇₄ N ₁₃ O ₁₂ ⁺
[M-NH ₂ + H] ⁺	1008.5387	1008.5364	-2.337	C ₄₈ H ₇₂ O ₁₂ N ₁₂ ⁺

[M-H ₂ O + H] ⁺	1006.5469*	1006.5447	-2.162	C ₄₈ H ₇₂ O ₁₁ N ₁₃ ⁺
[M-Asp ³ + H] ⁺	909.5305*	909.5329	2.652	C ₄₄ H ₆₉ O ₉ N ₁₂ ⁺
[Arg ⁴ -Adda ⁵ -Glu ⁶ -Dhb ⁷ -Ala ¹ + H] ⁺	753.4294*	753.4262	-4.243	C ₃₈ H ₅₇ O ₈ N ₈ ⁺
[Asp ³ -Arg ⁴ -Adda ⁵ -Glu ⁶ +H] ⁺	714.3821*	714.3797	-3.405	C ₃₅ H ₅₂ O ₉ N ₇ ⁺
[Arg ⁴ -Adda ⁵ -Glu ⁶ -Dhb ⁷ +H] ⁺	682.3923*	682.3931	1.241	C ₃₅ H ₅₂ O ₇ N ₇ ⁺
[Arg ⁴ -Adda ⁵ -Glu ⁶ + H] ⁺	599.3552*	599.3535	-2.802	C ₃₁ H ₄₇ O ₆ N ₆ ⁺
[Glu ⁶ -Dhb ⁷ -Ala ¹ -Arg ² -Asp ³ + H] ⁺	555.2522	555.2514	-1.317	C ₂₂ H ₃₅ O ₉ N ₈ ⁺
[Glu ⁶ -Dhb ⁷ -Ala ¹ -Arg ² + H] ⁺	440.2252	440.2260	1.753	C ₁₈ H ₃₀ O ₆ N ₇ ⁺
[Dhb ⁷ -Ala ¹ -Arg ² -Asp ³ + H] ⁺	426.2096	426.2089	-1.661	C ₁₇ H ₂₈ O ₆ N ₇ ⁺
[Adda ⁵ -Glu ⁶ -Dhb ⁷ -Adda frag. -NH ₂ + H] ⁺	375.1915	375.1911	-0.982	C ₂₀ H ₂₇ O ₅ N ₂
[Dhb ⁷ -Ala ¹ -Arg ² + H] ⁺	311.1826	311.1823	-0.852	C ₁₃ H ₂₃ O ₃ N ₆
[Asp ³ -Arg ⁴ +H] ⁺ /[Arg ² - Asp ³ + H] ⁺	272.1353	272.1345	-3.162	C ₁₀ H ₁₈ O ₄ N ₅ ⁺
[Glu ⁶ -Dhb ⁷ + H] ⁺	213.0870	213.0865	-2.409	C ₉ N ₁₃ O ₄ N ₂
[Asp ³ -Arg ⁴ -NH ₂] ⁺	255.1093	255.1081	-2.828	C ₁₀ H ₁₅ O ₄ N ₄ ⁺
[Arg ^{2/4} +H] ⁺	157.1084	157.1083	-0.558	C ₆ H ₁₃ ON ₄ ⁺
[Adda frag.+H] ⁺	135.0804	135.0803	-1.270	C ₉ H ₁₁ O ⁺

*Product ions also observed in tandem (MS²) ion trap mass spectra are marked with an asterisk.

Table 12: Assignments of the observed product ions and their m/z from high energy collision induced dissociation with [D-Asp³, Dhb⁷]MC-LR as [M+H]⁺. The exact mass of the product ions, the fragment formula and the accuracy is also shown.

Fragment ion assignment	Exact mass	m/z	Accuracy (ppm)	Molecular formula of product ion
[M+H] ⁺	981.5404	981.5379	-2.571	C ₄₈ H ₇₃ N ₁₀ O ₁₂ ⁺
[M-NH ₃ +H] ⁺	964.5139*	964.5160	-2.265	C ₄₈ H ₇₀ O ₁₂ N ₉ ⁺
[M - Co + H] ⁺	953.5455*	953.5422	-3.387	C ₄₇ H ₇₃ O ₁₁ N ₁₀ ⁺
[M-Asp ³ + H] ⁺	866.5135*	866.5142	0.910	C ₄₄ H ₆₈ O ₉ N ₉ ⁺
[M-Adda frag. + 2H] ⁺	847.4672	847.4689	1.960	C ₃₉ H ₆₃ O ₁₁ N ₁₀ ⁺
[M-Adda frag. -NH ₃ + H] ⁺	830.4407	830.4406	-0.157	C ₃₉ H ₆₀ O ₁₁ N ₉ ⁺
[Arg ⁴ -Adda ⁵ -Glu ⁶ -Dhb ⁷ -Ala ¹ + H] ⁺	753.4294*	753.4262	-4.243	C ₃₈ H ₅₇ O ₈ N ₈ ⁺
[Asp ³ -Arg ⁴ -Adda ⁵ -Glu ⁶ + H] ⁺	714.3821*	714.3795	-3.601	C ₃₅ H ₅₂ O ₉ N ₇ ⁺
[Arg ⁴ -Adda ⁵ -Glu ⁶ -Dhb ⁷ + H] ⁺	682.3923*	682.3923	0.039	C ₃₅ H ₅₂ O ₇ N ₇ ⁺

[Arg ⁴ -Adda ⁵ -Glu ⁶ + H] ⁺	599.3552*	599.3560	1.352	C ₃₁ H ₄₇ O ₆ N ₆ ⁺
[Ala ⁴ -Leu ² -Asp ³ -Arg ⁴ - NH ₃] ⁺	539.2936*	539.2944	1.498	C ₂₃ H ₃₉ O ₇ N ₈ ⁺
[Ala ⁴ -Leu ² -Asp ³ -Arg ⁴ + H] ⁺	456.2565*	456.2570	1.122	C ₁₉ H ₃₄ O ₆ N ₇ ⁺
[Ala ⁴ -Leu ² -Asp ³ -Arg ⁴ - NH ₃ + H] ⁺	439.2305*	439.2296	-0.749	C ₁₉ H ₃₁ O ₆ N ₆
[Leu ² -Asp ³ -Arg ⁴ + H] ⁺	385.2194	385.2189	-1.284	C ₁₆ H ₂₉ O ₅ N ₆ ⁺
[Dhb ⁷ -Ala ¹ -Leu ² -Asp ³ + H] ⁺	383.1925	426.2089	-1.661	C ₁₇ H ₂₇ O ₆ N ₄ ⁺
[Adda ⁵ -Glu ⁶ -Dhb ⁷ - Adda frag. - NH ₂ + H] ⁺	375.1915	375.1906	-2.235	C ₂₀ H ₂₇ O ₅ N ₂
[Asp ³ -Arg ⁴ + H] ⁺	272.1353	272.1347	-2.354	C ₁₀ H ₁₈ O ₄ N ₅ ⁺
[Dhb ⁷ -Ala ¹ -Leu ² + H] ⁺	268.1656	268.1659	1.424	C ₁₃ H ₂₂ O ₃ N ₃ ⁺
[Asp ³ -Arg ⁴ -NH ₂] ⁺	255.1093	255.1080	-3.259	C ₁₀ H ₁₅ O ₄ N ₄ ⁺
[Glu ⁶ -Dhb ⁷ + H] ⁺	213.0870	213.0865	-2.081	C ₉ N ₁₃ O ₄ N ₂ ⁺
[Arg ⁴ + H] ⁺	157.1084	157.1082	-1.067	C ₆ H ₁₃ ON ₄ ⁺
[Adda frag. + CH ₂ +CH ₂ +H] ⁺	163.1117	163.1115	-1.604	C ₁₁ H ₁₅ O ⁺
[Adda frag. + H] ⁺	135.0804	135.0802	-1.862	C ₉ H ₁₁ O ⁺

*Product ions also observed in tandem (MS²) ion trap mass spectra are marked with an asterisk.

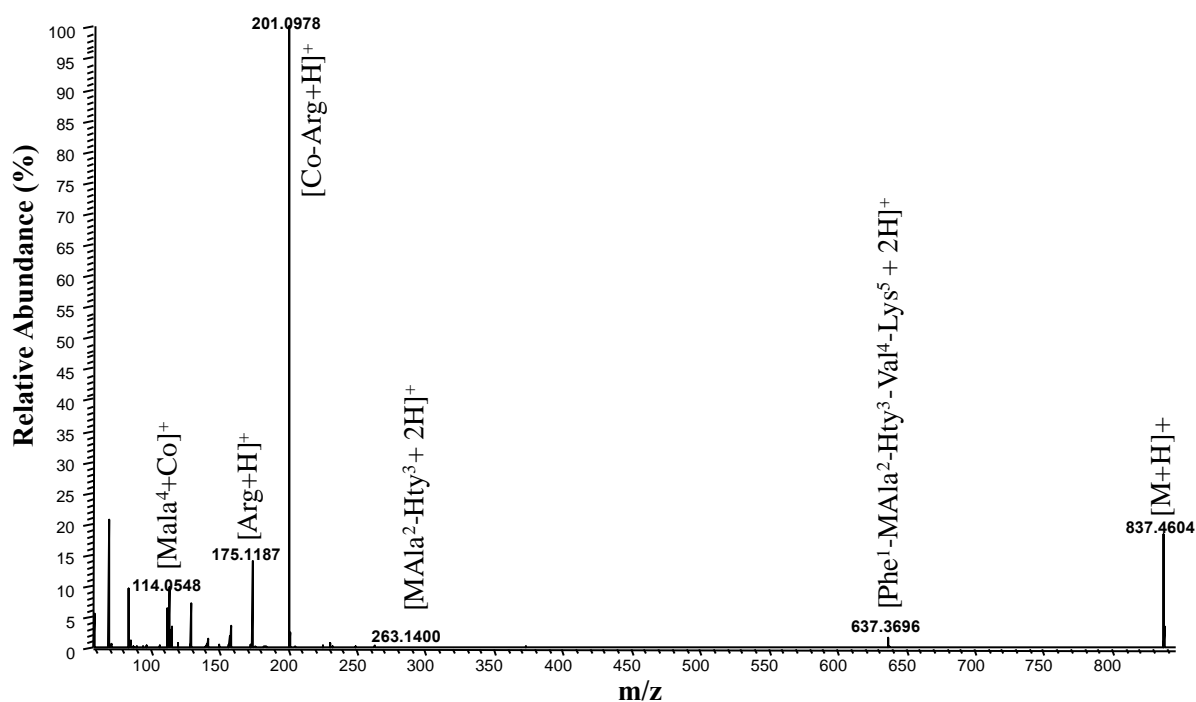


Figure 35: Tandem (MS²) mass spectrum from higher-energy collision induced dissociation of [M+H]⁺ of anabaenopeptin A (*m/z* of 837.4618.3) as [M+H]⁺. Product ions are shown with their assigned amino acid sequence in brackets.

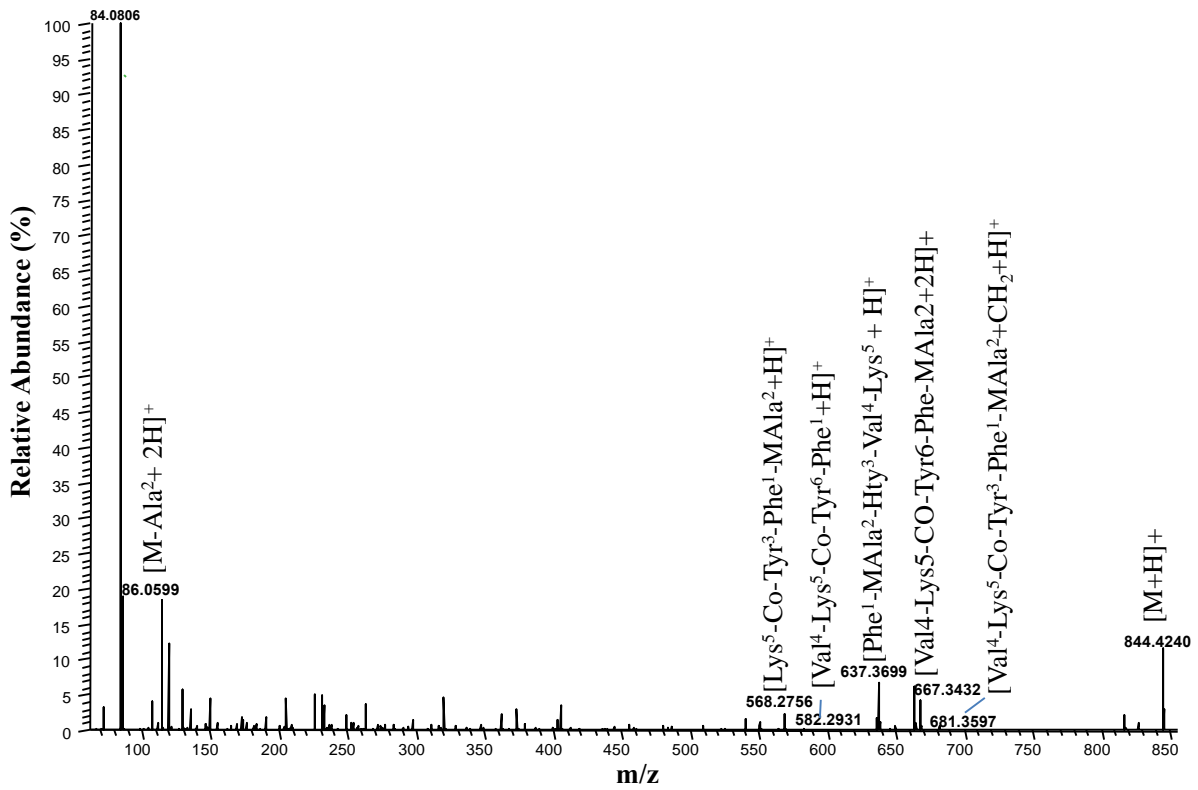


Figure 36: Tandem (MS²) mass spectrum from higher-energy collision induced dissociation of [M+H]⁺ of anabaenopeptin A (*m/z* of 844.4240) as [M+H]⁺. Product ions are shown with their assigned amino acid sequence in brackets.

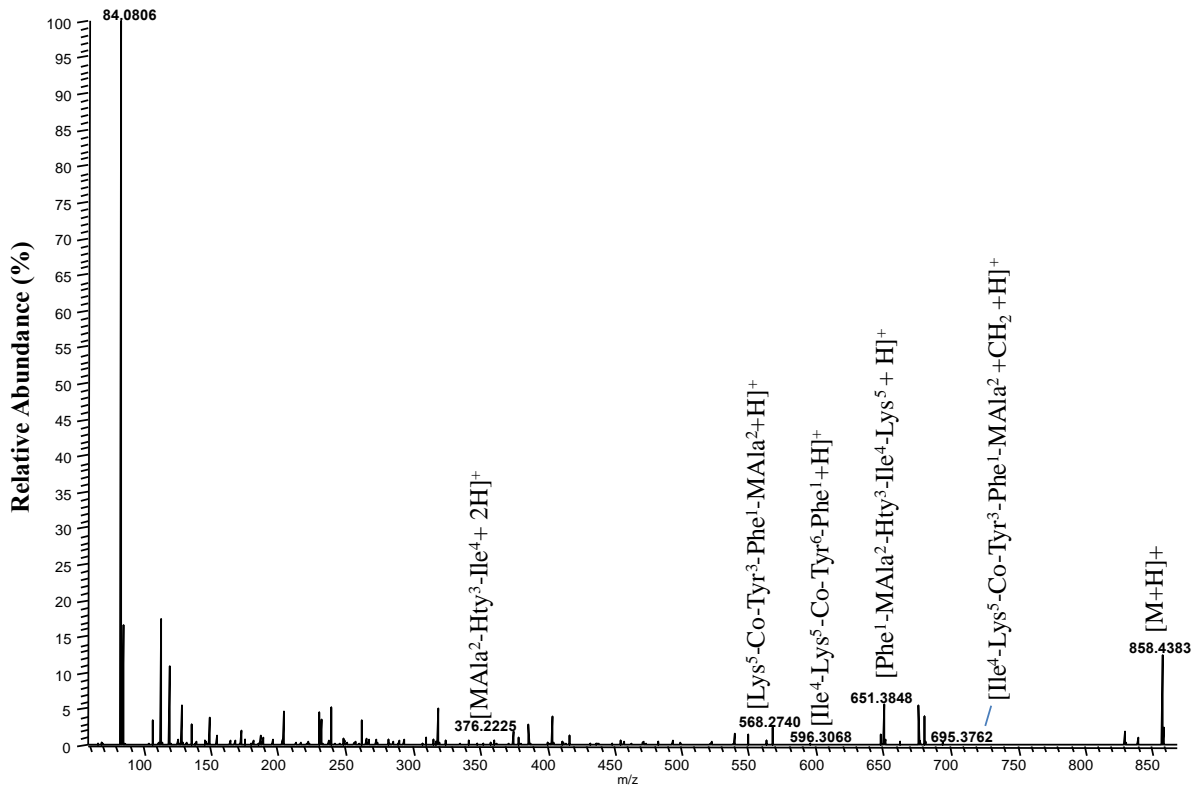


Figure 37: Tandem (MS²) mass spectrum from higher-energy collision induced dissociation of [M+H]⁺ of oscillamide Y (*m/z* of 858.4396) as [M+H]⁺. Product ions are shown with their assigned amino acid sequence in brackets.

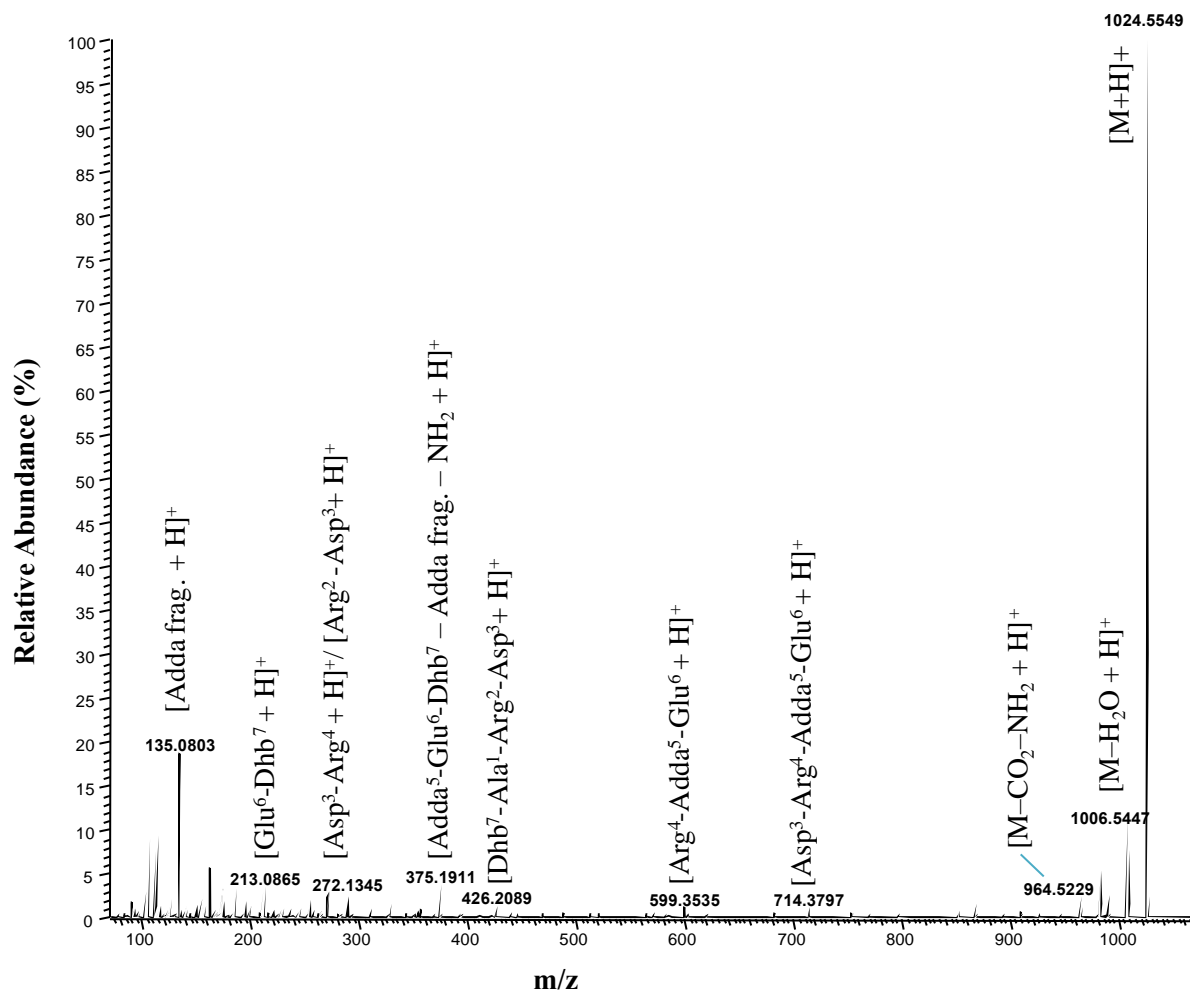


Figure 38: Tandem (MS²) mass spectrum from higher-energy collision induced dissociation of [M+H]⁺ of [D-Asp³, Dhb⁷]MC-RR (*m/z* of 1025.5574) as [M+H]⁺. Product ions are shown with their assigned amino acid sequence in brackets.

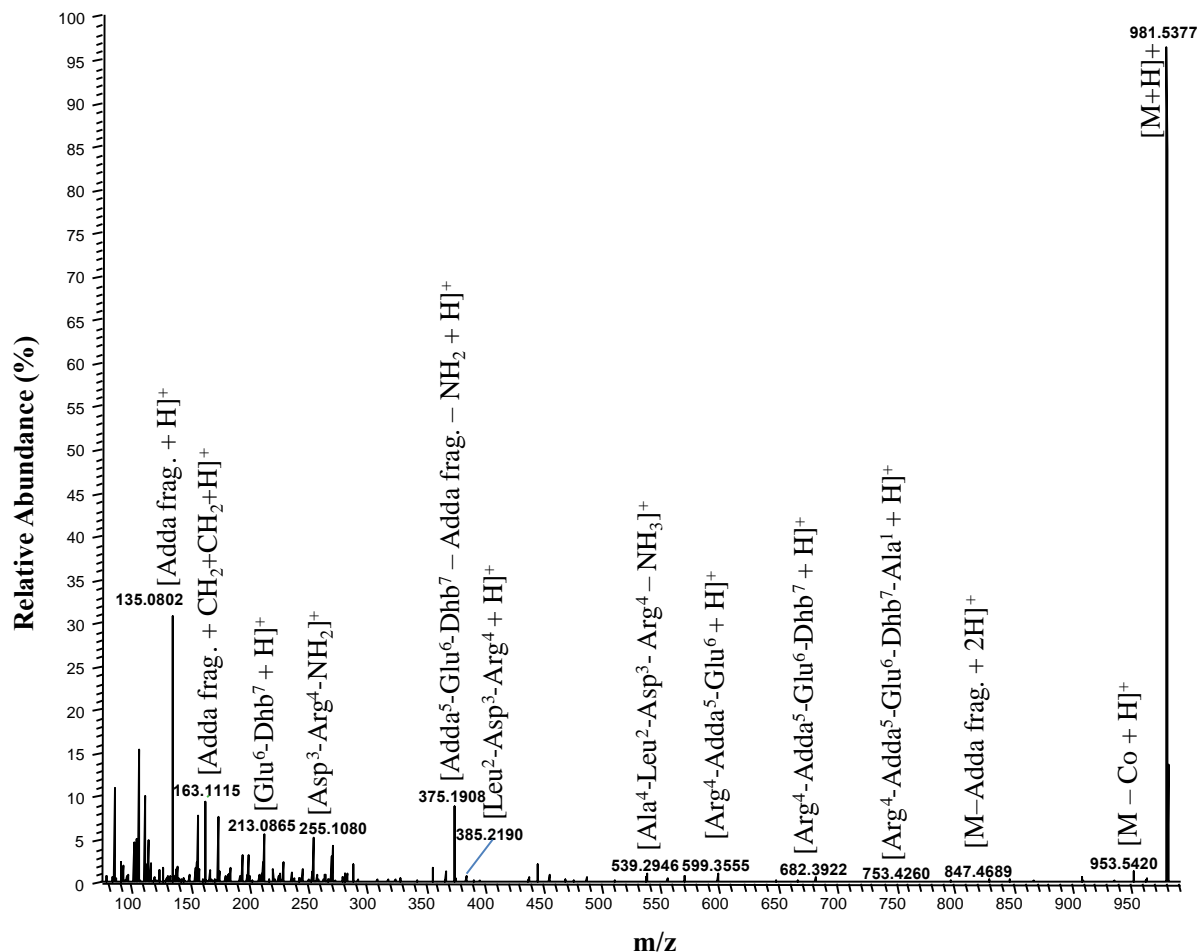


Figure 39: Tandem (MS²) mass spectrum from higher-energy collision induced dissociation of [M+H]⁺ of [D-Asp³, Dhb⁷]MC-LR (*m/z* of 981.5404) as [M+H]⁺. Product ions are shown with their assigned amino acid sequence in brackets.

HRMS/MS (Tab. 8-12 and Fig. 35-39) provided several product ions that were also obtained from (low-resolution) CID-MS/MS. The reference materials yielded similar results as NIVA-CYA98 in both HRMS/MS and CID-MS/MS. Combined with the assignment of amino acids to peaks, this made it possible to confirm the microcystins and anabaenopeptins in NIVA-CYA98.

5.6 Correction of concentration

The concentrations of the standards [Asp³]MC-LR and [Asp³, Dhb⁷]MC-RR from Enzo Life Science were analysed with NMR-quantitated standards of [Asp³]MC-LR and [Asp³, Dhb⁷]MC-RR from NRC. The original concentrations (Tab. 13, column 1) was then corrected according to the NRC standards (Tab. 13, column 2-3).

Table 13: Original concentrations of [Asp³]MC-LR and [Asp³, Dhb⁷]MC-RR standards and corrected concentrations using [Asp³]MC-LR and [Asp³, Dhb⁷]MC-RR.

Original concentration (ng/mL)	[D-Asp ³ , Dhb ⁷]MC-RR (ng/mL)	[D-Asp ³]MC-LR (ng/mL)
0.500	0.431	0.547
1.00	0.862	1.094
5.00	4.308	5.469
15.0	12.923	16.407
25.0	21.538	27.345
50.0	43.077	54.69
100	86.154	109.38

The results (Tab. 13) show a significant difference between the concentrations in the standards from Enzo Life Science (reference materials) and standards from NRC (certified reference materials). This type of correction should ideally have been done with all the quantified analytes, but these were the only ones available.

5.7 Microcystins and other cyanopeptides in NIVA-CYA98

Microcystins and other peptides in NIVA-CYA98 was identified using standards, β -mercaptoethanol derivatisation and tandem (MS^2) mass spectrometry. There has been a larger focus on determination of the analytes that were detectable in the crayfish samples. Use of standards determined the m/z (and accordingly the exact mass) of the analytes. This suggested that NIVA-CYA98 contained three microcystins with m/z of 1024.5574/512.7824, 1045.5353 and 981.5404. Standards were also used to compare retention time of analytes in standards and NIVA-CYA98. Subsequently, screening for MC analogs using various LC–HRMS approaches confirmed that the three analogs contained the characteristic Adda fragment (m/z 135.0804). It also clarified the abundance of the different analytes and showed that NIVA-CYA98 also contains an oxygenated analog of the predominating microcystin (Fig. 21). Mass spectra (Appendix C, Fig. C4-C7) of the microcystins in addition to the toxin mass list was used for further structure elucidation. There are various microcystins with identical m/z (Fig 3). Determination of the amino acid in position 7 made it possible to distinguish between different isoforms. β -mercaptoethanol derivatisation determined showed that NIVA-CYA98 produce microcystins with Dhb in position 7. Qualbrowser was used to calculate the molecular formula and mass error of other cyanopeptides, which were further confirmed with standards and MS^2 .

Tandem (MS^2) mass spectrometry was the final step in the structure elucidation. Ion trap tandem mass spectrometry, (low resolution) and quadrupole-orbitrap tandem mass

spectrometry, high resolution yielded product ions in both high- and low mass range. Assignment of amino acids to product ions in the tandem (MS²) mass spectra made it possible to complete the structure elucidation. NIVA-CYA98 contains [D-Asp³, Dhb⁷]MC-RR (predominant microcystin), oxygenated [D-Asp³, Dhb⁷]MC-RR, [D-Asp³, Dhb⁷]MC-LR, [D-Asp³, Dhb⁷]MC-HtyR, anabaenopeptin B, anabaenopeptin A and oscillamide Y. Of these, [D-Asp³, Dhb⁷]MC-RR, [D-Asp³, Dhb⁷]MC-LR, anabaenopeptin B, anabaenopeptin A and oscillamide Y were detectable in crayfish tissue.

5.8 Evaluation of method performance

The validation tools were used to determine the suitability of the chosen method.

5.8.1 LOQ and LOQ

The LOD and LOQ (Tab. 14) were calculated using matrix-matched standards from four different days. Signal suppression/enhancement was calculated from the same data material.

Table 14: LOD (ng/g), LOQ (ng/g) and SSE (%) for all detectable peptides in crayfish samples from muscle (M) and hepatopancreas (HP) tissue.

Peptide		Anabaenopeptin B	Anabaenopeptin A	Oscillamide Y	[D-Asp ³ , Dhb ⁷] MC-RR	[D-Asp ³ , Dhb ⁷] MC-LR
Tissue						
M	LOD (ng/g)	12.6	13.5	19.8	16.2	23.4
	LOQ (ng/g)	41.4	45.0	66.6	54.0	77.4
	SSE, %	104	86.9	90.1	78.3	112
HP	LOD (ng/g)	21.6	7.20	15.3	31.5	9.90
	LOQ (ng/g)	73.8	22.5	52.2	104	32.4
	SSE, %	87.5	57.0	73.0	93.5	85.8

The provisional TDI set by WHO is 0.04 µg per/kg body weight. This means that that a person of 70 kg may eat 2.8 µg MC each day without exceeding the TDI. A child of 30 kg can eat 1.2 µg without exceeding the limit. Considering that most people do not consume crayfish every day, these values may be translated to 19.6 µg and 8.4 µg per week.

A normal serving of crayfish usually includes 1 kg whole animals, approximately yielding 100 g muscle tissue. The LOQ for muscle tissue (Tab. 14) is 0.054 µg/g for [D-Asp³, Dhb⁷]MC-RR and 0.077 µg/g for [D-Asp³, Dhb⁷]MC-LR. A serving of crayfish will hence

give 5.4 μg [D-Asp³, Dhb⁷]MC-RR and 7.7 μg [D-Asp³, Dhb⁷]MC-LR. Considering these values separately for the two microcystins, results below LOQ (Tab. 14) will not be considered as harmful. A person of 70 kg would be able to eat 350 g/week without exceeding the provisional guidelines, while a child of 30 kg would be able to eat 150 g/week (if the crayfish only contained [D-Asp³, Dhb⁷]MC-RR). If the quantitative results yielded values <LOQ (but >LOD) for both microcystins, a serving of crayfish could possibly contain 13 μg microcystins without being quantified. This is still below the provisional guidelines for a person with a weight of 70 kg, but above the guidelines for children with a weight of 30 kg.

These calculations show that results below the value of LOQ will not exceed the guidelines given by WHO (for adults) and may hence be considered as not harmful when it comes to muscle tissue. For [D-Asp³, Dhb⁷]MC-RR in hepatopancrea tissue, LOQ is 0.104 $\mu\text{g}/\text{g}$ (Tab. 14). In this case one would exceed the provisional guidelines by eating less than two grams of hepatopancreas tissue. These values may therefore be harmful even if they are below LOQ. This is however not a problem because in this study because the majority of hepatopancreas tissue samples yielded microcystin values >LOQ. There are no provisional guidelines regarding anabaenopeptins.

Additionally, the results show that there was in part substantial signal suppression or enhancement of individual compounds, both in muscle and hepatopancreas tissues. Hepatopancreas tissue show signal suppression for all peptides, with the signal of anabaenopeptin A being most suppressed (57%). This percentage illustrates how much the matrix effects the calibration curve and indicates that the quantitative results (Appendix D, Fig D1-D2) for all peptides in the hepatopancreas tissue samples, and anabaenopeptin A, oscillamide Y and [D-Asp³, Dhb⁷]MC-RR in muscle tissue samples would have been underestimated without use of a matrix-matched standards. [D-Asp³, Dhb⁷]MC-LR and anabaenopeptin B would have been slightly overestimated in muscle tissue samples.

No matrix-matched standards are identical to the sample, and ideally one would have used an internal standard. Internal standards are however not available for microcystins due to the large variety of analogues and different times of elution.

5.8.2 Spike recovery

Spike-recovery trials were conducted in order to assess analyte accuracy. The measured concentrations of spiked muscle samples were $84\% \pm 14$ for anabaenopeptin B, $115\% \pm 10$ for [D-Asp³, Dhb⁷]MC-RR, $129\% \pm 11$ for anabaenopeptin A, $110\% \pm 28$ for oscillamide Y and $82\% \pm 6$ for [D-Asp³, Dhb⁷]MC-LR, N=3. The measured concentrations of spiked hepatopancreas samples were $45\% \pm 14.5$ for anabaenopeptin B, $55\% \pm 3$ for [D-Asp³, Dhb⁷]MC-RR, $71\% \pm 17$ for anabaenopeptin A, 85 ± 61 for oscillamide Y and $67\% \pm 15$ for [D-Asp³, Dhb⁷]MC-LR, N=3.

The results yielded good recovery for muscle tissue, but not as good for hepatopancreas tissue. It is however normal to observe low recovery in hepatopancreas (and liver) tissue. This is believed to be because of high enzymatic activity (Samdal, 2019).

5.8.3 Precision

The inter-day precision was obtained by injecting the same sample six times, on three different days (Appendix E, Fig. E1). An inter-day precision, RSiR (%), below 30% is considered as good on a high-resolution instrument like Q-Exactive (Ivanova et al., 2017). The results showed an inter-day precision between 11.1 % for anabaenopeptin B and 29.0 % for anabaenopeptin A.

5.9 Quantification of microcystins and anabaenopeptins using liquid chromatography–high resolution mass spectrometry

5.9.1 Quantification of microcystins and anabaenopeptins in NIVA-CYA98 (crayfish feed)

Liquid chromatography–high resolution mass spectrometry was performed by Q Exactive to quantify the microcystins and anabaenopeptins in NIVA-CYA98 and crayfish samples obtained from Lake Steinsfjorden. Results acquired with Quan browser, a segment of Xcalibur, made it possible to obtain the quantitative results. The quantification of microcystins and anabaenopeptins in NIVA-CYA98 resulted in good calibration curves (Appendix F, Fig. F2). The chromatograms (Fig. 40) showed narrow peaks, and the mass spectra showed a good accuracy (Fig. 40).

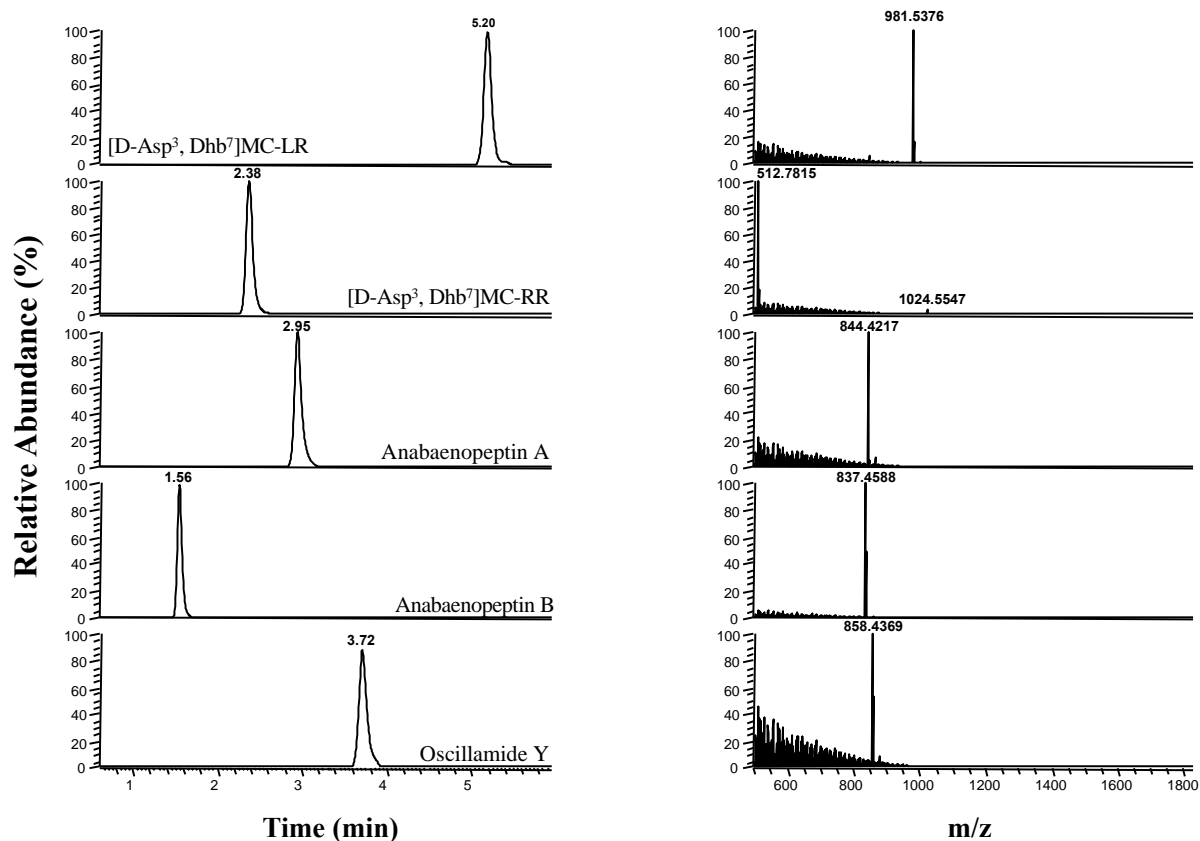


Figure 40: extracted ion chromatograms of $[D\text{-Asp}^3, Dhb^7]MC\text{-LR}$, $[D\text{-Asp}^3, Dhb^7]MC\text{-RR}$, anabaenopeptin A, anabaenopeptin B and oscillamide Y (in NIVA-CYA98) and their associated mass spectra.

Table 6 provides concentrations of analytes detected by LC-MS and ELISA in extracts of NIVA-CYA98. The results show that ELISA and LC-MS have detected an almost identical amount of microcystins (ELISA does not detect anabaenopeptins).

Table 6: Concentrations of the different microcystins and anabaenopeptins (for LC-MS) in the NIVA-CYA98 dry material extract. The result is based on a mean of two dilutions (1:100 and 1:1000). Both results were obtained from the same LC-MS analysis and are shown as ng/g.

NIVA-CYA98 (ng/g)	Anabaenopeptin B	Anabaenopeptin A	Oscillamide Y	$[D\text{-Asp}^3]MC\text{-RR}$	$[D\text{-Asp}^3]MC\text{-LR}$
LC-MS	143.991	1497.026	8048.127	2129.153	145.009
ELISA (total MC)					2217.32

5.9.2 Quantification of microcystins and anabaenopeptins in crayfish tissue

The microcystins and anabaenopeptins showed in Figure 34 are the molecules analysed for in the crayfish samples. [D-Asp³]MC-HtyR and the oxygenated [D-Asp³]MC-RR were not detectable in crayfish material, due to low concentrations in NIVA CYA-98.

The analyses of crayfish samples with matrix-matched standards provided chromatograms that showed good separation (Fig. 41) and acceptable peak shape. The matrix-matched standards resulted in good calibration curves, with an $R^2 > 0.99$ (Appendix F, Fig. F3-F4).

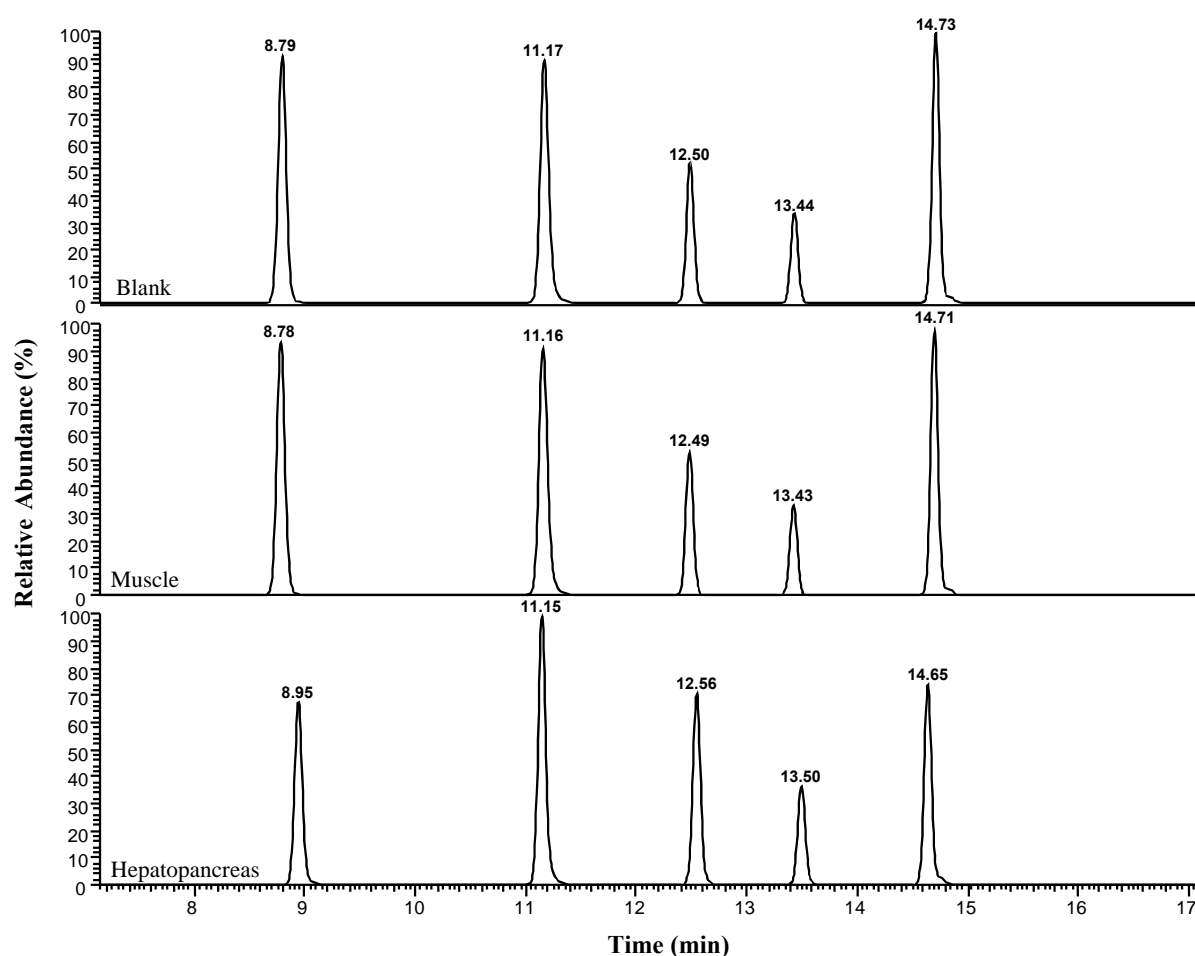


Figure 41: Extracted ion chromatogram of Microcystins and anabaenopeptins in the blank and matrix-matched standards (muscle and hepatopancreas). Retention time of the different species and mobile phase gradient is shown in Appendix B, Table B1.

The quantitative results (Appendix D, Fig. D1) showed that the majority of crayfish samples from muscle tissue yielded values of microcystins that were either not detected or $< \text{LOQ}$ and/or LOD . Muscle tissue samples provided detectable values of analyte in three different samples (five detected peptides), all in the group of crayfish that received NIVA-CYA98 as feed. The largest value of microcystins in crayfish muscle tissue was 82.5 ng/g [D-Asp³,

Dhb⁷]MC-RR in sample 5-D-M. The largest value of anabaenopeptins was 125.4 ng/g Oscillamide Y in sample 20-C-M. There was however possible to see a significant difference between the samples, based on what trial group they originated from. This is illustrated in Figure 42.

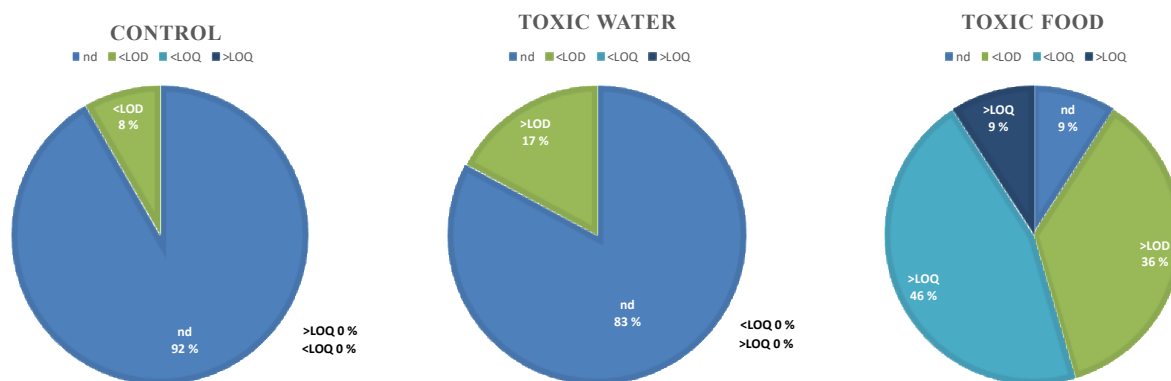


Figure 42: Sector diagram illustrating the percentage of samples that were not detected (n.d.), <LOD, <LOQ or >LOQ for the most abundant microcystin, [D-Asp³, Dhb⁷]MC-RR, in crayfish muscle tissue. The three sector diagrams represent the three different groups of crayfish that took part in the feeding trial; a control group, a group of crayfish receiving NIVA-CYA98 in the water and crayfish receiving NIVA-CYA98 as feed.

The sector diagrams (Fig. 42) illustrate that even though most of the toxins were not detected or showed values below LOD and LOQ, one can clearly see a difference between the three groups. In the group of control crayfish, the analyte was only detected in 6% of the samples, however below the limit of detection. For the group of crayfish that got NIVA-CYA98 added to the water, [D-Asp³, Dhb⁷]MC-RR were not detected in 83% of the samples, while the remaining 17% of the samples yielded results <LOD. For the group of crayfish that received NIVA-CYA98 as feed, 76% of the samples were detected. Only 3% below the limit of detection. This states that the toxins in the biomaterial of *P. rubescens* did have an impact on the crayfish samples.

Because muscle tissue is the part of crayfish that is mainly used as food, these are the results that are most interesting regarding toxic levels of microcystins for humans.

In hepatopancreas tissue samples, microcystins and anabaenopeptins were detected (>LOQ) in almost all the samples in the group that received NIVA-CYA98 as feed. The values were in the range 47.3 ng/g-12866.8 ng/g, with a mean of 2465.6 ng/g for microcystins. For the three

anabaenopeptins, the values were in the range 27.4 ng/g-9000.6 ng/g, with a mean of 1586.8 ng/g.

For microcystins, only one sample in the group that received NIVA-CYA98 in the water gave a value >LOQ. The majority of the samples in this group were detected, but the values was <LOD or/and >LOQ. For the anabaenopeptins, all but two samples in the group of Oscillamide Y were detected, with values ranging from 14.0 ng/g-256.4 ng/g and a mean of 104.0 ng/g. None of the samples in the group anabaenopeptin B gave results >LOQ, while some (nine) samples in the group anabaenopeptin A showed results >LOQ, but most being >LOQ. Also in hepatopancreas tissue samples, there was possible to observe a large difference between the samples in the groups of the feeding trial (Fig. 43). There is also possible to see a difference between the quantitative results from muscle tissue and hepatopancreas tissue.

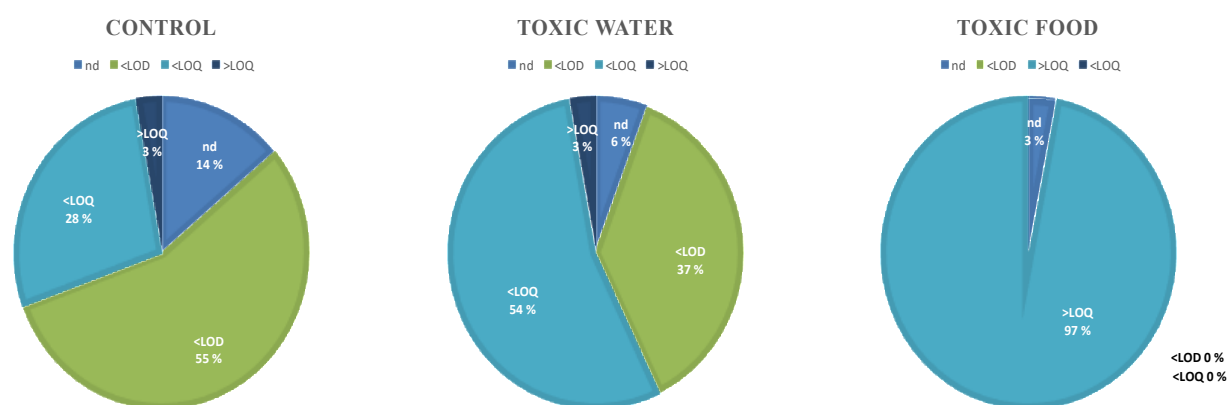


Figure 43: Sector diagram illustrating the percentage of samples that were not detected (n.d.), <LOD, <LOQ or >LOQ for the most abundant microcystin, [D-Asp³]MC-RR, in crayfish hepatopancreas tissue. The three sector diagrams represent the three different groups of crayfish that took part in the feeding trial; a control group, a group of crayfish receiving NIVA-CYA98 in the water and crayfish receiving NIVA-CYA98 as feed.

The group of crayfish that received NIVA-CYA98 as feed, contained detectable microcystins in their hepatopancreas tissue in 97% of the cases. The fact that the control group show detectable results in 31% of the control samples might be due to contamination. Early in the study, it was found that several samples from the control group showed significant signals of microcystins in both hepatopancreas and muscle tissue samples. Contamination of tissue may have happened in the ponds where the crayfish were bred. It was not collected water samples from these ponds. This is however unlikely, because the crayfish were kept inside six months prior to the feeding trial. During this time, all crayfish were treated as the control group. If the

contamination came from the pods, it would have disappeared by the time of the feeding trial. Most likely the contamination happened during homogenization of tissue.

The fact that only three crayfish samples yielded values above LOQ indicates that most samples contained less than 0.054 µg/g of MC-RR. For [D-Asp³, Dhb⁷]MC-LR, no samples yielded values above LOD (0.0234 µg/g), which means that the samples contain less than 0.0234 µg/g of [D-Asp³, Dhb⁷]MC-LR. The largest value of microcystins in muscle tissue is 0.0825 µg/g ([D-Asp³, Dhb⁷]MC-LR), which still allows an adult person to eat more than two servings of crayfish every week without exceeding the provisional tolerable daily intake of microcystins. The calculations do not take into account that one might obtain microcystins from other sources, for instance fish or recreational use (bathing) of the same Lake. The tolerable daily intake is though calculated as a guideline for long term exposure of water. Crayfish as food source does not have a TDI. It seems unlikely that one will receive harmful amounts of microcystins through crayfish (muscle tissue). One should however include other cyanopeptides in monitoring, as the results show that these are just as abundant in crayfish tissue as microcystins (and may also be toxic).

In the group of crayfish that received NIVA-CYA98 as food, the mean value of microcystins in the hepatopancreas samples was 2.46 µg/g. This means that one will exceed the TDI by eating only 1.5 g of hepatopancreas tissue. Hepatopancreas tissue is not considered as an edible part of the crayfish, but but some people eat a larger part of the crayfish. It has earlier been given public advise to remove the intestine when eating crayfish. This will remove over half the MC content in the crayfish tail (Haande et al., 2008). It might be a reasonable food safety precaution to also advise people to not eat hepatopancreas tissue.

The feeding trial was conducted over a time period of six weeks, where six crayfish was removed each week. A histogram showing the amount of detected microcystin [D-Asp³, Dhb⁷]MC-RR in crayfish samples over a time period of six weeks is shown in Figure 44.

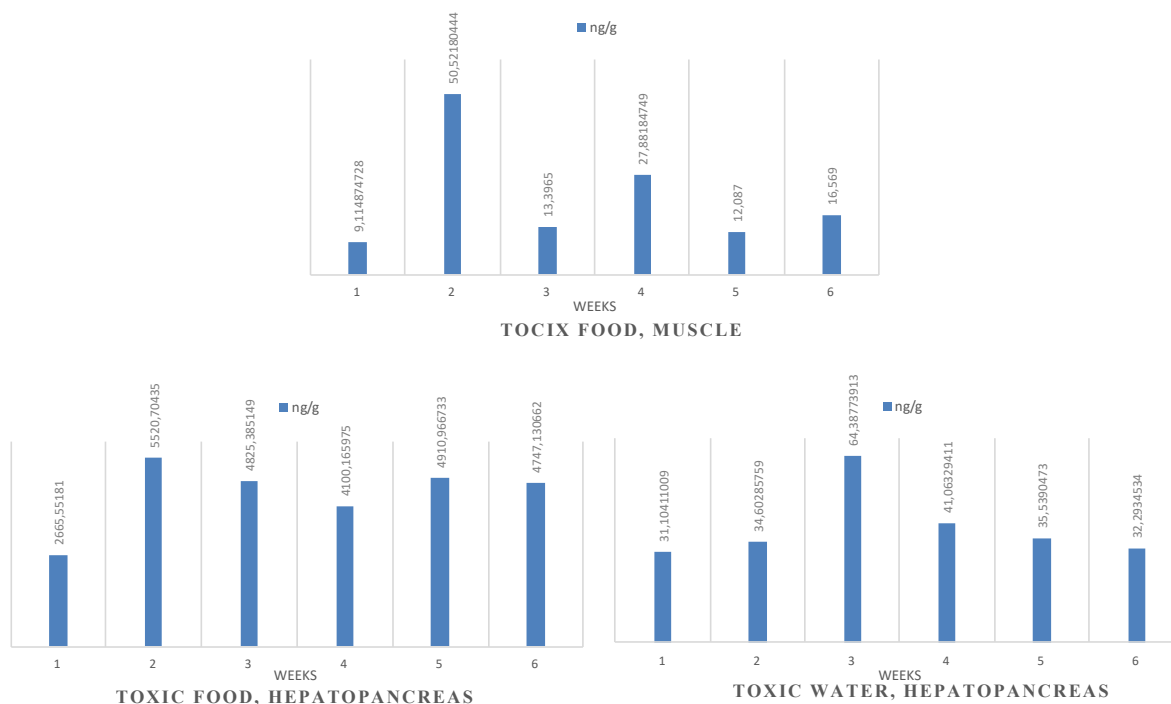


Figure 44: Histograms illustrating the amount (ng/g) of detected [D-Asp³, Dhb⁷]MC-RR in crayfish samples for muscle and hepatopancreas tissue in the groups Toxic Food and Toxic Water. There were not enough detected samples to make a histogram in the group Toxic Water for muscle samples. Results below LOD and LOD were treated as quantitative results.

Figure 44 illustrates that for the crayfish in this trial, time of exposure do not seem to have had an impact on the concentration of microcystins in the tissue. The results (Fig. 44) for [D-Asp³, Dhb⁷]MC-RR corresponds to those of [D-Asp³, Dhb⁷]MC-LR and the anabaenopeptins. This is however a small trial with only six crayfish samples per week.

5.10 Comparison with ELISA results

Due to the large variety of microcystins and the limitation in available standards, it can be challenging to measure the total amount of microcystins in a sample. ELISA is therefore used as a comparison to the quantitative results obtained by LC-MS. This comparison also gives a measure of the credibility of the two methods.

Quantitative results for [D-Asp³, Dhb⁷]MC-LR and [D-Asp³, Dhb⁷]MC-RR, obtained from LC-HRMS were compared with ELISA results. The ELISA method is specific for MCs and NODs and is designed to detect all MCs independent of which sidechains that are represented in position 2 and 4. This method will hence optimally include all the microcystins in the

sample. If the comparison expresses a large deviation between LC–MS and ELISA results, it might indicate that one or more microcystin is not found with LC–MS.

Figure 45 give a graphic comparison of ELISA and LC–MS results for both muscle and hepatopancreas samples.

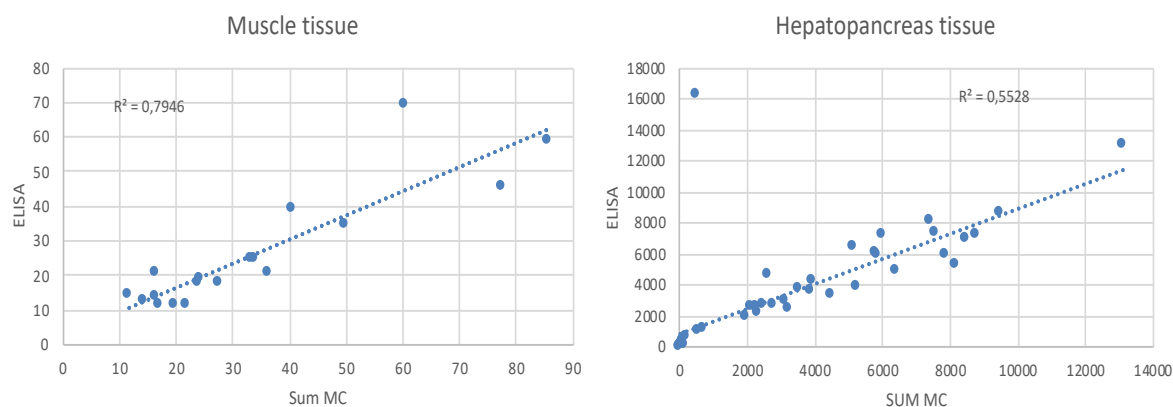


Figure 45: give correlation plots of ELISA and LC–MS for muscle and hepatopancreas crayfish samples. ELISA results (in ng/g) are shown on the y-axis, and LC–MS results (in ng/g) are shown on the x-axis. R^2 is shown in both plots.

The coefficient of determination, R^2 (Fig. 45) illustrate the degree of correlation between ELISA and LC–MS. For muscle tissue samples the R^2 is 0,79, which is good correlation considering the uncertainty of both methods. The relatively low R^2 in the LC–MS vs. ELISA plot for hepatopancreas tissue is the result of a possible outlier. When the possible outlier was removed, R^2 became 0,94. The ELISA result for this data point was 16.200 ng/g, while the LC–MS results was 503 ng/g. This sample was analysed by ELISA twice and gave the same result. For this data point, [D-Asp³, Dhb⁷]MC-RR (the predominant MC) was not found in the diluted sample and was outside the calibration curve in the undiluted sample (with a value of 1655 ng/mL or 14897 ng/g). Due to time limitation, the sample was not analysed a third time by LC–MS, but it is reason to believe that the LC–MS result do actually correlate with the ELISA results.

6. Suggestions for further work

The majority of crayfish muscle samples contained microcystins and other cyanopeptides below the limit of detection and/or the limit of quantification. This problem may be solved by trying to concentrate the crayfish samples by using less solvent/g crayfish tissue.

The biomaterial used as source of microcystins in the feeding trial did not contain any microcystins that can bind to protein. It may be of interest to investigate if these microcystins are detectable by the methods used during this study, and under what conditions the microcystins are released.

To give a more certain result for hepatopancreas samples, it would also be of interest find a method that obtains a higher recovery after addition of spike to hepatopancreas tissue. As this recovery is believed to be corresponding to the recovery in the actual samples.

7. Conclusion

The study revealed that NIVA-CYA98 (used in the feeding trial) contained four microcystins and three other cyanopeptides. By use of β -mercaptoethanol derivatisation, HRMS/MS and (low-resolution) CID-MS/MS, a complete microcystin profile was determined. Two microcystins, [D-Asp³, Dhb⁷]MC-RR and [D-Asp³, Dhb⁷]MC-LR, and three anabaenopeptins, anabaenopeptin A, anabaenopeptin B and oscillamide y, were detectable in crayfish tissue. The concentration of microcystins and anabaenopeptins in muscle tissue were low and fell below the limit of quantification (LOQ) in most of the samples. Hepatopancreas yielded significantly higher results and showed that microcystins and anabaenopeptins accumulates in hepatopancreas. The results found in the study indicate that it is safe to eat muscle tissue from crayfish. Hepatopancreas tissue contains higher concentrations but it not considered as harmful because is not an edible part of the crayfish.

The concentration of microcystins in NIVA-CYA98 obtained by LC-MS were almost identical to the concentration detected by ELISA. Quantitative results of microcystins in crayfish tissue showed good correlation with the earlier obtained ELISA results.

As for method validation, the results yielded acceptable precision, limits of detection (LODs) and limits of quantification (LOQs). Spike experiments showed a good recovery in crayfish muscle tissue, but not as good in hepatopancreas tissue. Quantification using matrix-matched standards provided good calibration curves, all with an R^2 above 0.99.

8. References

- Aune, T. R., H.; Skulleberg, O. M.; Underdal, B.; Yndestad, M.; Østensvik, Ø. . (1997). *Blågrønnalger i Steinsfjorden Sommeren 1997*. Norges Veterinærhøgskole: Institutt for Farmakologi, Mikrobiologi og Næringsmiddelhygiene.
- Bogialli, S., Bortolini, C., Di Gangi, I. M., Di Gregorio, F. N., Lucentini, L., Favaro, G. & Pastore, P. (2017). Liquid chromatography-high resolution mass spectrometric methods for the surveillance monitoring of cyanotoxins in freshwaters. *Talanta*, 170: 322-330. doi: 10.1016/j.talanta.2017.04.033.
- Caller, T., Henegan, P. & Stommel, E. (2018). The Potential Role of BMAA in Neurodegeneration. *Neurodegeneration, Neuroregeneration, Neurotrophic Action, and Neuroprotection*, 33 (1): 222-226. doi: 10.1007/s12640-017-9752-7.
- Carmichael, W. W., Azevedo, S. M., An, J. S., Molica, R. J., Jochimsen, E. M., Lau, S., Rinehart, K. L., Shaw, G. R. & Eaglesham, G. K. (2001). Human fatalities from cyanobacteria: chemical and biological evidence for cyanotoxins. *Environmental Health Perspectives*, 109 (7): 663-668. doi: 10.1289/ehp.01109663.
- Chorus, I., Falconer, I., Salas, H. J. & Bartram, J. (2000). *Health Risks Caused by Freshwater Cyanobacteria in Recreational Waters (Review)*, vol. 3.
- Crowther, J. R. (1995). *ELISA : theory and practice*. Methods in molecular biology, vol. 42. Totowa, N.J: Humana Press.
- Foss, A. J., Miles, C. O., Samdal, I. A., Løvberg, K. E., Wilkins, A. L., Rise, F., Jaabæk, J. A. H., McGowan, P. C. & Aabel, M. T. (2018). *Analysis of free and metabolized microcystins in samples following a bird mortality event*. Harmful Algae. pp. 117-129.
- Gault, P. M. & Marler, H. J. (2009). *Handbook on cyanobacteria : biochemistry, biotechnology and applications*. New York: Nova Science Publishers.
- Geekery, M. S. (2012). *LTQ ion trap*. Available at: <http://sco.lt/5m5XJB> (accessed: 07.05.2019).
- Gritti, F., Cavazzini, A., Marchetti, N. & Guiochon, G. (2007). *Comparison between the efficiencies of columns packed with fully and partially porous C18-bonded silica materials*. pp. 289-303.
- Gross, J. r. H. & Roepstorff, P. (2011). *Mass spectrometry : a textbook*. 2nd ed. ed. Heidelberg: Springer.
- Guiochon, G. & Gritti, F. (2011). Shell particles, trials, tribulations and triumphs. *Journal of Chromatography A*, 1218 (15): 1915-1938. doi: 10.1016/j.chroma.2011.01.080.
- Halasz, I. & Horvath, C. (1964). Micro Beads Coated with a Porous Thin Layer as Column Packing in Gas Chromatography. Some Properties of Graphitized Carbon Black as the Stationary Phase. *Analytical Chemistry*, 36 (7): 1178-1186. doi: 10.1021/ac60213a007.
- Hayes, R., Ahmed, A., Edge, T. & Zhang, H. (2014). Core-Shell Particles: preparation, fundamentals and applications in HPLC. *Journal of Chromatography A*, 1357. doi: 10.1016/j.chroma.2014.05.010.
- Ho, C. S., Lam, C. W. K., Chan, M. H. M., Cheung, R. C. K., Law, L. K., Lit, L. C. W., Ng, K. F., Suen, M. W. M. & Tai, H. L. (2003). Electrospray ionisation mass spectrometry: principles and clinical applications. *The Clinical biochemist. Reviews*, 24 (1): 3.
- Hosseini, S. (2018). *Enzyme-linked immunosorbent assay (ELISA) : from A to Z*. Singapore: Springer.

- Huisman, J., Codd, G. A., Paerl, H. W., Ibelings, B. W., Verspagen, J. M. H. & Visser, P. M. (2018). Cyanobacterial blooms. *Nature Reviews Microbiology*, 16 (8): 471-483. doi: 10.1038/s41579-018-0040-1.
- Haande, Sigrid, Samdal Ingunn A., Ballot Andreas, Rusch Johannes, Strand David, Løvberg Kjersti E., Miles Christopher O. & Trude, V. (2008). Microcystins in European noble crayfish (*Astacus astacus*) in Lake Steinsfjorden, a cyanobacterial (*Planktothrix*) dominated lake.
- Institute, F. E. (2017). *Observation of cyanobacteria from Landsat 8 satellite*.
- Ivanova, L., Sahlstrøm, S., Rud, I., Uhlig, S., Fæste, C. K., Eriksen, G. S. & Divon, H. H. (2017). *Effect of primary processing on the distribution of free and modified Fusarium mycotoxins in naturally contaminated oats*. pp. 73-88.
- Janssen, E. M. L. (2019). Cyanobacterial peptides beyond microcystins – A review on co-occurrence, toxicity, and challenges for risk assessment. *Water Research*, 151: 488-499. doi: 10.1016/j.watres.2018.12.048.
- John, D. V., Meng-Qiu, D., James, W., Andrew, D. & John, R. Y. (2004). Automated approach for quantitative analysis of complex peptide mixtures from tandem mass spectra. *Nature Methods*, 1 (1): 39. doi: 10.1038/nmeth705.
- John Gravas, J. R. (2013). *Mass Spectrometry for the Novice*: Taylor & Francis Inc.
- Kebarle, P. & Tang, L. (1993). From ions in solution to ions in the gas phase - the mechanism of electrospray mass spectrometry. *Analytical Chemistry*, 65 (22): 972A-986A. doi: 10.1021/ac00070a001.
- Kim, M. S., Kim, H.-H., Lee, K.-M., Lee, H.-J. & Lee, C. (2017). Oxidation of microcystin-LR by ferrous-tetrapolyphosphate in the presence of oxygen and hydrogen peroxide. *Water Research*, 114: 277-285. doi: 10.1016/j.watres.2017.02.038.
- Krienitz, L., Ballot, A., Kotut, K., Wiegand, C., Pütz, S., Metcalf, J. S., Codd, G. A. & Pflugmacher, S. (2003). Contribution of hot spring cyanobacteria to the mysterious deaths of Lesser Flamingos at Lake Bogoria, Kenya. *FEMS Microbiology Ecology*, 43 (2): 141-148. doi: 10.1111/j.1574-6941.2003.tb01053.x.
- Kurmayer, R., Li, D. & Elisabeth, E. (2016). Role of toxic and bioactive secondary metabolites in colonization and bloom formation by filamentous cyanobacteria *Planktothrix*. *Role of toxic and bioactive secondary metabolites in colonization and bloom formation by filamentous cyanobacteria Planktothrix*, 54: 69-86.
- Laboratoryinfo. (2019). High Performance Liquid Chromatography (HPLC) : Principle, Types, Instrumentation and Applications.
- Learning, N. P. o. T. E. *Mass Spectrometry-II*. Image. Available at: <https://nptel.ac.in/courses/102103044/module2/lec12/5.html> (accessed: 07.05.2019).
- Martens, S. (2017). *Handbook of Cyanobacterial Monitoring and Cyanotoxin Analysis*, vol. 8.
- Meriluoto, Jussi, Spoof, L. & Codd, G. A. (2017). *Handbook of cyanobacterial monitoring and cyanotoxin analysis*. Chichester, West Sussex: Wiley.
- Meriluoto, J., Spoof, L. & Codd, G. A. (2017). *Handbook of Cyanobacterial Monitoring and Cyanotoxin Analysis*: Wiley.
- Miles, C. (2018). *Personal communication*.
- Miles, C. O., Sandvik, M., Nonga, H. E., Rundberget, T., Wilkins, A. L., Rise, F. & Ballot, A. (2012). Thiol derivatization for LC-MS identification of microcystins in complex matrices. *Environmental science & technology*, 46 (16): 8937. doi: 10.1021/es301808h.

- Miles, C. O., Sandvik, M., Haande, S., Nonga, H. & Ballot, A. (2013). LC-MS Analysis with Thiol Derivatization to Differentiate [Dhb7]- from [Mdha7]-Microcystins: Analysis of Cyanobacterial Blooms, Planktothrix Cultures and European Crayfish from Lake Steinsfjorden, Norway. *Environmental Science & Technology*, 47 (9): 4080-4087. doi: 10.1021/es305202p.
- Miles, C. O. & Stirling, D. (2017). *Toxin Mass List, Version 15 [WWW Document]*. Available at: [https://www.researchgate.net/publication/316605326 Toxin mass list version 15?channel=doi&linkId=5907416aaca272116d35c5a4&showFulltext=true](https://www.researchgate.net/publication/316605326_Toxin_mass_list_version_15?channel=doi&linkId=5907416aaca272116d35c5a4&showFulltext=true).
- Miller, J. M. (2005). *Chromatography: Concepts and Contrasts*: Wiley.
- Neilan, B. A., Pearson, L. A., Muenchhoff, J., Moffitt, M. C. & Dittmann, E. (2013). *Environmental conditions that influence toxin biosynthesis in cyanobacteria*, 15. Oxford, UK. pp. 1239-1253.
- Orbitrap mass analyzer. Image. Creative Proteomics. Available at: <https://www.creative-proteomics.com/support/q-exactive-hybrid-quadrupole-orbitrap-mass-spectrometer.htm> (accessed: 07.05.2019).
- Orbitrap mass analyzer. (2012). Available at: [https://commons.wikimedia.org/wiki/File:Orbitrap mass analyzer - partial cross-section.JPG](https://commons.wikimedia.org/wiki/File:Orbitrap_mass_analyzer_-_partial_cross-section.JPG) (accessed: 07.05.2019).
- organisation, T. N. P. (2002). *The Noble Prize in Chemistry 2002*. Available at: <https://www.nobelprize.org/prizes/chemistry/2002/summary/> (accessed: 13.05.2019).
- Organization, W. H. (2017). Guidelines for Drinking-Water Quality. *Fourth Edition Incorporating the first Addendum*: 344-346.
- Pearson, L., Mihali, T., Moffitt, M., Kellmann, R. & Neilan, B. (2010). On the Chemistry, Toxicology and Genetics of the Cyanobacterial Toxins, Microcystin, Nodularin, Saxitoxin and Cylindrospermopsin. *Marine Drugs*, 8 (5): 1650.
- Phenomenex. (2019). *Kinetex F5* Available at: <https://www.phenomenex.com/Info/Page/f5> (accessed: 07.05.2019).
- Rohrlack, T., Edvardsen, B., Skulberg, R., Halstvedt, C. B., Utkilen, H. C., Ptacnik, R. & Skulberg, O. M. (2008). Oligopeptide chemotypes of the toxic freshwater cyanobacterium Planktothrix can form sub-populations with dissimilar ecological traits. *Limnology and Oceanography*, 53 (4): 1279-1293. doi: 10.4319/lo.2008.53.4.1279.
- Rønning, P. O. (2017). *Innføring i massespektrometri*. Høgskolen i Oslo og Akershus: Institutt for maskin, elektronikk og kjemi.
- Samdal, I. A., Ballot, A., Løvberg, K. E. & Miles, C. O. (2014). Multihapten approach leading to a sensitive ELISA with broad cross-reactivity to microcystins and nodularin. *Environmental science & technology*, 48 (14): 8035. doi: 10.1021/es5012675.
- Samdal, I. A. (2019). *Comments on recovery in hepatopancreas tissue*.
- Skoog, D. A., West, D. M., Holler, F. J. & Crouch, S. R. (2014). *Fundamentals of Analytical Chemistry*: Cengage Learning.
- Thompson, M., Ellison, S. L. R., Fajgelj, A., Willetts, P. & Wood, R. (1999). Harmonized guidelines for the use of recovery information in analytical measurement. *Pure and Applied Chemistry*, 71 (2). doi: 10.1351/pac199971020337.
- University, F. A. (2018). *Study finds source of toxic green algal blooms and the results stink*. Available at: <https://phys.org/news/2018-01-source-toxic-green-algal-blooms.html> (accessed: 13.05.2019).

- Vial, J. & Jarde, A. (1999). Experimental Comparison of the Different Approaches To Estimate LOD and LOQ of an HPLC Method. *Analytical Chemistry*, 71 (14): 2672-2677. doi: 10.1021/ac981179n.
- Webb, Penelope, M., Stewart, I., Schluter Philip, J. & Shaw Glen, R. (2006). Recreational and occupational field exposure to freshwater cyanobacteria – a review of anecdotal and case reports, epidemiological studies and the challenges for epidemiologic assessment. *Environmental Health*, 5 (1): 6. doi: 10.1186/1476-069X-5-6.
- Welker, M. & Von Döhren, H. (2006). Cyanobacterial peptides – Nature's own combinatorial biosynthesis. *FEMS Microbiology Reviews*, 30 (4): 530-563. doi: 10.1111/j.1574-6976.2006.00022.x.
- Örnemark, B. M. a. U. (2014). Eurachem Guide: the fitness for Purpose of Analytical Methods - A Laboratory Guide to Method Validation and Related Topics. *Eurachem*.

Appendix A

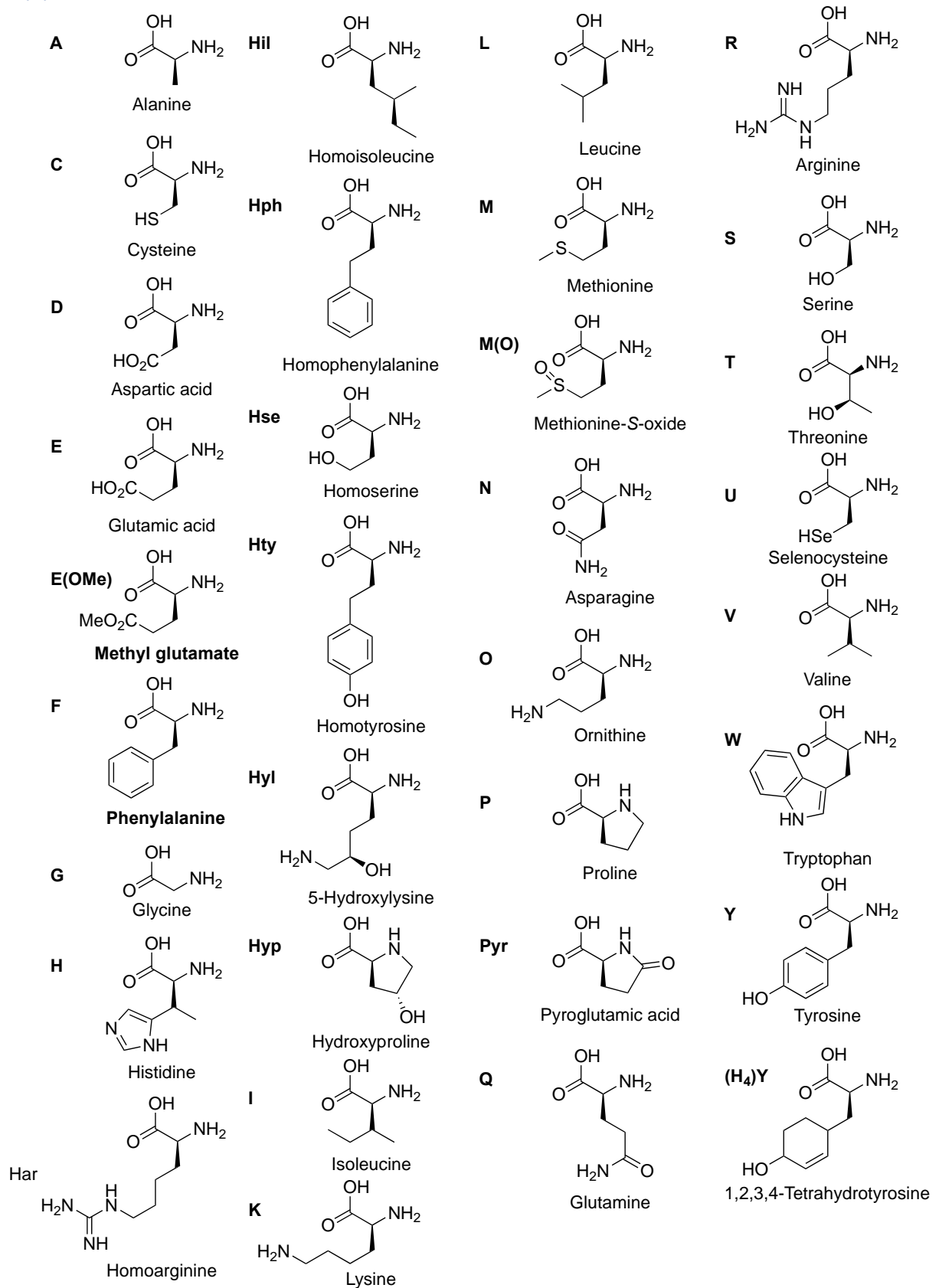


Figure A1: The molecular structure of the different amino acids that can occur in position 2 and 4 in the microcystin structure, with their name and letter abbreviation. The figure is adopted from Chris Miles personal data, with permission.

Appendix B



Figure B1: Mobile phase gradient profile 1, shown as a graph with percent on the y-axis and time on the x-axis.



Figure B2: Mobile phase gradient profile 2, shown as a graph with percent on the y-axis and time on the x-axis.

Table B1: The peaks and retention time of the microcystins and anabaenopeptins using the two different mobile phase gradient profiles.

Retention time, gradient profile 1	Retention time, gradient profile 2	Microcystin/anabaenopeptin
1.55-1.68	8.78-8.95	Anabaenopeptin B
2.37-2.41	11.15-11.17	[D-Asp ³ , Dhb ⁷]MC-RR
2.95-2.98	12.49-12.56	Anabaenopeptin A
3.70-3.73	13.43-13.50	Oscillamide Y
5.19-5.26	14.65-14.73	[D-Asp ³ , Dhb ⁷]MC-LR

Appendix C

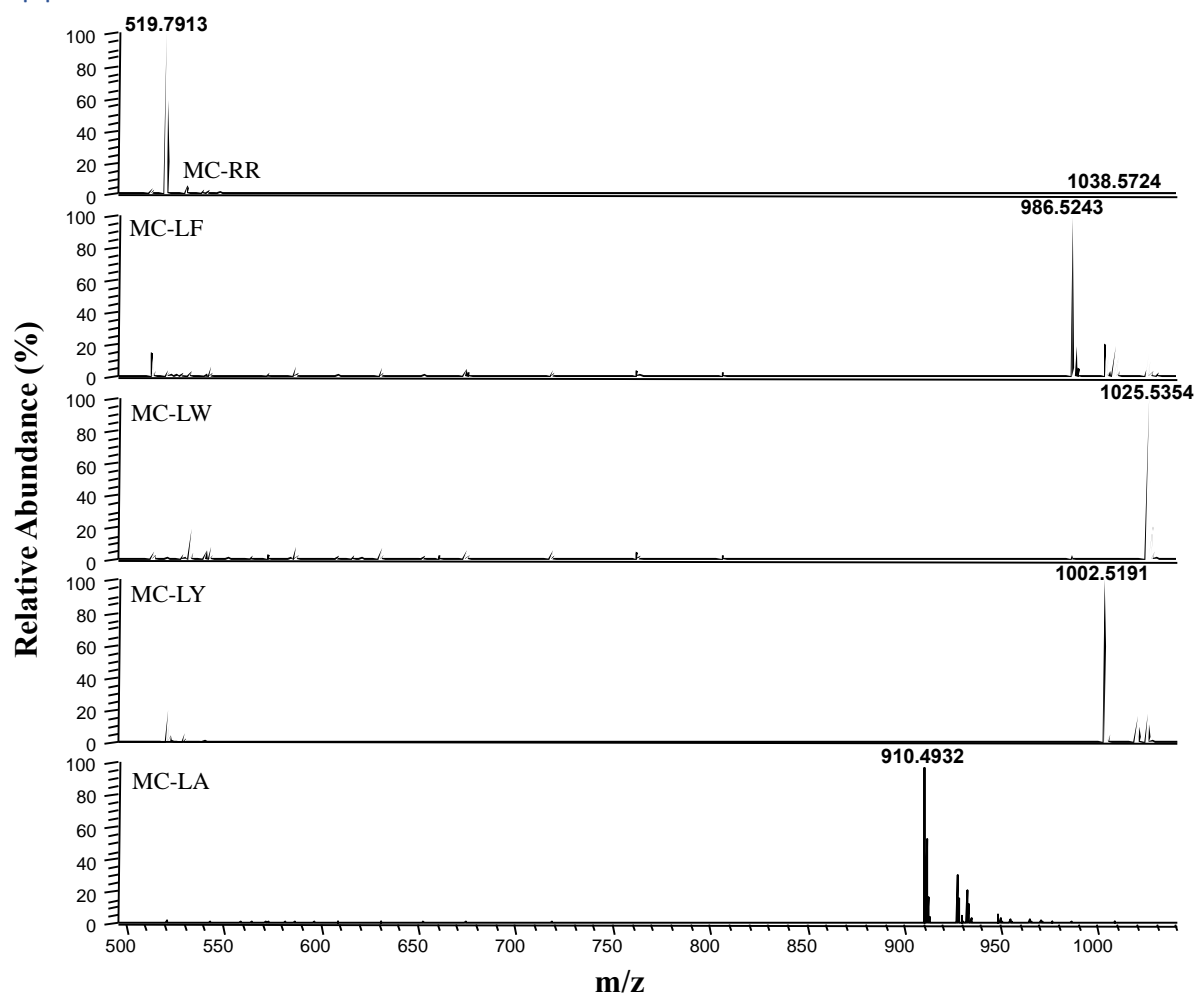


Figure C1: Full ms mass spectra of MC-RR, MC-LF, MC-LW, MC-LY, MC-LA, from a mixed standard solution, 200 ng/mL.

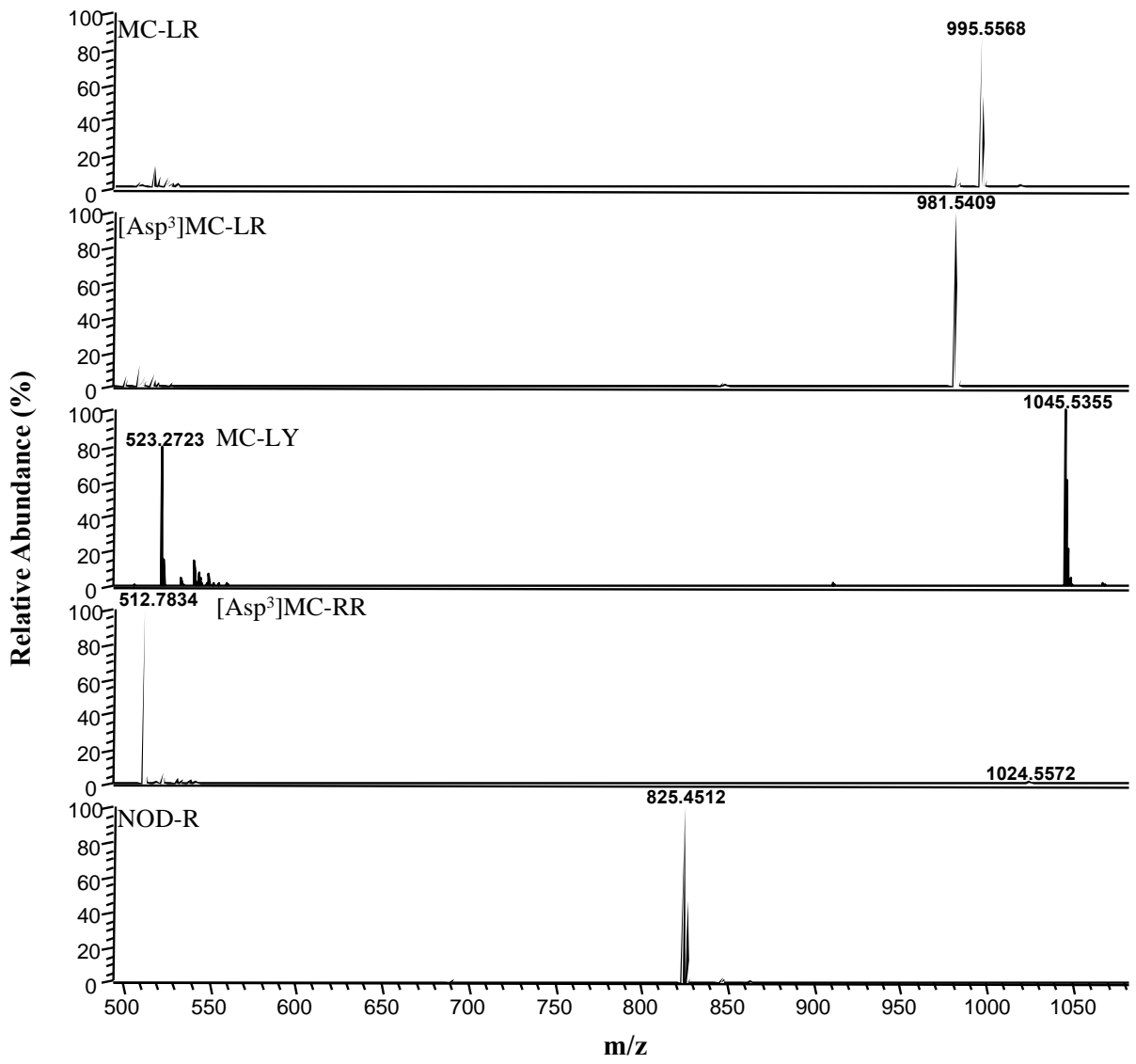


Figure C2: Full ms mass spectra of MC-LR, [Asp³]MC-LR, MC-LY, [Asp³]MC-RR and NOD-R, from a mixed standard solution, 200 ng/mL.

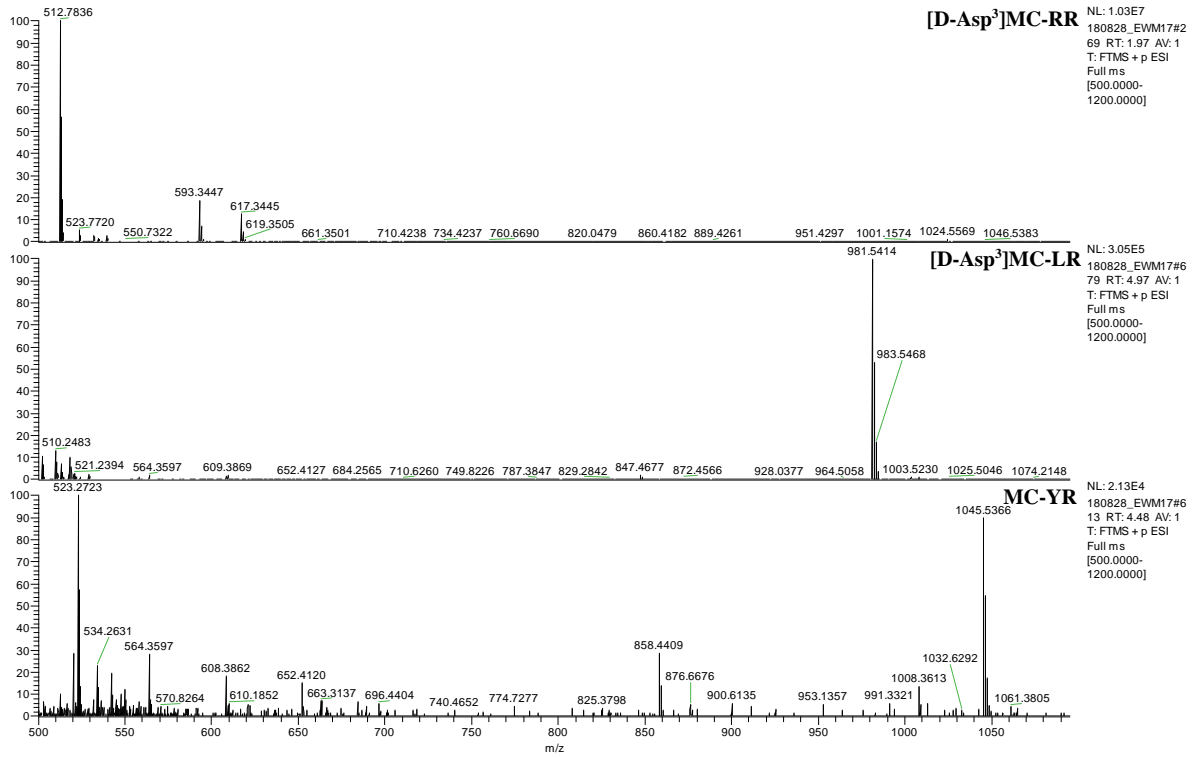


Figure C3: gives the mass spectra of the MC's found in CYA-98.

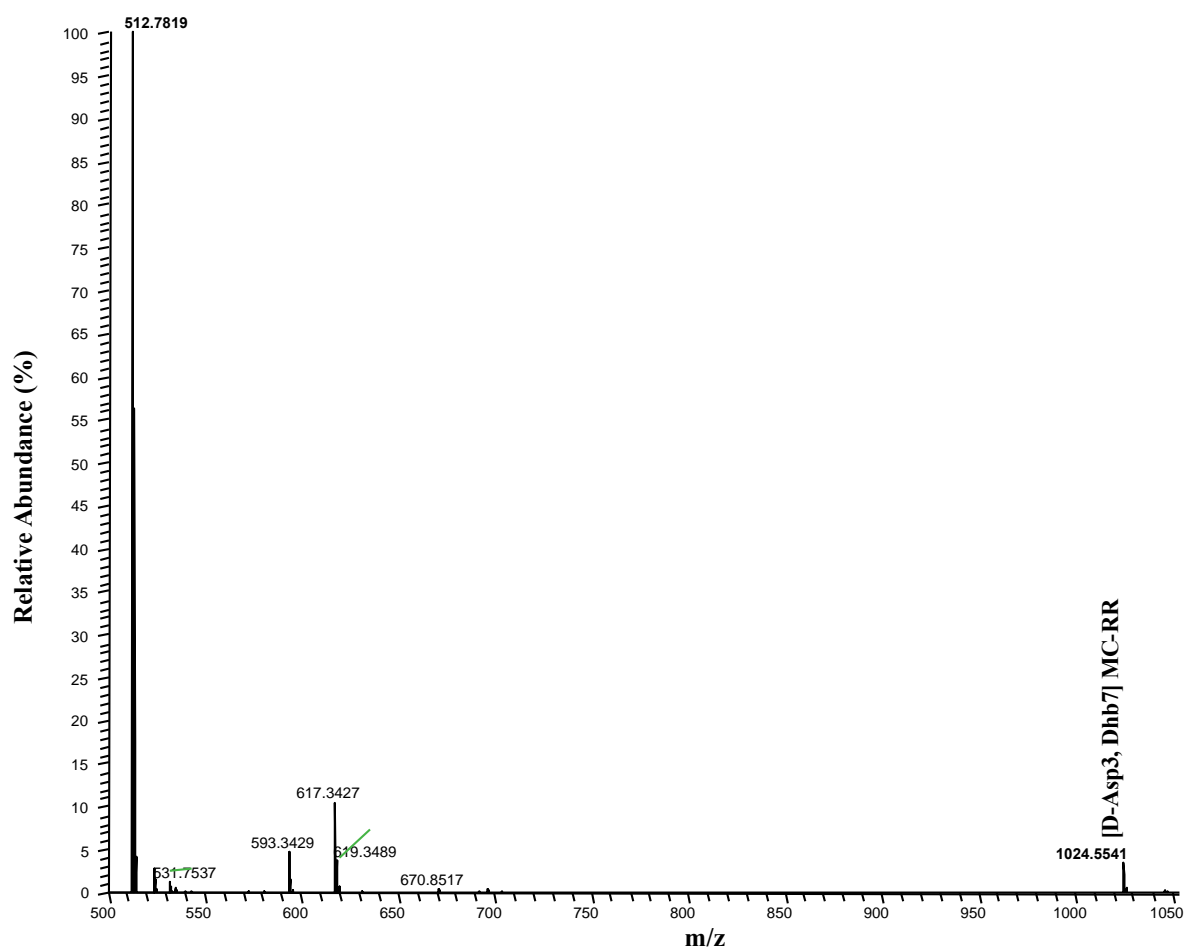


Figure C4: Mass spectra of the specie eluting at 1.98 min, full ms mass spectra associated to the largest peak in the extracted ion chromatogram of 135.0804 *m/z*.

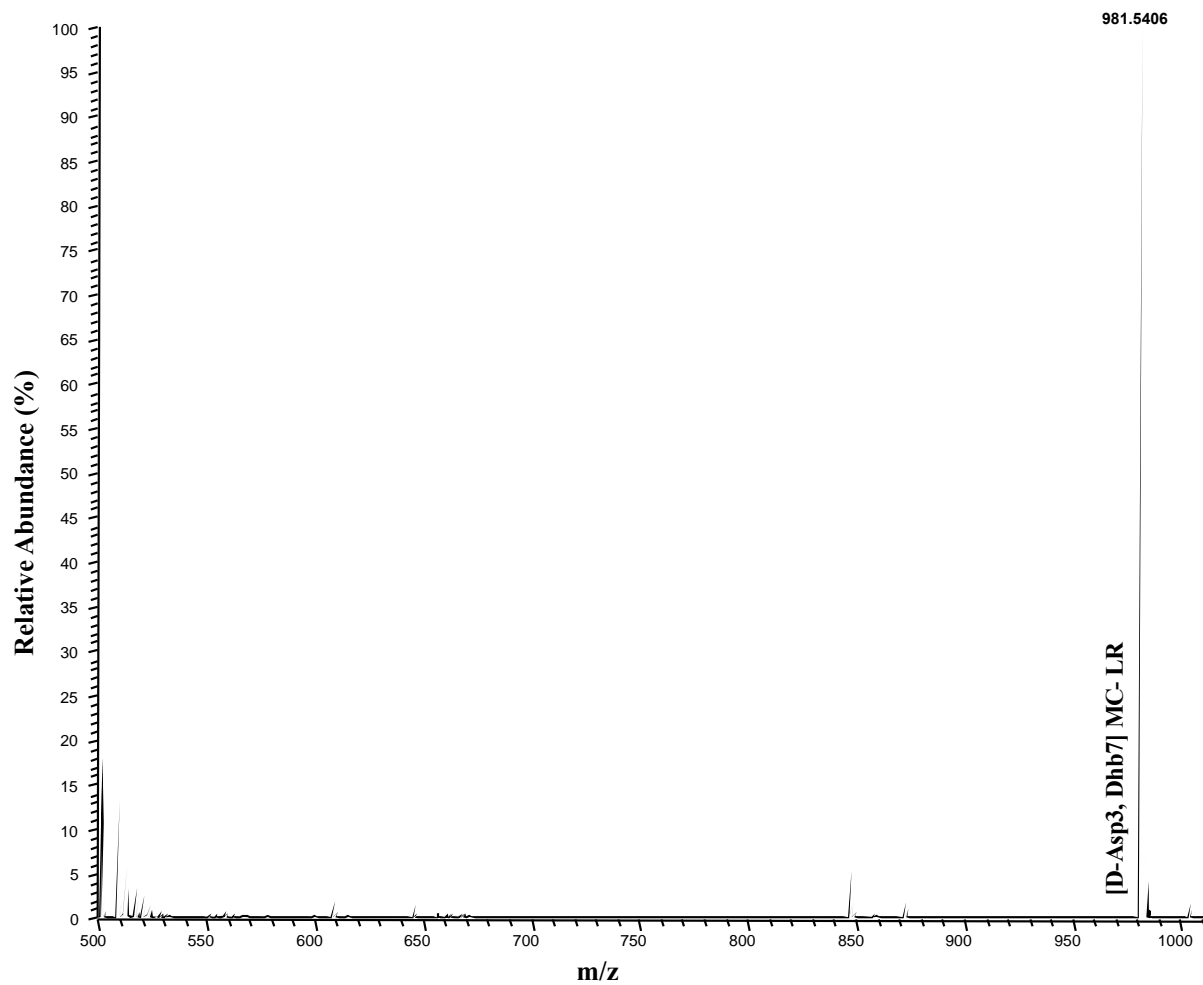


Figure C5: Mass spectra of the specie eluting at 4.99 min, full ms mass spectra associated to the peak in the extracted ion chromatogram of 135.0804 m/z .

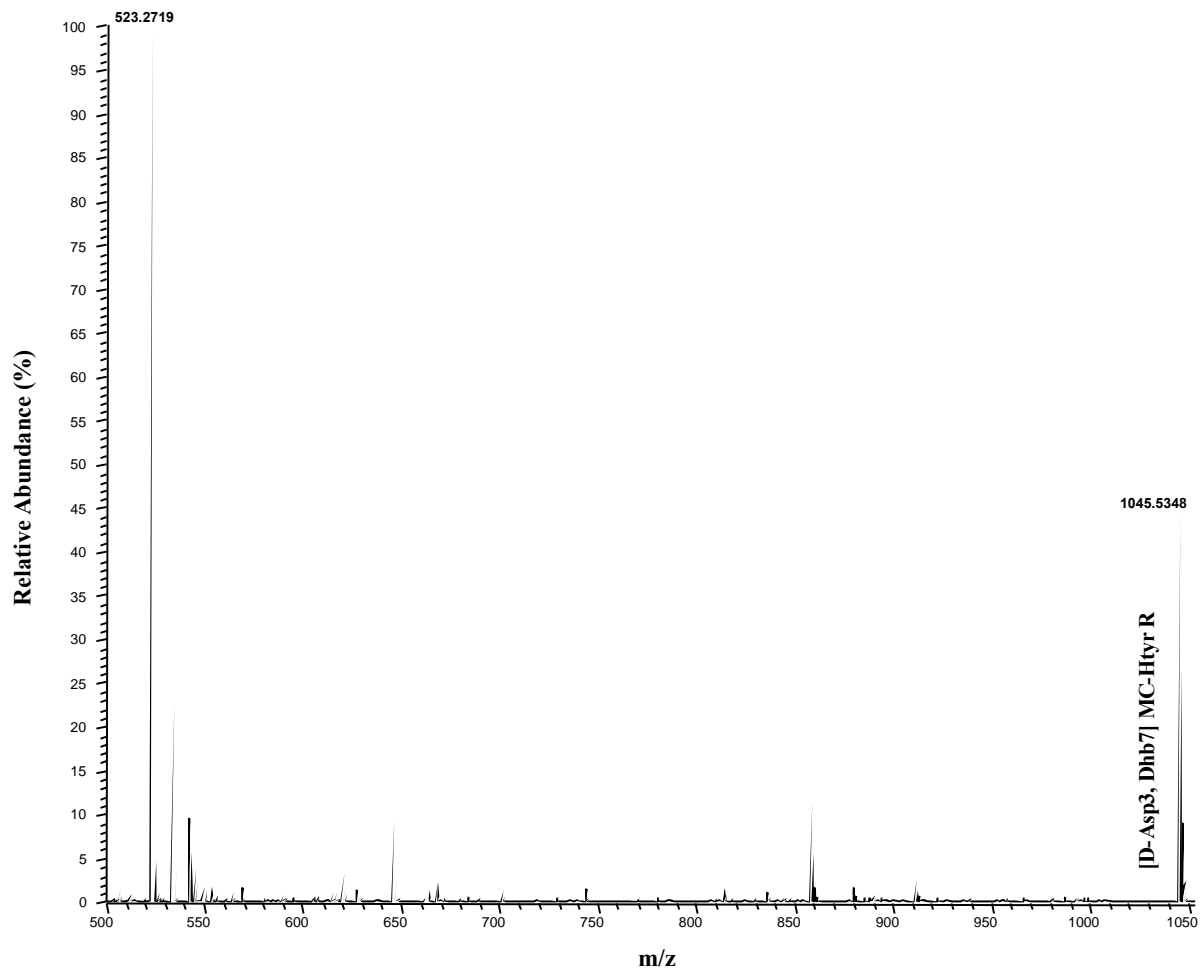


Figure C6: Mass spectra of the specie eluting at 4.51 min, full ms mass spectra associated to the peak in the extracted ion chromatogram of 135.0804 m/z .

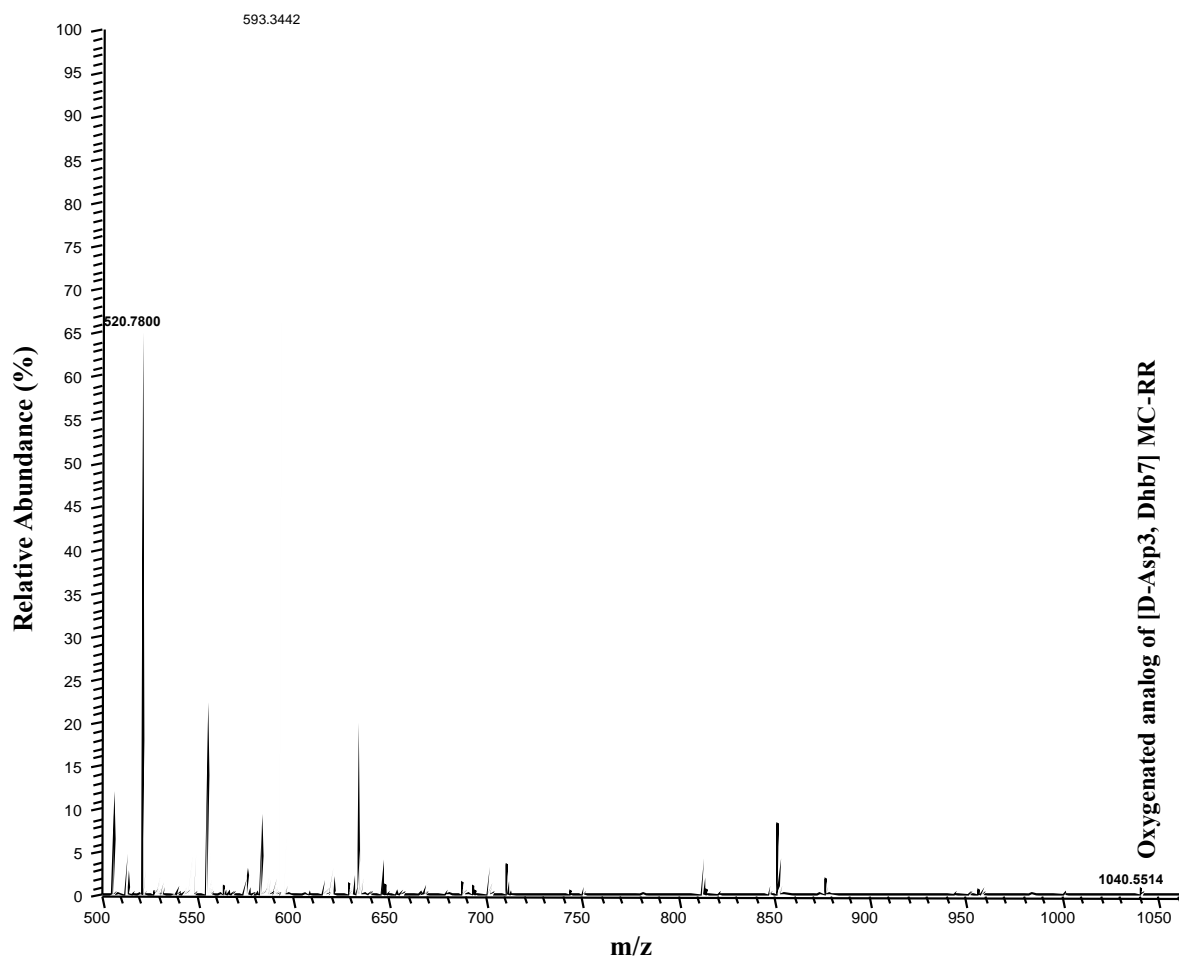


Figure C7: Mass spectra showing the oxygenated analog of [D-Asp³]MC-RR/ [D-Asp³, Dhb⁷]MC-RR.

Appendix D

Sample	Anabaenopeptin A	Anabaenopeptin B	Oscillamide Y	D-Asp3, Dhb7 MC-RR	D-Asp3, Dhb7 MC-LR
1-A-M Control	nd	nd	nd	nd	nd
1-B-M Control	nd	nd	nd	nd	nd
1-C-M Control	nd	nd	nd	nd	nd
1-D-M Control	nd	nd	nd	nd	nd
2-B-M Toxic Food	1,4*	1,8*	15,9	39,2	0,9*
2-C-M Toxic Food	nd	nd	nd	7,3	nd
2-D-M Toxic Food	nd	1,8*	nd	31,6	1,8*
3-A-M Toxic Water	nd	nd	nd	nd	nd
3-B-M Toxic Water	nd	nd	nd	nd	nd
3-C-M Toxic Water	nd	nd	nd	4,7	nd
3-D-M Toxic Water	nd	nd	nd	nd	nd
4-A-M Control	nd	nd	nd	nd	nd
4-B-M Control	nd	nd	nd	nd	nd
4-C-M Control	nd	nd	nd	nd	nd
4-D-M Control	nd	nd	nd	0,9*	nd
5-A-M Toxic Food	nd	0,9*	nd	14,3	nd
5-B-M Toxic Food	4,1*	nd	nd	6,8	0,9*
5-C-M Toxic Food	nd	nd	nd	10,1	nd
5-D-M Toxic Food	11,3	6,0	39,6	82,5	2,7*
6-A-M Toxic Water	nd	nd	nd	0,6*	nd
6-B-M Toxic Water	nd	nd	nd	nd	nd
6-C-M Toxic Water	nd	nd	nd	nd	nd
6-D-M Toxic Water	nd	nd	nd	nd	nd
7-A-M Control	nd	nd	nd	nd	nd
7-B-M Control	nd	nd	nd	nd	nd
7-C-M Control	nd	nd	nd	nd	nd
7-D-M Control	nd	nd	nd	nd	nd
8-A-M Toxic Food	nd	1,8*	22,4	23,9	nd
8-B-M Toxic Food	4,9	0,9*	30,1	16,3	nd
8-C-M Toxic Food	nd	nd	nd	2,3*	0,9*
9-A-M Toxic Water	nd	nd	nd	nd	nd
9-B-M Toxic Water	nd	nd	nd	nd	nd
9-C-M Toxic Water	nd	nd	nd	nd	nd
9-D-M Toxic Water	nd	nd	nd	nd	nd
10-A-M Control	nd	nd	nd	nd	nd
10-B-M Control	nd	nd	nd	nd	nd
10-C-M Control	nd	nd	nd	nd	nd
10-D-M Control	nd	nd	nd	nd	nd
11-A-M Toxic Food	4,5*	1,8*	27,5	26,7	0,9*
11-B-M Toxic Food	4,4*	1,8*	18,5	35,5	0,9*
11-C-M Toxic Food	nd	0,9*	nd	18,3	nd
11-D-M Toxic Food	16,7	3,6*	nd	48,4	0,9*
12-B-M Toxic Water	nd	nd	nd	nd	nd
12-C-M Toxic Water	nd	nd	nd	nd	nd
12-D1-M Toxic Water	nd	nd	nd	nd	nd
12-D-M Toxic Water	nd	nd	nd	nd	0,9*
13-A-M Control	nd	nd	nd	nd	nd
13-B-M Control	nd	nd	nd	nd	nd
13-C-M Control	nd	nd	nd	nd	nd
13-D-M Control	nd	nd	nd	nd	nd
14-A-M Toxic Food	nd	0,9*	nd	9,6	0,9*
14-B-M Toxic Food	nd	0,9*	nd	3,6*	nd
14-C-M Toxic Food	14,0	3,6*	64,8	32,0	1,8*
14-D-M Toxic Food	nd	0,9*	nd	11,3	0,9*
15-B-M Toxic Water	nd	nd	nd	nd	nd
15-C-M Toxic Water	nd	nd	nd	0,9*	0,9*
15-D-M Toxic Water	nd	nd	nd	0,9*	nd
16-A-M Control	nd	nd	nd	nd	nd
16-B-M Control	nd	nd	nd	nd	nd
16-C-M Control	nd	nd	nd	nd	nd
16-D-M Control	nd	nd	nd	nd	nd
17-A-M Toxic Food	nd	nd	nd	16,1	nd
17-B-M Toxic Food	nd	0,9*	12,5	11,4	0,9*
17-C-M Toxic Food	nd	0,9*	0,9*	20,8	0,9*
17-D-M Toxic Food	nd	0,9*	nd	4,4*	nd
18-A1-M Toxic Water	nd	nd	nd	1,8*	nd
18-A2-M Toxic Water	nd	nd	nd	nd	nd
18-C-M Toxic Water	nd	nd	nd	nd	nd
18-D-M Toxic Water	nd	nd	nd	nd	nd
19-A-M Control	nd	nd	nd	nd	nd
19-B-M Control	nd	nd	nd	nd	nd
19-C-M Control	nd	nd	nd	nd	nd
19-D-M Control	nd	nd	nd	nd	nd
20-A-M Toxic Food	4,4*	2,7*	21,7	23,3	0,9*
20-B-M Toxic Food	nd	0,9*	nd	15,9	0,9*
20-C-M Toxic Food	19,3	5,8	125,4	74,8	2,7*
21-A-M Toxic Water	nd	nd	nd	nd	nd
21-B-M Toxic Water	nd	nd	nd	nd	nd
21-C-M Toxic Water	nd	nd	nd	nd	nd
21-D-M Toxic Water	nd	nd	nd	nd	nd
22-A-M Control	nd	nd	nd	nd	nd
22-B-M Control	nd	nd	nd	1,8*	nd
22-C-M Control	nd	nd	nd	nd	nd
22-D-M Control	nd	0,9*	nd	0,9*	0,9*
23-A-M Toxic Food	nd	nd	nd	4,8	0,9*
23-B-M Toxic Food	7,1	nd	nd	nd	nd
23-C-M Toxic Food	10,8	1,8*	48,7	19,2	0,9*
23-D-M Toxic Food	nd	3,6*	76,6	59,4	0,9*
24-A-M Toxic Water	nd	nd	nd	nd	nd
24-B-M Toxic Water	nd	nd	nd	nd	nd
24-C-M Toxic Water	nd	nd	nd	nd	nd
24-D-M Toxic Water	nd	nd	nd	nd	0,9*
25-A-M Control	nd	nd	nd	nd	nd
25-B-M Control	nd	nd	nd	nd	nd
25-C-M Control	nd	nd	nd	nd	nd
25-D-M Control	nd	nd	nd	nd	nd
26-A-M Toxic Food	nd	nd	nd	nd	nd
26-B-M Toxic Food	nd	nd	nd	nd	nd
26-C-M Toxic Food	9,3	1,8*	35,7	15,8	0,9*
26-D-M Toxic Food	nd	0,9*	14,0	10,8	0,9*
27-A-M Toxic Water	nd	nd	nd	nd	nd
27-B-M Toxic Water	nd	nd	nd	nd	nd
27-C-M Toxic Water	nd	nd	nd	nd	nd
27-D-M Toxic Water	nd	nd	nd	7,0	nd

Figure D1: quantitative results of microcystins and anabaenopeptins (ng/g) in muscle tissue. Results <LOQ marked in light red, results <LOD is marked in dark red.

Sample	Anabaenopeptin A	Anabaenopeptin B	Oscillamide Y	D-Asp3, Dhb7 MC-RR	D-Asp3, Dhb7 MC-LR
1-A-HP Control	32,0	1,8*	162,9	77,5	3,1*
1-B-HP Control	nd	nd	nd	nd	1,7*
1-C-HP Control	31,8	1,8*	170,6	54,5	2,1*
1-D-HP Control	20,2	nd	105,0	40,1	1,8*
2-A-HP Toxic Food	1166,3	229,9	6241,9	4574,3	342,8
2-B-HP Toxic Food	528,3	493,6	3493,4	8094,6	658,9
2-C-HP Toxic Food	27,4	246,7	195,1	7771,2	395,5
2-D-HP Toxic Food	477,6	441,6	2445,2	4686,0	277,6
3-A-HP Toxic Water	36,2	1,8*	182,9	57,1	3,6*
3-B-HP Toxic Water	10,6	nd	63,6	32,0	nd
3-C-HP Toxic Water	12,3	nd	81,0	34,5	1,8*
3-D-HP Toxic Water	29,7	4,5	184,0	66,2	2,4*
4-A-HP Control	3,4	nd	31,7	5,4	nd
4-B-HP Control	16,5	nd	84,9	23,8	1,8*
4-C-HP Control	61,1	3,6*	316,3	114,3	4,5
4-D-HP Control	51,6	1,8*	264,0	85,5	4,4*
5-A-HP Toxic Food	299,1	188,7	235,8	2747,7	368,9
5-B-HP Toxic Food	551,3	235,1	3700,2	2184,1	267,0
5-C-HP Toxic Food	737,7	336,3	6157,7	3571,2	298,1
5-D-HP Toxic Food	434,9	278,0	489,5	7487,8	356,8
6-A-HP Toxic Water	31,3	nd	184,6	54,0	3,7*
6-B-HP Toxic Water	10,8	nd	66,9	15,6	nd
6-C-HP Toxic Water	9,1	nd	57,8	27,0	1,9*
6-D-HP Toxic Water	4,3	nd	24,0	13,0	nd
7-A-HP Control	17,7	nd	69,6	10,1	nd
7-B-HP Control	19,5	nd	92,5	21,0	1,6*
7-C-HP Control	0,9*	nd	nd	nd	1,6*
7-D-HP Control	nd	nd	nd	nd	nd
8-A-HP Toxic Food	1472,5	615,4	8851,5	9006,1	438,8
8-B-HP Toxic Food	807,7	194,4	4964,5	3356,2	154,0
8-C-HP Toxic Food	836,8	189,9	4549,3	1800,2	133,8
9-A-HP Toxic Water	15,1	nd	97,9	32,9	1,7*
9-B-HP Toxic Water	18,3	nd	104,1	13,4	nd
9-C-HP Toxic Water	8,6	nd	48,9	23,3	1,8*
9-D-HP Toxic Water	17,6	nd	102,1	50,5	2,7*
10-A-HP Control	14,1	nd	80,9	15,9	1,8*
10-B-HP Control	5,9	nd	34,5	7,9	nd
10-C-HP Control	13,7	nd	72,7	17,1	1,8*
10-D-HP Control	1,8*	nd	28,8	4,8*	nd
11-A-HP Toxic Food	581,4	127,1	1281,1	1970,0	136,3
11-B-HP Toxic Food	344,7	254,0	2193,9	4975,6	259,9
11-C-HP Toxic Food	101,0	119,3	nd	5515,0	260,5
11-D-HP Toxic Food	1648,6	689,3	9000,6	7014,2	401,5
12-A-HP Toxic Water	34,5	1,8*	173,5	37,5	3,4*
12-B-HP Toxic Water	16,8	nd	96,4	27,6	1,9*
12-C-HP Toxic Water	18,3	1,8*	103,8	31,2	2,3*
12-D-HP Toxic Water	7,5	nd	47,3	16,5	nd
13-A-HP Control	16,8	nd	95,3	19,3	1,6*
13-B-HP Control	22,4	1,8*	122,3	32,1	1,9*
13-C-HP Control	26,3	1,8*	125,7	25,8	2,5*
13-D-HP Control	3,6*	nd	20,6	3,6*	1,6*
14-A-HP Toxic Food	212,6	310,9	nd	3583,6	324,9
14-B-HP Toxic Food	859,4	214,5	5909,2	2577,8	173,9
14-C-HP Toxic Food	1365,5	589,7	8464,0	7778,8	657,7
14-D-HP Toxic Food	753,1	281,8	1329,4	4261,9	226,3
15-B-HP Toxic Water	21,7	nd	120,8	49,3	3,2*
15-C-HP Toxic Water	34,4	2,7*	191,2	139,4	5,8
15-D-HP Toxic Water	12,9	nd	83,7	34,2	2,6*
16-A-HP Control	16,4	nd	75,2	19,6	2,2*
16-B-HP Control	17,9	nd	81,6	9,0	nd
16-C-HP Control	8,9	nd	42,3	6,2	1,7*
16-D-HP Control	42,8	1,8*	262,9	91,1	6,7
17-A-HP Toxic Food	41,3	1,8*	257,4	5111,7	5,3
17-B-HP Toxic Food	256,6	90,9	4599,8	1946,7	304,4
17-C-HP Toxic Food	1436,5	384,7	8712,4	12866,8	234,9
17-D-HP Toxic Food	47,3	436,0	553,4	2237,9	974,7
18-A-HP Toxic Water	nd	nd	1,8*	nd	nd
18-A2-HP Toxic Water	8,8	nd	61,0	23,4	1,6*
18-C-HP Toxic Water	6,6	nd	41,7	13,7	nd
18-D-HP Toxic Water	5,6	nd	38,0	20,4	nd
19-A-HP Control	19,3	nd	118,0	45,3	2,5*
19-B-HP Control	nd	1,8*	3,7	nd	nd
19-C-HP Control	18,1	1,8*	102,8	34,1	1,9*
19-D-HP Control	3,0*	nd	14,9	4,5	1,6*
20-A-HP Toxic Food	1108,3	224,5	6751,3	7255,8	303,4
20-B-HP Toxic Food	332,8	120,7	1281,6	5746,1	254,4
20-C-HP Toxic Food	nd	604,5	nd	nd	503,3
21-A-HP Toxic Water	12,1	nd	75,6	43,6	2,5*
21-B-HP Toxic Water	25,4	1,8*	138,8	73,4	3,4*
21-C-HP Toxic Water	10,6	nd	63,0	23,9	3,0*
21-D-HP Toxic Water	20,3	3,6*	101,7	28,6	2,2
22-A-HP Control	2,7*	nd	18,4	12,6	nd
22-B-HP Control	12,3	nd	63,3	21,7	nd
22-C-HP Control	7,6	nd	34,3	10,4	nd
22-D-HP Control	25,6	1,8*	133,7	79,3	2,8*
23-A-HP Toxic Food	228,5	14,8	nd	169,6	23,1
23-B-HP Toxic Food	136,5	86,5	3279,7	445,8	69,5
23-C-HP Toxic Food	493,7	225,3	7262,3	5494,4	317,7
23-D-HP Toxic Food	1200,2	103,1	3362,1	6156,0	240,0
24-A-HP Toxic Water	17,1	nd	89,4	54,6	2,2*
24-B-HP Toxic Water	14,5	nd	73,8	70,6	2,1*
24-C-HP Toxic Water	56,5	2,7*	256,4	54,3	3,9*
24-D-HP Toxic Water	18,3	nd	86,9	42,2	2,2*
25-A-HP Control	0,9*	nd	nd	nd	1,6*
25-B-HP Control	3,6*	nd	15,2	2,7*	nd
25-C-HP Control	73,9	nd	421,5	59,3	4,6
25-D-HP Control	1,8*	nd	11,6	5,6	nd
26-A-HP Toxic Food	510,4	108,2	3626,0	2223,3	89,1
26-B-HP Toxic Food	708,7	46,5	1529,4	649,5	47,3
26-D-HP Toxic Food	523,8	40,2	3444,9	2491,4	108,0
27-A-HP Toxic Water	28,0	2,7*	157,7	83,0	3,5*
27-B-HP Toxic Water	1,8*	1,8*	14,0	5,4	nd
27-C-HP Toxic Water	nd	nd	nd	nd	1,6*
27-D-HP Toxic Water	45,8	nd	220,3	93,4	4,0*

Figure D2: quantitative results of microstystins and anabaenopeptins (ng/g) in hepatopancreas tissue. Results <LOQ marked in light red, results <LOD is marked in dark red, results marked in blue have been diluted (1:100)

because they were outside the calibration curve (upper limit). Results marked with an asterisk are outside the calibration curve (lower limit). The result marked in orange shows the undiluted value in ng/mL. The diluted value was negative and could consequently not be used.

Appendix E

Parallels	A	B	C	Anabaenopeptin B		Parallels	A	B	C	Anabaenopeptin A					
1	2,3	1,8	1,4			1	2,7	2,1	2,8						
2	2,2	1,9	2,0			2	3,0	1,8	2,7						
3	2,1	1,8	1,9			3	2,9	1,6	2,7						
4	2,0	1,9	1,8			4	2,9	1,5	3,1						
5	2,2	1,8	1,8			5	2,6	1,6	2,8						
6	2,1	1,6	2,0			6	3,0	1,3	2,8						
Repeatability				Between series				Repeatability				Between series			
Mean	2,15	1,80	1,83	Mean of means	1,93	Mean	2,85	1,63	2,82	Mean of means	2,43				
SD	0,12	0,09	0,25	Sx=SD of mean	0,19	SD	0,14	0,26	0,15	Sx=SD of mean	0,69				
Combined SD, Sr	0,17			SL ² =sx ² -sr ² /n	0,03	Combined SD, Sr	0,19			SL ² =sx ² -sr ² /n	0,47				
Combined RSDr (%)	5,18			RSDL ² =(sx/mean) ² -sr ² /n	96,72	Combined RSDr (%)	5,83			RSDL ² =(sx/mean) ² -sr ² /n	805,43				
SiR=rot(sr ² +sL ²)	0,25			RSiR(%)=rot(RSDr ² +RSDL ²)	11,11	SiR=rot(sr ² +sL ²)	0,71			RSiR(%)=rot(RSDr ² +RSDL ²)	28,97				
MU=2*u=2*SiR=	0,49					MU=2*u=2*SiR=	1,43								
Parallels	A	B	C	Oscillamide Y		Parallels	A	B	C	[D-Asp3, Dhn7]MC-RR					
1	3,6	2,1	2,7			1	2,4	1,4	2,5						
2	2,3	2,1	2,8			2	2,5	1,5	3,2						
3	3,0	2,3	3,6			3	2,4	1,5	2,4						
4	2,2	2,3	3,4			4	2,3	1,5	2,1						
5	3,2	2,4	3,1			5	2,5	1,4	2,1						
6	2,9	2,3	3,3			6	2,4	1,6	2,0						
Repeatability				Between series				Repeatability				Between series			
Mean	2,86	2,26	3,15	Mean of means	2,76	Mean	2,42	1,48	2,38	Mean of means	2,10				
SD	0,55	0,14	0,36	Sx=SD of mean	0,45	SD	0,08	0,05	0,44	Sx=SD of mean	0,53				
Combined SD, Sr	0,39			SL ² =sx ² -sr ² /n	0,18	Combined SD, Sr	0,26			SL ² =sx ² -sr ² /n	0,27				
Combined RSDr (%)	7,72			RSDL ² =(sx/mean) ² -sr ² /n	261,23	Combined RSDr (%)	6,42			RSDL ² =(sx/mean) ² -sr ² /n	635,36				
SiR=rot(sr ² +sL ²)	0,58			RSiR(%)=rot(RSDr ² +RSDL ²)	17,91	SiR=rot(sr ² +sL ²)	0,58			RSiR(%)=rot(RSDr ² +RSDL ²)	26,01				
MU=2*u=2*SiR=	1,15					MU=2*u=2*SiR=	1,17								
Parallels	A	B	C	[D-Asp3, Dhn7]MC-LR		Parallels	A	B	C						
1	1,9	1,5	1,9												
2	1,5	1,5	1,7												
3	1,8	1,4	1,9												
4	1,8	1,4	1,8												
5	1,7	1,4	2,0												
6	1,9	1,4	1,9												
Repeatability				Between series				Repeatability				Between series			
Mean	1,77	1,43	1,88	Mean of means	1,69	Mean				Mean of means					
SD	0,16	0,04	0,09	Sx=SD of mean	0,23	SD				Sx=SD of mean					
Combined SD, Sr	0,11			SL ² =sx ² -sr ² /n	0,05	Combined SD, Sr				SL ² =sx ² -sr ² /n					
Combined RSDr (%)	3,61			RSDL ² =(sx/mean) ² -sr ² /n	184,27	Combined RSDr (%)				RSDL ² =(sx/mean) ² -sr ² /n					
SiR=rot(sr ² +sL ²)	0,25			RSiR(%)=rot(RSDr ² +RSDL ²)	14,05	SiR=rot(sr ² +sL ²)				RSiR(%)=rot(RSDr ² +RSDL ²)					
MU=2*u=2*SiR=	0,50					MU=2*u=2*SiR=									

Figure F1: Calculations of inter-day-precision for microcystins and anabaenopeptins.

Appendix F

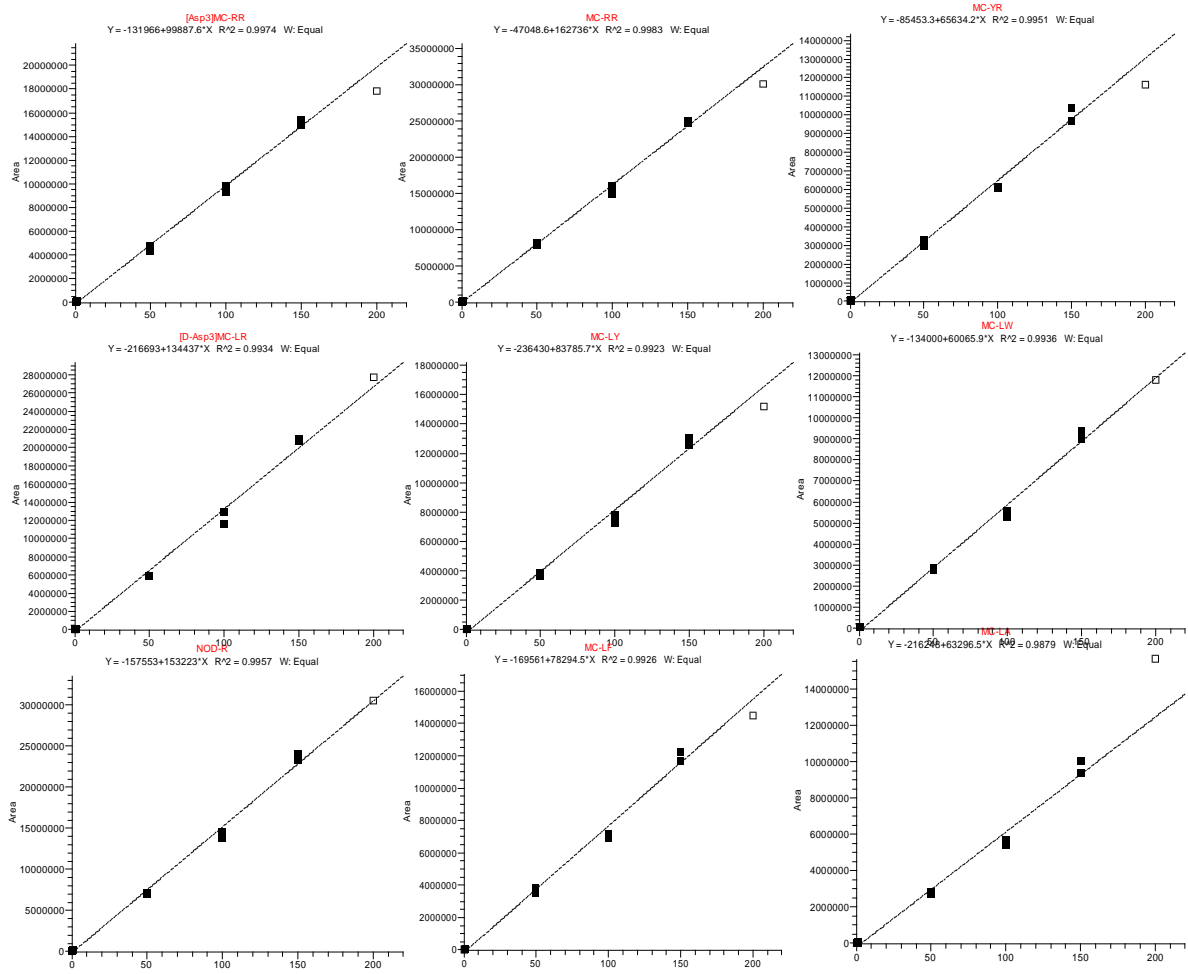


Figure F1: Calibration curves of MCs and nodularin in the mixed standard solution.

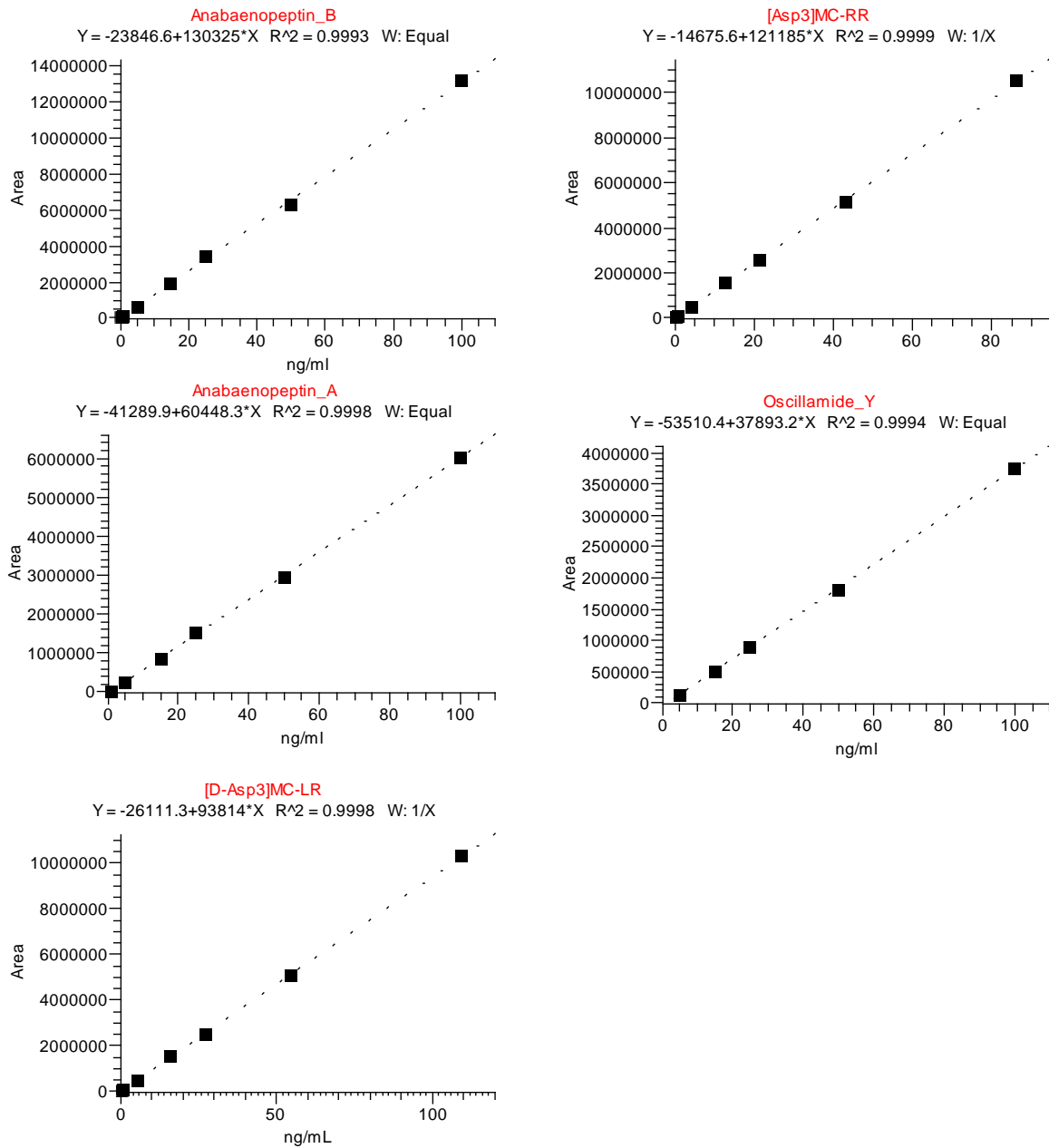


Figure F2: Calibration curves of the microcystins and anabaenopeptins detectable in crayfish, blank standards.

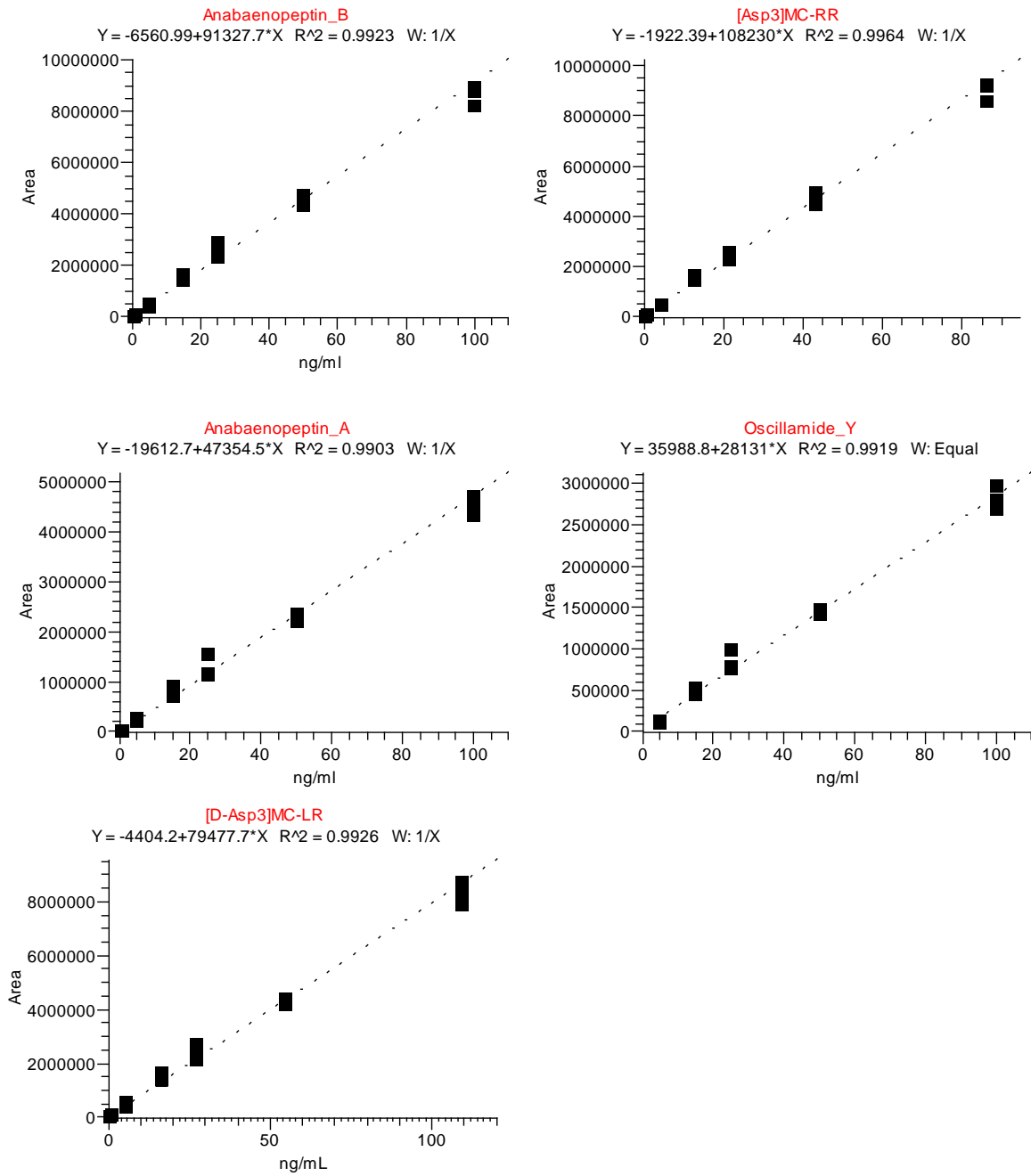


Figure F3: Calibration curves of the microcystins and anabaenopeptins detectable in crayfish, muscle matrix standards.

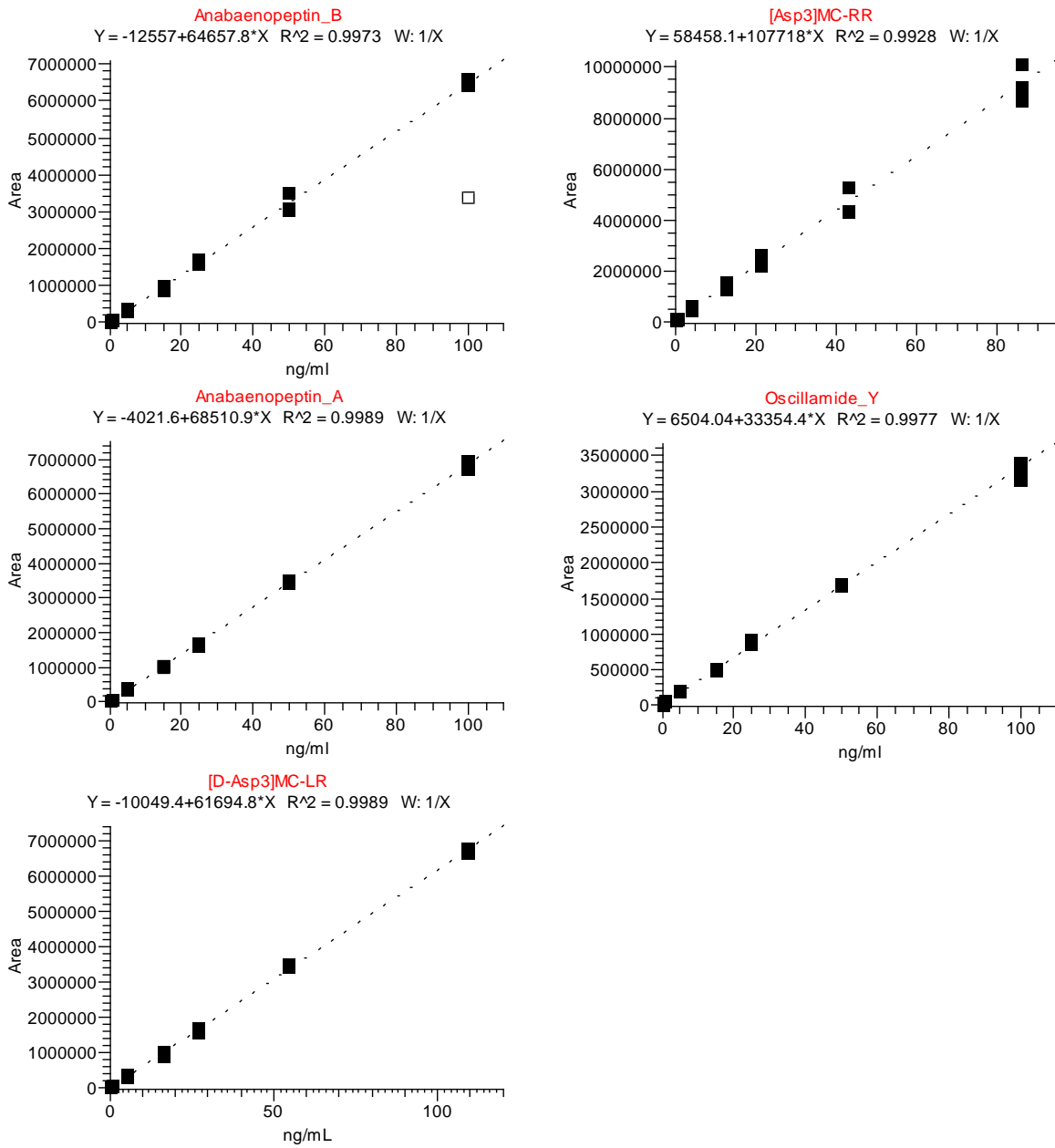


Figure F4: Calibration curves of the microcystins and anabaenopeptins detectable in crayfish, muscle matrix standards.

Appendix G

E:\082318\...082318_EWM15

2018-08-23 21:05:32

EWM 10 x fortynting

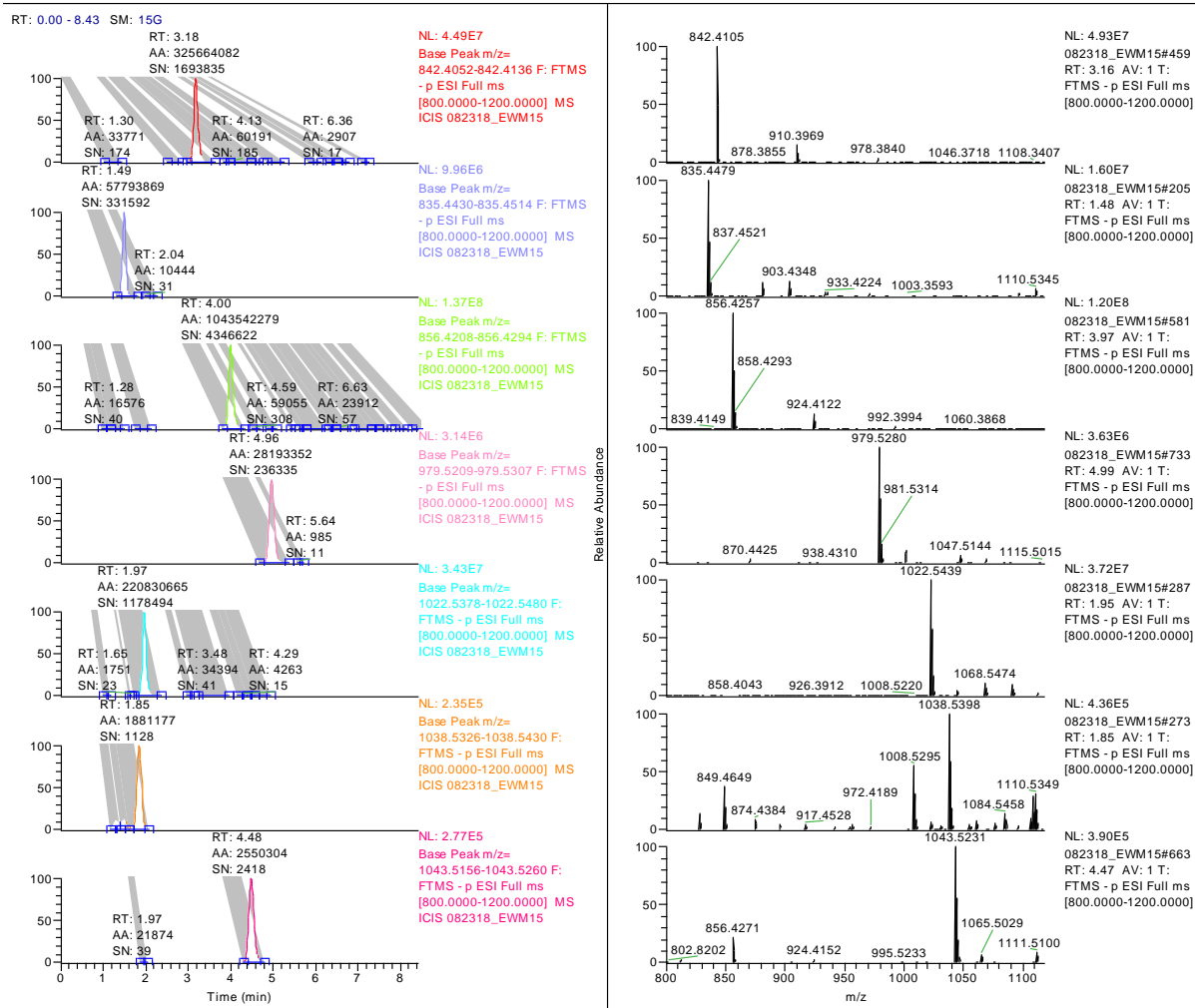


Figure G1: Chromatograms and mass spectra showing all microcystins and anabaenopeptins in a 1:10 dilution of a NIVA-CYA98 extract, negative mode.

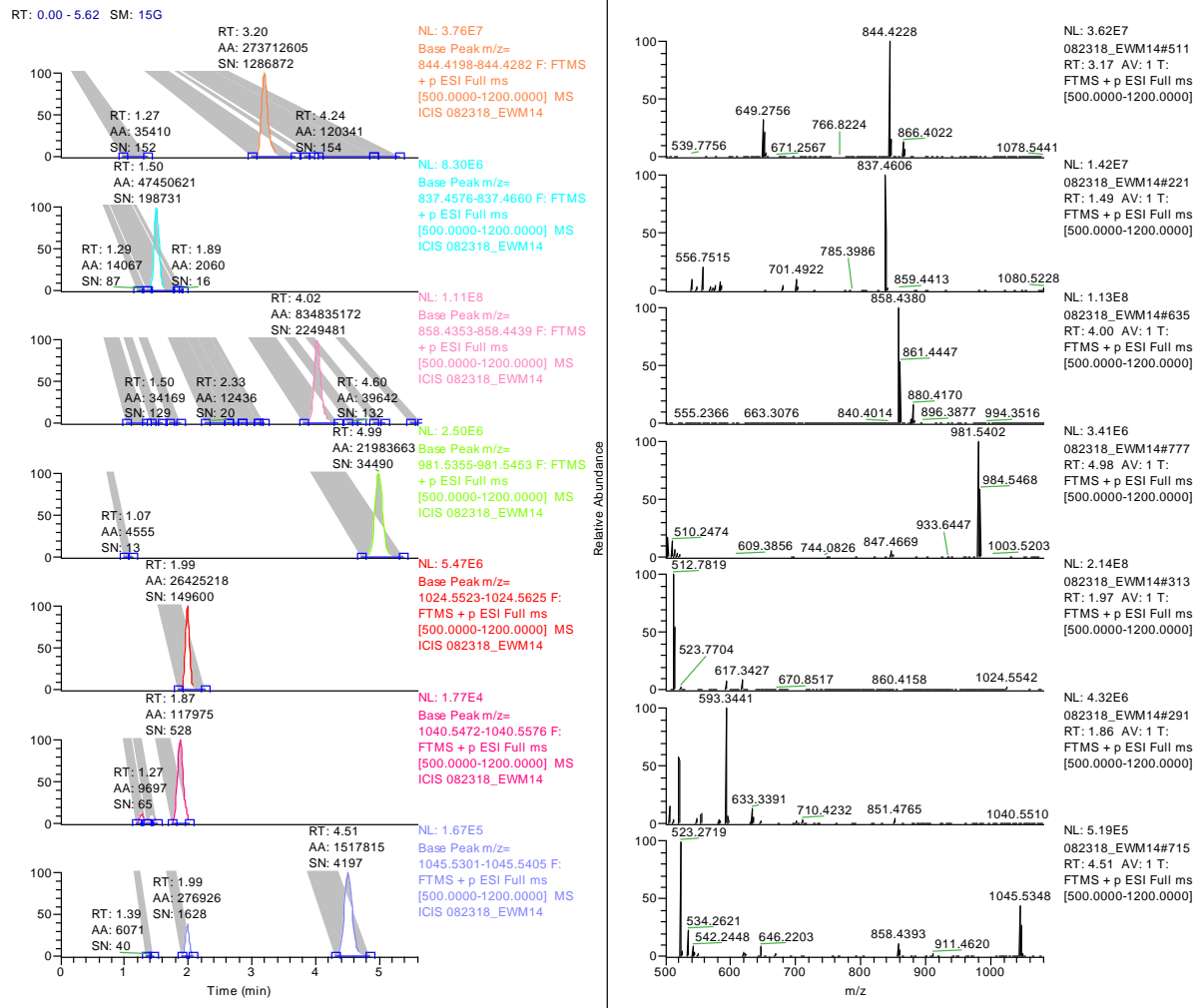


Figure G2: Chromatograms and mass spectra showing all microcystins and anabaenopeptins in a 1:10 dilution of a NIVA-CYA98 extract, positive mode.



Norges miljø- og biovitenskapelige universitet
Noregs miljø- og biovitenskapelige universitet
Norwegian University of Life Sciences

Postboks 5003
NO-1432 Ås
Norway